



TÉCNICO
LISBOA



Decentralized Voltage Control Strategies

for Microgeneration in Low-Voltage Distribution Grids

by

João Carlos Costa Botas de Campos

Thesis to obtain the Master of Science Degree in
Electrical and Computing Engineering

Supervisors: Prof. Pedro Manuel dos Santos Carvalho
Eng. José Ferreira Pinto

Examination Committee

Chairperson: Prof. Rui Manuel Gameiro de Castro

Supervisor: Prof. Pedro Manuel Santos de Carvalho

Member of the Committee: Prof. Sónia Maria Nunes dos Santos Paulo Ferreira Pinto

November 2016

Agradecimentos

Aos meus pais e família pelo apoio prestado durante todo o meu percurso acadêmico, e por terem que aturar dois anos de “*Tá andando*” em tom meio-morto como resposta ao progresso da tese. Aos meus colegas de curso, que apesar das muitas distrações que providenciaram também me deram animo ao longo destes sete anos, e que espero que consigam despachar a deles mais depressa do que eu. Ao meu coordenador, pela ajuda prestada e pelos vários blackouts de comunicação (meus) que teve que sofrer. Finalmente, à Internet pela informação que me pode prestar, mas mãe maldita da procrastinação que me ancora. Mas mãe é mãe, e não se vive sem ela...

Abstract

The growth of distributed generation (DG) presents a rising challenge for the regulation of the nodal profile in low-voltage (LV) networks. To lessen the impact caused by ***distributed energy resources*** (DERs), namely due to voltage rise, ***decentralized voltage control strategies*** have been gaining prominence. However, these methods carry several, often overlooked, drawbacks that can compromise a grid's voltage profile. In this thesis, we examine such limitations, concurrently proposing an adequate autonomous system model that can act as a suitable workaround, within possibility. We model several reduced circuit networks and a basic control algorithm, then expanding upon the latter as the issues accrue. Of these, the main hindrance comes in the form of ***system instability***, due to a non-convergent behavior of the algorithm, followed by restrictions on the generators' power output. An ***alternating power controller*** is thus put forward, using each ***controller's power gain*** as a means to ensure the system's stability, and afterwards computationally simulated. The base network model is then expanded upon to account for the effects on stability that concentrating DG and distancing the generating busses have. We finalize with the proposal of an alternate ***voltage error integration*** based controller that removes the controllers' operation simultaneity, responsible for the inherent unpredictability of the profile's behavior tied to the unbalanced distribution of DERs through the phases. While theoretical feasible, this thesis ultimately demonstrates that the large-scale adoption of a decentralized strategy cannot go without a much more in-depth study on its limitations, particularly using a more realistic study scenario.

Index terms – Distributed energy resources, decentralized voltage control strategy, system instability, alternating power controller, controller power gain, voltage error integration.

Resumo Analítico

Com o crescimento de geração distribuída (GD), existe um desafio crescente em relação à regulação do perfil de tensão em redes de baixa tensão (BT). Para atenuar o impacto causado por elevações de tensão devido à inclusão de **recursos de energia distribuídos** (RED), **estratégias de controlo de tensão descentralizadas** têm ganhado tracção. Porém, estas estratégias acarretam desvantagens (frequentemente negligenciadas) que podem comprometer o perfil de uma rede eléctrica. Nesta tese, examinamos tais limitações, propondo concorrentemente um modelo de controlo autónomo que logre contorna-las, dentro do possível. Modelos de circuito reduzido e um algoritmo de controlo básico foram concebidos, desenvolvendo este último ao longo do trabalho. O principal entrave advém de **instabilidade no sistema**, devido à uma não-convergência do erro de tensão, seguido de restrições na potência gerada. Um **controlador de potência alternado** é então apresentado, utilizando o **ganho de potência** de cada gerador para assegurar a estabilidade, e depois simulado computacionalmente. A rede original é seguidamente expandida, contabilizando os efeitos que a concentração e a dispersão de GD têm na sua estabilidade. Finalizamos com a proposta de um controlador alternativo, baseado na **integração da área do erro de tensão**, que remove a simultaneidade operacional dos controladores responsável pela imprevisibilidade do comportamento do perfil, ligada à distribuição desequilibrada dos REDs pelas fases. Embora teoricamente factível, em última análise, esta tese demonstra que a adopção em larga escala de estratégias descentralizadas não pode ocorrer sem um estudo mais aprofundado sobre as suas limitações, particularmente recorrendo a um cenário de estudo mais realista.

Palavras-chave – Recursos de energia distribuídos, estratégias de controlo de tensão descentralizadas, controlador de potência alternado, instabilidade no sistema, ganho de potência, integração da área do erro de tensão.

Table of Contents

1	Introduction	1
1.1	State-of-the-art and Motivation	1
1.2	Objective and Structure	3
2	Decentralized System Modeling	5
2.1	Low-Voltage Network Outline	5
2.1.1	Reduced Circuit Characterization	5
2.1.2	Study Models	9
2.2	Decentralized Controller Logic	12
2.2.1	Basic Voltage Control Algorithm	12
2.2.2	Algorithm Convergence Criteria	13
2.2.3	Instability and Oscillation Power Gain Threshold	16
3	Limits to Fully Decentralized Voltage Control	18
3.1	Approaches to the Controllers' Power Gain	18
3.1.1	Common Network Gain	18
3.1.2	Gain through Inverse Impedance	22
3.1.3	Alternative Strategies	25
3.2	Limitations on Injected Power	27
3.2.1	Generator Operational Area	27
3.2.2	Power Coordinates Solution Line Set	30
3.3	Updated Controller Logic	32
3.3.1	Bounded to the Maximum Apparent Power Limit Curve	33
3.3.2	Active Power Shift by Foresight	34
4	Simulation Results	36
4.1	Establishing the Initial Voltage Error	36
4.2	Voltage Error Behavior and System Performance	38
4.3	Power Gains and Optimal Performance	46
4.4	Active and Reactive Power Curtailment	48
4.5	Additional Alteration to the Algorithm	53
5	Expanding the Study Model	54
5.1	Concentrated Distributed Generation	54
5.1.1	Effects on Stability	54
5.1.2	Effects on the Initial Voltage Error	56
5.2	Anchoring	60
5.3	Dispersion of Distributed Generation	61

6 Voltage Error Area Integration	66
6.1 Voltage Error Area Correction	67
6.2 Voltage Error Behavior and System Performance	69
6.3 Dynamic Error Sampling	72
6.4 Applied to a Full Grid	75
7 Conclusions	77
7.1 Summary	77
7.2 Outlook	80
Bibliography	81
Annex A - MATLAB Code for Discrete Controller	82
Annex B - MATLAB Code for Continuous Controller	84
Annex C - MATLAB Code for <i>ini_cond_error</i> Func.	87
Annex D - MATLAB Code for <i>matrixbuild</i> Func.	88
Annex E - MATLAB Code for <i>pf3ph</i> Func.	90
Annex F - MATLAB Code for <i>setlineadj</i> Func.	91

List of Figures

Chapter 2

- 2.1 Single line model of a feeder network with a load and a DER. 5
- 2.2 Figurative example of a voltage rise in phase R, ΔV^{RN} , and the resulting voltage drop in phase T, ΔV^{TN} , induced by an active power injection change, ΔP_{iG} . 7
- 2.3 Four-wired LV test circuit used as a foundation for the study on DER injection. We can notice two generators (blue and red), and how their loop resistances R_{ii}^{el} and R_{jj}^{el} are obtained. Additionally, we can also see their common-path resistance (inside the purple box), from which the respective non-diagonal terms of $[R]$, in this case $-\frac{1}{4} R_{ij}^{el}$, will be derived from. 9
- 2.4 Plane representation of the stability criteria for the control system. If the eigenvalues of $[A]$, $\lambda(A)$, are all contained within the pink area the system will be able to converge. Furthermore, this convergence will be non-oscillatory iff all eigenvalues are contained within the blue line segment. 15

Chapter 3

- 3.1 Eigenvalue gradients Δ_i for the different study models, with $[k] = \alpha[I]$. Note that the colors are NOT indicative of the DERs themselves, as was the case in Table I and II. 18
- 3.2 Diagonal terms of $[k_{stb}]$ for the different study models, with $[k] = \alpha[I]$. 18
- 3.3 Effects of distancing (i.e. adding more impedance) the DG cluster from the source bus on the maximum α . The topmost line represents the same example as Fig 3.2, with each subsequent line below representative of an gradual increase in the loop impedance between the cluster and the source. In matrix terms, this amounts to a $R_{ii} + 2z = R_{ii} + 2 \times 0.2$ increment when compared with the line immediately above. 20
- 3.4 Eigenvalue gradients Δ_i for the different study models, with $[k] = \alpha[R_I]$. Note that, again, the colors are NOT indicative of the DERs themselves, as was the case in Table I and II. 22
- 3.5 Diagonal terms of $[k_{stb}]$ for the different study models, with $[k] = \alpha[R_I]$. The colors ARE indicative of the DERs and we see that, for the same phase distribution, the terms of $[k_{stb}]$ are consistent per their positioning. 22
- 3.6 Comparison of the effects of distancing the DG cluster from the source bus with a common network (dotted lines) and an admittance based (full lines) power gain on the maximum α . As in Fig 3.3, the topmost line represents the same example as Fig 3.2, with each subsequent line below representative of an gradual increase in the loop impedance between the cluster and the source. In matrix terms, this amounts to a $R_{ii} + 2z = R_{ii} + 2 \times 0.2$ increment when compared with the line immediately above. 24
- 3.7 Global Horizontal Irradiation values for Continental Portugal. Source: Solargis, GHI Solar Map © 2015. 27
- 3.8 $[P, Q]$ plane representation of the maximum apparent power S_M (green semi-circumference) and the operational area of a generator (light green area), assuming $S_M \leq P_A$. (a), (b) and (c) denote the restrictions imposed on the system by the armature current, the field current, and the end region heating limit, respectively. Yellow areas represent the zones within S_M where the injected power violates the last two provisions. We opted to define S_M towards the rated VA as that limit will be more pertinent for cases of voltage spikes. 28

- 3.9 $[P, Q]$ plane hypothetical representations of (27), assuming that $p_{f2} \leq P_A$ for demonstrative purposes. The highlighted blue line segment contains all the possible solutions for active and reactive power. Two scenarios are shown; in the first the leftmost abscissa is positive while in the second its null due to the set restrictions. In a situation where (26) is equal to zero, (27) will be tangent to the semi-circumference. 30
- 3.10 $[P, Q]$ plane hypothetical representations of the possible applications of the inherent properties of (27). In the leftmost, we see how the system would handle an unexpected drop in available active power P_A , and in the rightmost how it would fix the power coordinates to a specific $PF = \cos(\theta)$. In both cases, the network's voltage profile would remain unchanged despite the variation in the injected active and reactive power. 31
- 3.11 Examples of possible power coordinates solution sets in a $[P, Q]$ plane, with each hypothetical line corresponding to a specific voltage profile, and (2) and (3) defining the generator's operational range. 31
- 3.12 $[P, Q]$ plane hypothetical representations the logical steps taken by the controller when correcting an instance of nodal voltage deviation, when using the S_M bounded strategy. Green vertical arrows represent $Q(V)$, purple horizontal arrows $P(V)$ and the red line the solution set of values per (27). 33
- 3.13 $[P, Q]$ plane hypothetical representations the logical steps taken by the controller when correcting an instance of nodal voltage deviation, when using an the foresight strategy. Green vertical arrows represent $Q(V)$, purple horizontal arrows $P(V)$ and the red line the solution set of values per (27). 34

Chapter 4

- 4.1-4.2 Evolution of the state variable error for the evenly-distributed per phase study model 1, with $[k] = 0.95[k_{osc}]$ (left) and $[k] = 1.95[k_{osc}]$ (right), up to twenty iterations. 38
- 4.3-4.4 Evolution of the state variable error for the evenly-distributed per phase study model 2, with $[k] = 0.95[k_{osc}]$ (left) and $[k] = 1.95[k_{osc}]$ (right), up to twenty iterations. 39
- 4.5-4.6 Evolution of the state variable error for the evenly-distributed per phase study model 3, with $[k] = 0.95[k_{osc}]$ (left) and $[k] = 1.95[k_{osc}]$ (right), up to twenty iterations. 39
- 4.7-4.8 Evolution of the state variable error for the evenly-distributed per phase study model 4, with $[k] = 0.95[k_{osc}]$ (left) and $[k] = 1.95[k_{osc}]$ (right), up to twenty iterations. 40
- 4.9-4.10 Evolution of the state variable error for the evenly-distributed per phase study model 5, with $[k] = 0.95[k_{osc}]$ (left) and $[k] = 1.95[k_{osc}]$ (right), up to twenty iterations. 40
- 4.11-4.12 Evolution of the state variable error for the evenly-distributed per phase study model 6, with $[k] = 0.95[k_{osc}]$ (left) and $[k] = 1.95[k_{osc}]$ (right), up to twenty iterations. 41
- 4.13-4.14 Evolution of the state variable error for the unevenly-distributed per phase study model 7, with $[k] = 0.95[k_{osc}]$ (left) and $[k] = 1.95[k_{osc}]$ (right), up to twenty iterations. 42
- 4.15-4.16 Evolution of the state variable error for the unevenly-distributed per phase study model 8, with $[k] = 0.95[k_{osc}]$ (left) and $[k] = 1.95[k_{osc}]$ (right), up to twenty iterations. 42
- 4.17-4.18 Evolution of the state variable error for the unevenly-distributed per phase study model 9, with $[k] = 0.95[k_{osc}]$ (left) and $[k] = 1.95[k_{osc}]$ (right), up to twenty iterations. 43
- 4.19-4.20 Evolution of the state variable error for the unevenly-distributed per phase study model 10, with $[k] = 0.95[k_{osc}]$ (left) and $[k] = 1.95[k_{osc}]$ (right), up to twenty iterations. 43
- 4.21-4.22 Evolution of the state variable error for the unevenly-distributed per phase study model 11, with $[k] = 0.95[k_{osc}]$ (left) and $[k] = 1.95[k_{osc}]$ (right), up to twenty iterations. 44

4.23-4.24	<i>Evolution of the state variable error for the unevenly-distributed per phase study model 12, with $[k] = 0.95[k_{osc}]$ (left) and $[k] = 1.95[k_{osc}]$ (right), up to twenty iterations.</i>	44
4.25-4.26	<i>Evolution of the state variable error for the unevenly-distributed per phase study model 13, with $[k] = 0.95[k_{osc}]$ (left) and $[k] = 1.95[k_{osc}]$ (right), up to twenty iterations.</i>	45
4.27-4.28	<i>Evolution of the state variable error for the unevenly-distributed per phase study model 14, with $[k] = 0.95[k_{osc}]$ (left) and $[k] = 1.95[k_{osc}]$ (right), up to twenty iterations.</i>	45
4.29-4.30	<i>Evolution of the control variables for the studied models 1 and 2, with $[k] = 1.5[k_{osc}]$, up to a hundred iterations.</i>	48
4.31-4.34	<i>Evolution of the control variables for the studied models 3 through 6, with $[k] = 1.5[k_{osc}]$, up to a hundred iterations.</i>	49
4.35-4.38	<i>Evolution of the control variables for the studied models 7 through 10, with $[k] = 1.5[k_{osc}]$, up to a hundred iterations.</i>	50
4.39-4.42	<i>Evolution of the control variables for the studied models 11 through 14, with $[k] = 1.5[k_{osc}]$, up to a hundred iterations.</i>	51
4.43	<i>[P, Q] plane hypothetical representations the logical steps taken by the controller when applying the abovementioned function, represented by the dashed yellow arrow. The dotted red line represents the $-x \text{ or }^{-1}$ slope line. Note that both purple arrows, depicting the active power shift, have the same length.</i>	53

Chapter 5

5.1	<i>Evolution of the state variable error with 6 DERs, for $\alpha = 0.3$, with the same initial values as the ones listed in Table XIV.</i>	58
5.2	<i>Evolution of the state variable error with 7 DERs, for $\alpha = 0.3$, with the same initial values as the ones listed in Table XIV.</i>	59
5.3	<i>General representation of the relation between the power gain and lag, and the shift created by the "reduction" of [A]. Notice how the lowest point in both curves is closer to their respective stability limit $[k_{stb}]$ rather than $[k_{osc}] = 0.5[k_{stb}]$, which is the case for most scenarios involving unbalanced DG through RST.</i>	60
5.4	<i>Evolution of the Maximum Common Gain Factor for Study Model 6 in function of the line impedance coefficient x.</i>	62
5.5	<i>Evolution of the Maximum Common Gain Factor for Study Model 6 in function of the line impedance coefficient x (quadratic variant).</i>	63
5.6	<i>Evolution of the R_{11}/R_{22} and R_{22}/R_{33} ratios in function of the line impedance coefficient x: left \rightarrow linear increment (Fig 5.4), right \rightarrow quadratic increment (Fig 5.5). The major difference between the two cases lies in that the R_{22}/R_{33} ratio plateaus just above 0.5 in the first case, indicating that $A_{23}(x \rightarrow \infty) = -0.25\alpha$, while in the latter it decays towards zero as x increases, similar to R_{11}/R_{22}.</i>	64
5.7	<i>Comparison between the two different spacing methods. As stated, the bottom bus distribution results in a higher Maximum Common Gain Factor α, though the distance between generating busses (1) and (4) remains unaltered for both cases.</i>	64
5.8	<i>Evolution of the Maximum Common Gain Factor for a full 3bus-by-3phase node grid (9 DERs) in function of the line impedance coefficient x, for both spacing variants.</i>	65

Chapter 6

- 6.1 *Variation of the lag over a hundred simulations as a result of the extra term with a random value between -1% and $+1\%$ of $(V^0 - V^*)$, for study model 6 (left) and the full grid scenario in Chapter 5 (right). The dotted lines represent their values without these fluctuations, and the red ones stand for the average lag.* 66
- 6.2 *Demonstrative example of an integral voltage error correction over a period of time. The algorithm will act upon the voltage difference only when the darkened integral area surpasses a set limit A_X .* 68
- 6.3 *Hypothetical voltage error curve, and its respective means taken from the entire area and sampled from the dashed demarcation. The latter, as we can see, is closer to the error at the endmost, and thus more adequate for the controller to use as a basis for the consequent power shift.* 68
- 6.4-6.5 *Evolution of the state variable error for a continuous system, for study model 1, employing integration of the voltage error area, during a one second interval, with $\alpha = 1$.* 69
- 6.6-6.7 *Evolution of the state variable error for a continuous system, for study model 6, employing integration of the voltage error area, during a one second interval, with $\alpha = 1$.* 70
- 6.8-6.9 *Evolution of the state variable error for a continuous system, for study model 9, employing integration of the voltage error area, during a one second interval, with $\alpha = 1$.* 70
- 6.10-6.11 *Evolution of the state variable error for a continuous system, for study model 14, employing integration of the voltage error area, during a one second interval, with $\alpha = 1$.* 71
- 6.13-6.14 *Evolution of the state variable error for a continuous system, for study model 1, employing integration of the voltage error area and dynamic sampling, during a one second interval, with $\alpha = 1$.* 73
- 6.15-6.16 *Evolution of the state variable error for a continuous system, for study model 6, employing integration of the voltage error area and dynamic sampling, during a one second interval, with $\alpha = 1$.* 74
- 6.17-6.18 *Evolution of the state variable error for a continuous system, for study model 9, employing integration of the voltage error area and dynamic sampling, during a one second interval, with $\alpha = 1$.* 74
- 6.19-6.20 *Evolution of the state variable error for a continuous system, for study model 14, employing integration of the voltage error area and dynamic sampling, during a one second interval, with $\alpha = 1$.* 75
- 6.21-6.22 *Evolution of the state variable error in a full grid (9 DERs), following the same setup as the previous eight figures. Each color stands for one of the nine DERs connected to the feeder grid.* 76

List of Equations

- (1) $V_{0G} = V_0 - V_G \approx \frac{R \cdot P_N + X \cdot Q_N}{V_G}$ 6
- (2) $V_{0G} \approx R \cdot P_N + X \cdot Q_N$ 6
- (3) $\Delta V_{0G} \approx -R \cdot \Delta P_G - X \cdot \Delta Q_G$ 6
- (4) $\Delta V_G = -\Delta V_{0G} \approx R \cdot \Delta P_G + X \cdot \Delta Q_G$ 6
- (5) $R_{ij} = \begin{cases} R_{0i\cap 0j}^p + R_{0i\cap 0j}^N & \text{if } i \text{ and } j \text{ are in phase } (p) \\ -1/2 R_{0i\cap 0j}^N & \text{otherwise} \end{cases}$ 7
- (6) $R_{ij} = \begin{cases} R_{ij}^{el} & \text{if } i \text{ and } j \text{ are in phase } (p) \\ -1/4 R_{ij}^{el} & \text{otherwise} \end{cases}$ 7
- (7) $\Delta V_i^p \approx \begin{cases} R_{ij}^{el} (\Delta P_{jG} + x^{or} \Delta Q_{jG}) & \text{if } i \text{ and } j \text{ are in phase } (p) \\ -1/4 R_{ij}^{el} (\Delta P_{jG} + x^{or} \Delta Q_{jG}) & \text{otherwise} \end{cases}$ 7
- (8) $[\Delta V] = [R]([\Delta P_G] + x^{or} [\Delta Q_G])$ 8
- (9.1) $p^{k+1} = p^k + [k_p](V^* - V^k)$ 13
- (9.2) $q^{k+1} = q^k + [k_Q](V^* - V^k)$ 13
- (10) $V^{k+1} = V^k + [R]((p^{k+1} - p^k) + x^{or}(q^{k+1} - q^k))$ 13
- (11) $V^{k+1} = ([I] - [R][k])V^k + ([R][k])V^*$ 13
- (12) $[A] = [I] - [R][k]$ 14
- (13) $[A] - \lambda[I] = \begin{bmatrix} 1 - k_1 R_{11} - \lambda & -k_2 R_{12} & -k_3 R_{13} \\ -k_1 R_{12} & 1 - k_2 R_{22} - \lambda & -k_3 R_{23} \\ -k_1 R_{13} & -k_2 R_{23} & 1 - k_3 R_{33} - \lambda \end{bmatrix}$ 16
- (14) $\lambda^3 + a([R.k])\lambda^2 + b([R.k])\lambda + c([R.k]) = 0$ 16
- (15.1) $a([R.k]) = k_1 R_{11} + k_2 R_{22} + k_3 R_{33} - 3$ 16
- (15.2) $b([R.k]) = k_1 k_2 R_{11} R_{22} + k_1 k_3 R_{11} R_{33} + k_2 k_3 R_{22} R_{33} - k_1 k_2 R_{12}^2 - k_1 k_3 R_{13}^2 - k_2 k_3 R_{23}^2 - 2a([R.k]) - 3$ 16
- (15.3) $c([R.k]) = k_1 k_2 k_3 (R_{11} R_{22} R_{33} + 2R_{12} R_{13} R_{23} - R_{11} R_{23}^2 - R_{22} R_{13}^2 - R_{33} R_{12}^2) + a([R.k]) - b([R.k]) - 1$ 16
- (16) $\lambda^3 + (a_1 + \alpha a_2([R.K]))\lambda^2 + (b_1 + \alpha b_2([R.K]) + \alpha^2 b_3([R.K]))\lambda + (c_1 + \alpha c_2([R.K]) + \alpha^2 c_3([R.K]) + \alpha^3 c_4([R.K])) = 0$ 16
- (17) $\prod_{i=1}^n (\lambda_i - \Delta_i([R.K]) \alpha - B_i) = 0$ 17
- (18) $\Delta^3 + a_\Delta([R.K])\Delta^2 + b_\Delta([R.K])\Delta + c_\Delta([R.K]) = 0$ 17

$$(19.1) \quad a_{\Delta}([R, K]) = K_1 R_{11} + K_2 R_{22} + K_3 R_{33} \quad 17$$

$$(19.2) \quad b_{\Delta}([R, K]) = K_1 K_2 R_{11} R_{22} + K_1 K_3 R_{11} R_{33} + K_2 K_3 R_{22} R_{33} - K_1 K_2 R_{12}^2 - K_1 K_3 R_{13}^2 - K_2 K_3 R_{23}^2 \quad 17$$

$$(19.3) \quad c_{\Delta}([R, K]) = K_1 K_2 K_3 (R_{11} R_{22} R_{33} + 2R_{12} R_{13} R_{23} - R_{11} R_{23}^2 - R_{22} R_{13}^2 - R_{33} R_{12}^2) \quad 17$$

$$(20) \quad [k_{stb}] = \frac{2}{\text{Max}|\Delta_i([R, K])|} [K] \quad 17$$

$$(21) \quad [A] = \begin{bmatrix} 1 & 0 & R_{1i} k_{ii} & 0 & 0 \\ 0 & 1 & \vdots & 0 & 0 \\ 0 & 0 & (1 - R_{ii} k_{ii}) & 0 & 0 \\ 0 & 0 & \vdots & 1 & 0 \\ 0 & 0 & R_{ni} k_{ii} & 0 & 1 \end{bmatrix} \quad 25$$

$$(22) \quad S_M^2 \geq P_G^2 + Q_G^2 \quad 28$$

$$(23) \quad V^* = V^0 + [R]((p_f - p^0) + x \circ r (q_f - q^0)) \quad 29$$

$$(24) \quad C_0 = ([R]^{-1}(V^* - V^0) + p^0) x \circ r^{-1} + q^0 \quad 29$$

$$(25) \quad p_f = \frac{C_0 x \circ r^{-1} \mp \sqrt{(1 + x \circ r^{-2}) S_M^2 - C_0^2}}{(1 + x \circ r^{-2})} \quad 29$$

$$(26) \quad \left[\sqrt{(1 + x \circ r^2) S_M} - |[R]^{-1}(V^* - V^0) + p^0 + x \circ r q^0| \right]_i \geq 0 \quad 29$$

$$(27) \quad q_f(p_f) = C_0 - x \circ r^{-1} p_f \quad 30$$

$$(28) \quad S_M x \circ r^{-1} (1 + x \circ r^2)^{1/2} \geq [C_0]_i \geq -S_M \quad 32$$

List of Tables

I	Evenly Distributed per Phase Models	10
II	Unevenly Distributed per Phase Models	11
III	Logical Steps of a Voltage Dependent $Q(V)/P(V)$ Power Controller	12
IV	Eigenvalues and Error Behavior for each Study Model with Unitary Gain	14
V	Eigenvalue Gradients and Maximum Allowed Power Gains with $[k] = \alpha[I]$	19
VI	Eigenvalue Gradients and Maximum Allowed Power Gains with $[k] = \alpha[R_I]$	23
VII	Logical Steps of a Voltage Dependent Alternating $Q(V)/P(V)$ Power Controller with $Q(V)$ precedence – Bounded	33
VIII	Logical Steps of a Voltage Dependent Alternating $Q(V)/P(V)$ Power Controller with $Q(V)$ precedence – Foresight	34
IX	Initial Voltage Values for Evenly Distributed per Phase Models	37
X	Initial Voltage Values for Unevenly Distributed per Phase Models	37
XI	Optimal Gains for Evenly Distributed per Phase Models	46
XII	Optimal Gains for Unevenly Distributed per Phase Models	46
XIII	Maximum Eigenvalue Gradient and respective Common Gain Factor	55
XIV	Initial Values for Nodal Voltage and subsequent System Performance	55

Nomenclature

DG	distributed generation
LV	low-voltage
DER	distributed energy resource
DNO	distributed network operator
PV	photovoltaic
RST, N	network phases, neutral
V^0	initial nodal voltage
V_G	generated voltage
V^*	voltage set-point
ΔV	voltage error
Q_G, P_G	generated reactive, active power
q^0, p^0	initial reactive, active injected power
q_f, p_f	final (post-correction) reactive, active injected power
S_M	maximum apparent power
P_A	available active power
z	bus-to-bus line impedance
$x \circ r$	network's internodal line reactance-to-resistance ratio
$[R]$	reduced resistance matrix
C_0	initial conditions variable
$[R_I]$	inverse diagonal resistance matrix
$Q(V), P(V)$	voltage dependent reactive, active power controller
PF	power factor
k_Q, k_P	controller reactive, active power gain
$[k]$	overall gain matrix
α	common gain factor
$[K]$	controller specific power gain
$[A]$	iteration coefficient matrix
$\lambda(A)$	eigenvalues of the iteration coefficient matrix
Δ	eigenvalue gradient
$[k_{stb}]$	instable behavior threshold overall gain matrix
$[k_{osc}]$	oscillatory behavior threshold overall gain matrix
A_x	voltage error area set-point

Chapter 1

Introduction

1.1 State-of-the-art and Motivation

Microgeneration, defined as local small-scale production of renewable electric power by traditional consumers as to achieve energetic self-sufficiency and/or to sell it back to the Distribution Network Operator (DNO), has been steadily rising in prominence over the past two decades. And, in light of the present-day tendency towards achieving a sustainable development, it is reasonable to expect that it will continue to expand over the foreseeable future, particularly in developed countries as an integral cornerstone of a larger energetic sustainability model [1]-[3]. The advent of smaller and, perhaps most importantly, affordable photovoltaic (PV) panels, as a direct outcome of an expanding and ever-evolving manufacture process of PV components [4], has resulted in the considerable growth of scaled-down generation sites located downstream in the low-voltage (LV) electric network. This trend has raised several pressing concerns within the pertaining academia seeing that most of the current distribution network's infrastructure wasn't originally conceived to have a large number of distributed generation (DG) clusters connected to it [5]. Naturally, this issue becomes tied to the notion of a grid's hosting capacity: the limit of Distributed Energy Resource (DER) penetration under which a power system can effectively operate, expounded in [6].

The primary matter of contention is related to the phenomenon of voltage rise, which can be observed in distribution networks, where the reactance-to-resistance ratio is small (such as is the case with LV), with a significant number of installed DERs [7]. This unwanted deviation in the network's voltage profile comes as a consequence of the inversion of the regular power flow, caused by the substantial injection of active power into the grid by the connected DG. As the name implies, in addition to causing an unbalance in the grid's nodal voltage values, these occurrences will often also raise their values past their safety limits. The network's functionality as a whole can thus be compromised, and perhaps even paralyzed in a worst case scenario. Compounding the issue further, due to the decentralized nature of production, the load distribution throughout the LV networks (typically three-phased in Europe) will invariably be unbalanced owing to the inherently single-phase characteristics of the DG elements. In such circumstances, a corrective voltage reduction in one phase will result in a proportional increase in the remaining two phases' nodes, which in turn may cause them to go over the limit, thus perpetuating the problem [8]. It's this issue of voltage cascading that will further exacerbate the negative impact of the previously mentioned instances of voltage rise, and will be and will be at the core of the matter when designing a control strategy for the DG system.

In order to avoid these situations, it has been proposed, and extensively researched as in [9]-[11], that the each individual nodal voltage be regulated directly by the DNO. The company would monitor the entire grid around-the-clock, compiling the gathered data and using it to ensure that its voltage profile remains stabilized, issuing remote orders to all of the individual power controllers, which regulate the power injected by each DER. This is referred to as a centralized control strategy. Adopting such approach would allow for a maximization of a network's overall hosting capacity, while at the same time ensuring a fairer distribution of the incurred burden, spreading it as evenly as possible throughout its users. However, such degree of control is too heavily reliant on intra-network communications, making it less than optimal given the ever-present possibility of disruptions and/or delays in said links. Moreover, the sheer scale of the existing (and projected) DG makes this method considerably difficult and costly to implement due to the amount of supplementary equipment that is required for its proper execution. Ultimately, the hefty price associated with such investment would be passed on to the micro-producers, making it economically unappealing to both them and the PV manufacturers.

On account of the aforementioned disadvantages, distributed (i.e. decentralized) voltage control strategies have been gaining prominence as a more practical alternative to the above method [12]-[14]. Their general aim is to have the injected active and reactive power in each of the generating nodes regulated in an autonomous manner, based solely on the observed nodal voltage, by a local power controller, without any (or at times minimal) input from an outside source, be it the DNO or the remaining DERs. In essence, each individual controller would be responsible for keeping the voltage of its respective node fixed at a certain preset value, automatically increasing or decreasing the power injected to the grid to counterbalance any detected deviations. Theoretically, this self-dependency would reduce the impact DG has on any feeder network's voltage profile to a virtual non-issue, thus keeping it largely undisturbed. Couple that with a dispensable study of the network's intricate topological details and a more cost-competitive investment in infrastructure, makes this approach all the more ideal for the often poorly characterized LV grids and in the face of rapidly expanding number of DG installations.

However, despite its many benefits (enumerated and otherwise), adopting a fully decentralized voltage control stratagem poses its significant share of underlying drawbacks, of which there's been a somewhat startling lack of effort to address. The most egregious of all pertains to stability of a distribution network's voltage profile, which cannot be wholly guaranteed without any sort of master controller to oversee the control system's operation. Examples due a lack thereof, ranging from voltage oscillation to outright crippling spikes and/or drops in grid's nodes, have already been documented [15]. Beyond the absence of a supervising mechanism, we can conjecture that the above-mentioned phenomenon of voltage rise is the main contributor for these occurrences, alongside the unbalanced load conditions throughout the grid and limitations inherent to the controllers' electronics.

Overall, there seems to be a worrying underestimation of just how the entire autonomous control process is influenced by the number and distribution of the DERs, and how it affects the calculated power flow solution. And, as a consequence, how small variations in the grid's scheme, be it the inclusion/removal or simply altering a generator's position, can yield vastly different results in terms of initial voltage deviation, error behavior and final values for the injected power. Finally, there's also the ubiquitous environmental factor and the various physical limits of the pertinent electrical equipment to take into account, which will inevitably place further constraints relating to the generators' power output.

1.2 Objective and Structure

The scope of this work is thus to properly identify and then expound on these inherent concerns lying at the heart of a fully decentralized voltage control scheme, that chiefly arise as a consequence of voltage rise occurrences in downstream distribution networks with concentrated DG. In particular, we aim to demonstrate the large degree of fallibility in an autonomous control system when it comes to its stability, that is its ability to correct any deviation from the voltage profile set-point, when pressed by the myriad of factors that affect a feeder network. Concurrently, we'll also strive to propose and properly test an adequate theoretical voltage control scheme, as part of a wider strategy to consign micro-producers as voltage regulators, that can (at least partially) counteract these flaws.

We'll start in **Chapter 2** by defining a suitable model for a LV network to use as our base, as well as an array of study cases derived from it. Employing then a basic voltage control algorithm, we'll study the problems that may arise during its operational period, gradually building a more robust system for the controllers, to lessen the encountered issues. As stated before, ensuring that the control algorithm remains stable stands as the most pressing drawback of a fully decentralized control scheme. Our main focus in the following chapters will hence fall upon determining and analyzing the convergence of the evaluated control algorithm, as its iterative nature can compromise the convergence of its state variable (i.e. the nodal voltage) to its predefined set-point.

It's through delineating the system's tipping-point, relating to its stability, that in **Chapter 3** we'll be able to then compare the different methodologies that can be employed for the controllers power gains. Properly defining these values becomes critical in this context, as they'll will greatly influence the behavior of the voltage error, and thus the convergence of the state variable and performance (i.e. speed) of the system's operation. Beyond stability, we'll also define the restrictions on injected power, inherent to the physical attributes of a DER. While these won't affect the algorithm's convergence, their presence necessitates a reevaluation nonetheless, so that a generator can properly operate within its defined operational area.

Beyond theoretical assessments, **Chapter 4** is dedicated to testing the system's behavior and performance with the aforementioned conditioning, via computer simulations run through MATLAB. These trials will focus primarily on analyzing its speed and the final obtained values for the injected power, as a means to corroborate the previously exposed hypotheses.

After running through the base criteria and testing phase, **Chapter 5** expands upon the original network, in an effort to shift from ideal conditions towards more realistic ones, to demonstrate how the controllers' performance changes (or, in this specific case, deteriorates). The two main focus will be on the concentration and dispersion of DG. The former concerns the inclusion of more generators onto the same 3bus-by-3phase grid, and how these inclusions adversely affect both stability, performance, and the initial voltage error. The latter relates to the distancing of the generating busses, by increasing the in-between line impedance, and how it can be used to better isolate DG clusters from another, thus enhancing the overall system robustness.

The study will conclude in **Chapter 6** with a concise examination into a time-based voltage error integration method as a possible alternative to the discrete iterative algorithm presented up until that point. The motivation for this stems from the inclusion of voltage fluctuations in the generating nodes, that greatly disturb the system's operation, exacerbating its performance issues. To counteract these inconsistencies, rather than a constant operation, the controller will only act upon a voltage deviation when the integral error area surpasses a certain set-point, then basing the corrective power shift on its average.

By the point we reach our conclusions, we hope that we'll be able to provide a better understanding of the underlying issues that plague a fully decentralized voltage control scheme, while contributing with a viable voltage regulation strategy for micro-producers, as was originally requested of this work.

Chapter 2

Decentralized System Modeling

2.1 Low-Voltage Network Outline

First and foremost, for us to elaborate on the possible methods for voltage control in downstream LV networks, it's necessary to assemble a suitable model of a basic feeder network under unbalanced load and generation conditions. All arranged so that we can use it to simulate the behavior of the different state and control variables involved. To study the voltage variation resultant from DER injections, the typical methodology dictates the compilation of the nodal admittance matrix and Thévenin impedances, which in turn are necessary to calculate the power flow. To compose the former, it becomes essential to know all of the intricate details of the feeder network, such as its overall configuration, arrangement and characteristics of every single wire that composes it. Given the sheer complexity and scope of the involved LV networks, this analysis naturally comes off as a highly impractical for any intended examination of the voltage variation, this one included.

2.1.1 Reduced Circuit Characterization

A more viable alternative is therefore preferable. As it's more thoroughly delineated in [6], a substitute impedance matrix can be built based solely on the network's nodes that are connected to a DER, and consequently much more pertinent to our interest. Not only is the resulting proxy vastly more simplified than its counterpart, this reduced circuit characterization is based on a simplistic topological inspection of a standard three-phased (plus neutral) feeder network and the cables ohmic characteristics, making it less information demanding. Such impedance matrix encloses sufficient information to analyze voltage control algorithms as it represents the sensitivities of nodal voltages with regard to power injections [8].

Before tackling the four-wire case, however, we'll first take a look at the hypothetical example presented below.

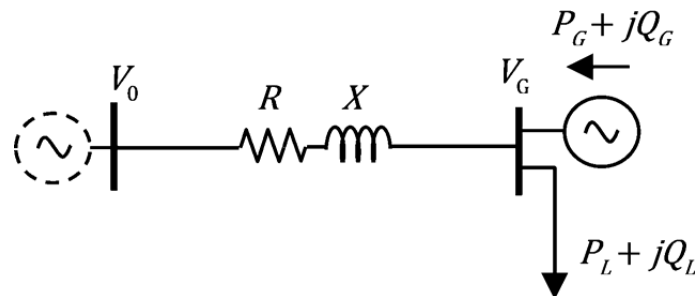


Fig. 2.1 Single line model of a feeder network with a load and a DER.

Calculating the approximate voltage drop V_{0G} in the line between bus V_0 and V_G in Fig. 2.1, with $P_N = P_L - P_G$ and $Q_N = Q_L - Q_G$ representing respectively the net real and reactive power associated with the DER generator, we arrive at the expression:

$$V_{0G} = V_0 - V_G \approx \frac{R \cdot P_N + X \cdot Q_N}{V_G} \quad (1)$$

Considering the latter's voltage value as unitary (in *per unit*), we attain:

$$V_{0G} \approx R \cdot P_N + X \cdot Q_N \quad (2)$$

If one then assumes that the load at each generating node remains more or less equal, and by applying the principal of linearity in (2), a subsequent voltage drop increase or decrease will be the result solely of the variation in the DER's injected power. Therefore:

$$\Delta V_{0G} \approx -R \cdot \Delta P_G - X \cdot \Delta Q_G \quad (3)$$

Going back to (1), assuming that the voltage at the source bus V_0 remains constant, we can conclude:

$$\Delta V_G = -\Delta V_{0G} \approx R \cdot \Delta P_G + X \cdot \Delta Q_G \quad (4)$$

Expanding now (4) to a three-phase (R,S,T) plus neutral (N) system, the proxy impedance matrix will be equal to $[z] = [R] + j[X]$ or, if the network's internodal line reactance-to-resistance ratio $x \circ r$ is constant throughout its entirety, further simplified to $[z] = [R](1 + j x \circ r)$.

As a result, $[R]$ will have the same n -by- n dimensions, with n being the number of connected DER generators, and the remaining terms become n -length vectors representing the voltage and injected power at each generating node. The diagonal terms of $[R]$ express the total upstream resistance seen by each DER, that is to say, the sum of both the source-to-node i through p resistance R_{0i}^p and the node-to-source through the neutral N resistance R_{0i}^N . Moreover, the non-diagonal terms of the matrix are representative of the influence a variation of the injected power in one of the nodes will have on the voltage of its remaining counterparts, and are affected not only by the distance to the source but also the grid configuration itself. Fig 2.2 showcases an illustrative example of the effect of an induced voltage rise ΔV^{RN} has on both phase R and its propagating effect on phase T ΔV^{TN} .

As shown below, the phasorial sum of V^{TN} with the orthogonal projection of the neutral voltage rise $R_{0i}^N \Delta P_{iG}$ in phase R, results in an overall drop of the amplitude in T. As the expression of the new voltage is indicative of, this phenomenon results from the mutually shared neutral resistance R_{0i}^N between the two phases, assuming in this case that both are equally distant to the source 0. Further supposing, that the neutral currents are all delayed and advanced by 120° degrees in relation to one another and in-phase with their respective line-to-neutral voltages, we can estimate that $\Delta V^{TN} = 0.5 R_{0i}^N \cdot \Delta P_{iG}$.

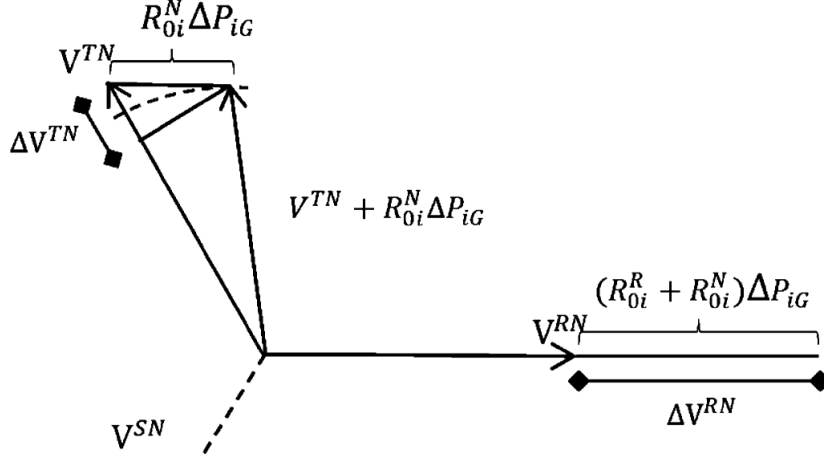


Fig. 2.2 Figurative example of a voltage rise in phase R, ΔV^{RN} , and the resulting voltage drop in phase T, ΔV^{TN} , induced by an active power injection change, ΔP_{iG} .

Applying this assumption to a feeder network with a n -number of DERs, each single one possibly connected to different phases and with varying distances to the source, we can write the terms of the resistance matrix $[R]$ as:

$$R_{ij} = \begin{cases} R_{0i0j}^p + R_{0i0j}^N & \text{if } i \text{ and } j \text{ are in phase } (p) \\ -1/2 R_{0i0j}^N & \text{otherwise} \end{cases} \quad (5)$$

where R_{0i0j} denotes what is known as the common-path resistance between i and j which, as the name implies, refers to the overlapping source-to-node resistance seen by the two generating nodes, both through p and N . Going further as to consider that the cable impedance between two buses of the grid, connected or otherwise, is always the same in both the three phases and the neutral, (5) can be simplified into:

$$R_{ij} = \begin{cases} R_{ij}^{el} & \text{if } i \text{ and } j \text{ are in phase } (p) \\ -1/4 R_{ij}^{el} & \text{otherwise} \end{cases} \quad (6)$$

where R_{ij}^{el} stands for the *smallest* loop resistance between i and j , in other words whichever $R_{0i}^p + R_{0i}^N$ and $R_{0j}^p + R_{0j}^N$ is the smallest of the two. Combining (4) and (6), we lastly arrive at the general expression for a feeder network's phase-to-neutral voltage profile variation at a generating node i , when subjected to alterations in the injected power in a node j :

$$\Delta V_i^p \approx \begin{cases} R_{ij}^{el} (\Delta P_{jG} + x^{or} \Delta Q_{jG}) & \text{if } i \text{ and } j \text{ are in phase } (p) \\ -1/4 R_{ij}^{el} (\Delta P_{jG} + x^{or} \Delta Q_{jG}) & \text{otherwise} \end{cases} \quad (7)$$

or expanded in matrix form to take in account simultaneous fluctuations in the DER injection:

$$[\Delta V] = [R](\Delta P_G + x_{or} \Delta Q_G) \quad (8)$$

With the intent to verify the relative accuracy of the proposed approximation, several tests were conducted, comparing the theoretical model resistance matrix with that obtained in practice through power-flow study, using a several grid configurations and loading situations. Results show that for light loads, both active and reactive, and purely resistive cables, the error for the taken approach is in the magnitude of 1%, well within what could be considered a satisfactory margin. As the reactance-to-resistance ratio rises, this error increases as expected, reaching the order of 10% with a $x_{or} = 0.5$, and nearly to 20% with a heavier load. However, given that that the scope of this work chiefly concerns itself with issues occurring at low voltage networks, where the x_{or} is small, and at periods where the overall DER load is relatively light, we can surmise that the proposed reduced circuit characterization is more than appropriate for usage in any follow-up calculations and simulations for the remainder of this study.

2.1.2 Study Models

Having acquired a method to construct a resistance matrix, serving as a stand-in for the impedance $[z]$ seeing as $[z] = [R](1 + jx\omega r)$, out of a simplified analysis of any given four-wire feeder network, we now need to define a spectrum of exemplary grid models to be subjected for review. These study cases will serve to illustrate a broad range of situations that can potentially be found in any typical LV network with DG, allowing for a more comprehensive assessment of the evolution of their voltage profile based on the variation of the injected power. Perhaps more important, it will be the comparison between the different configurations that will be illustrative of the sensitivity inherent to integration of DERs so far downstream, especially when it comes to the effects of an unbalanced load. This examination will demonstrate how fragile these systems' stability can be, based on the positioning of the generators and the characteristics of the electrical cables alone, and how the simple act of moving a single generator can be potentially compromising. Ultimately, it'll also aid us in building a robust model for a distributed control solution to mitigate the innate problems that arise with the high concentration of DG clusters and the subsequent inversion of the power flow, and draw conclusions about its limitations.

Firstly, we will characterize the LV test feeder, in this case a standard four-wire circuit with five busses (including the source), as seen below in Fig 2.3. To simplify future calculations, and in line with the reduced circuit characterization we've chosen to employ, the cable impedance between two nodes is considered equal throughout the entire network, as is the reactance-to-resistance ratio. For trialing purposes, three DER generators will be connected to this grid, spread throughout the three most downstream busses in a number of possible arrangements, to simulate the effects an unbalanced load will have on the overall evolution of the voltage profile at their nodes. With this archetype, we can provide a reasonable theoretical evaluation on the behavior of the nodal voltage under single-phase distributed generation, particularly on the effects of voltage rise which will then factor in the development of a decentralized control system. Moreover, it provides a basis that can be further expanded upon with the insertion of more DERs and/or busses.

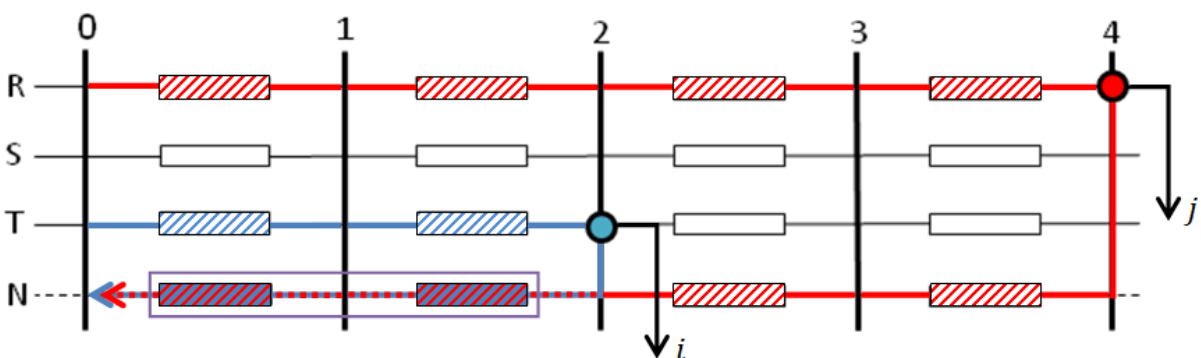


Fig. 2.3 Four-wired LV test circuit used as a foundation for the study on DER injection. We can notice two generators (blue and red), and how their loop resistances R_{ii}^{el} and R_{jj}^{el} are obtained. Additionally, we can also see their common-path resistance (inside the purple box), from which the respective non-diagonal terms of $[R]$, in this case $-\frac{1}{4}R_{ij}^{el}$, will be derived from.

Table I and Table II provide 14 distinct cases in total, all the possible non-redundant combinations for the relative positioning to the leftmost generator in a 3bus-by-3phase grid by the remaining two, each numerated from one to fourteen. The former pertains to an equal distribution of DG through the phases, only varying the distance of each to the source, while the latter contains the remainder, where more than one generator is connected to one phase. These will be used as the fundamental examples from which we'll to draw our main conclusions, ranging from its effects on stability to the behavior of in autonomous voltage control. A simplified diagram of the test feeder circuit is displayed in the second column, representing busses 2, 3 and 4 from Fig. 2.3, illustrating the position of the three DERs for each test model. The rightmost section contain the resulting resistance matrix for the feeder's configuration, assuming an internodal impedance of $0.2 p.u.$, for a $100 kVA$ and a $400 V$ base, which will figure predominantly in the coming simulations. These matrixes are arranged so that their diagonal terms are ordered from lowest, corresponding to the generator closest to the source, to highest, corresponding to the farthest.

Table I
Evenly Distributed per Phase Models

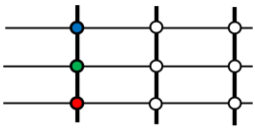
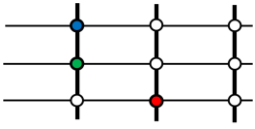
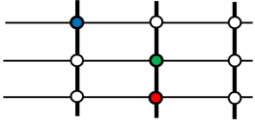



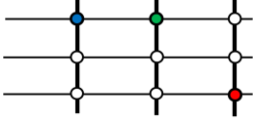
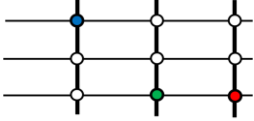
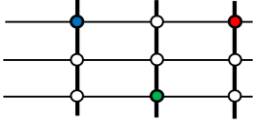
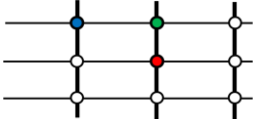
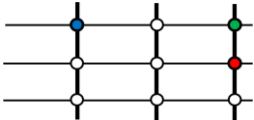
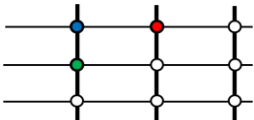
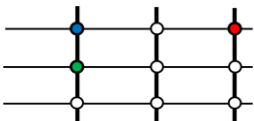
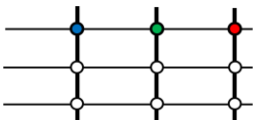
Model #	DER Grid Configuration	Resulting $[R]$ matrix
1		$R_1 = \begin{bmatrix} 0.8 & -0.2 & -0.2 \\ -0.2 & 0.8 & -0.2 \\ -0.2 & -0.2 & 0.8 \end{bmatrix}$
2		$R_2 = \begin{bmatrix} 0.8 & -0.2 & -0.2 \\ -0.2 & 0.8 & -0.2 \\ -0.2 & -0.2 & 1.2 \end{bmatrix}$
3		$R_3 = \begin{bmatrix} 0.8 & -0.2 & -0.2 \\ -0.2 & 1.2 & -0.3 \\ -0.2 & -0.3 & 1.2 \end{bmatrix}$
4		$R_4 = \begin{bmatrix} 0.8 & -0.2 & -0.2 \\ -0.2 & 0.8 & -0.2 \\ -0.2 & -0.2 & 1.6 \end{bmatrix}$
5		$R_5 = \begin{bmatrix} 0.8 & -0.2 & -0.2 \\ -0.2 & 1.6 & -0.4 \\ -0.2 & -0.4 & 1.6 \end{bmatrix}$
6		$R_6 = \begin{bmatrix} 0.8 & -0.2 & -0.2 \\ -0.2 & 1.2 & -0.3 \\ -0.2 & -0.3 & 1.6 \end{bmatrix}$

Table II
Unevenly Distributed per Phase Models

Model #	DER Grid Configuration	Resulting [R] matrix
7		$R_7 = \begin{bmatrix} 0.8 & 0.8 & -0.2 \\ 0.8 & 1.2 & -0.3 \\ -0.2 & -0.3 & 1.6 \end{bmatrix}$
8		$R_8 = \begin{bmatrix} 0.8 & -0.2 & -0.2 \\ -0.2 & 1.2 & 1.2 \\ -0.2 & 1.2 & 1.6 \end{bmatrix}$
9		$R_9 = \begin{bmatrix} 0.8 & -0.2 & 0.8 \\ -0.2 & 1.2 & -0.3 \\ 0.8 & -0.3 & 1.6 \end{bmatrix}$
10		$R_{10} = \begin{bmatrix} 0.8 & 0.8 & -0.2 \\ 0.8 & 1.2 & -0.3 \\ -0.2 & -0.3 & 1.2 \end{bmatrix}$
11		$R_{11} = \begin{bmatrix} 0.8 & 0.8 & -0.2 \\ 0.8 & 1.6 & -0.4 \\ -0.2 & -0.4 & 1.6 \end{bmatrix}$
12		$R_{12} = \begin{bmatrix} 0.8 & -0.2 & 0.8 \\ -0.2 & 0.8 & -0.2 \\ 0.8 & -0.2 & 1.2 \end{bmatrix}$
13		$R_{13} = \begin{bmatrix} 0.8 & -0.2 & 0.8 \\ -0.2 & 0.8 & -0.2 \\ 0.8 & -0.2 & 1.6 \end{bmatrix}$
14		$R_{14} = \begin{bmatrix} 0.8 & 0.8 & 0.8 \\ 0.8 & 1.2 & 1.2 \\ 0.8 & 1.2 & 1.6 \end{bmatrix}$

For convenience's sake, and from here on out, we'll be keeping the same color mnemonic used in Tables I and II. The blue coded DER will correspond to the first line of the matrix [R], that is the closest to the source, with the red DER representing the last, i.e. the farthest, and the green DER standing in-between the two.

2.2 Decentralized Controller Logic

In response to the challenge that arises from the introduction of DG in downstream LV networks, chiefly concerning the stability of its voltage profile and the health of its various hardware components, we now move to discuss the basics of the power regulating method we are to employ. The commonly practiced solution for occurrences of overvoltage in the generating nodes, resulting from the unbalanced conditions often found in real-life scenarios, revolves around disconnecting the pertaining DER from the grid, thus reducing its voltage, as per (8). This approach is referred to as an ON/OFF or 0/1 type controller. However, we've to consider the interconnectivity between generators since, as we saw, any change in the injected power will have a propagating effect. While shutting down a DER may resolve the issue in the connecting node, such action may lead to a substantial rise in the voltage of the remaining phases, hence the negative non-diagonal terms of $[R]$, and possibly inducing another instance of overvoltage, requiring additional shutdowns. This cascading effect may lead to an overall major loss in DER power generation from the slightest violations of the set voltage boundaries. Thus a controller design hinging on a less drastic power curtailment, as a means to regulate the voltage profile, is a preferable alternative. The objective is to keep the power curtailment to a minimum, thus maximizing the available of DG, while attain a controller capable of eliminating any voltage violation.

2.2.1 Basic Voltage Control Algorithm

For these reasons, and in lieu of the conclusions arrived at back in section 2.1, our basic voltage control algorithm relies on the discrete integration of the voltage error, obtained by the difference between its current value and a previously set-point V^* . As we will want to maximize the injected active power as much as possible, this value will be $V^* = V_{max} - e_V$, in which V_{max} stands for the maximum allowed nodal voltage and e_V the safety tolerance. By employing gradual and consecutive adjustments to both the injected active and reactive power based on this error, it will be able to counteract any irregularity it detects, until the nodal voltage reaches its desired set-point. This iterative process algorithm, as [8] describes it, can be summed up as in the following table:

Table III
Logical Steps of a Voltage Dependent Q(V)/P(V) Power Controller

Step 1	Compare set-point V^* and actual voltage to obtain error $\Delta V_i = V^* - V_i$;
Step 2	Compute power-shifts ΔP_i and ΔQ_i based on ΔV_i and gains $\Delta P_i = k_p \Delta V_i$, $\Delta Q_i = k_Q \Delta V_i$;
Step 3	Update V_i based on the new values of P_i and Q_i $V_i = V^0 + [R](\Delta P_i + x_{or} \Delta Q_i)$;
Step 4	Check if $V_i \neq V^*$, \forall_i If True \rightarrow return to Step 1; Else \rightarrow stop;

Accordingly, and with (8) in mind, the control and state equations concerning Step 2 and 3 of Table III are respectively given as:

$$p^{k+1} = p^k + [k_p](V^* - V^k) \quad (9.1)$$

$$q^{k+1} = q^k + [k_q](V^* - V^k) \quad (9.2)$$

$$V^{k+1} = V^k + [R]((p^{k+1} - p^k) + x_{or}(q^{k+1} - q^k)) \quad (10)$$

where k_p and k_q represent the active and reactive power gains w.r.t. to the nodal voltage of each DER. As seen by (7), the interconnectivity of each DER generator means any form of power correction will have effects on the remainder, mathematically represented by the non-null terms for the reduced resistance matrix. In an ideal case scenario, these gains would be equal to the inverse matrix of $[R]$ and $[X]$ respectively, requiring the algorithm to run only for one iteration to correct the original error. For an autonomous local control, where DER is responsible for regulating their own voltage with local information only, the non-diagonal elements of these sensitivity matrices are null, reflecting the lack of outside input each decentralized controller has in the feeder grid.

This method is not without its setbacks. Being an iterative process, such form of control brings about several key concerns in theory alone. Chief among them, the possibility of the system being unable to properly converge due to its innate characteristics or, to a lesser degree of severity, having oscillations occurring during its process. The number of necessary iterations for the voltage to enter an acceptable range is also important, as, in a real life situation, it's in our best interest that any instances of overvoltage be corrected as swiftly as possible as to limit any risks placed on the grid's perceived quality of service. Thus, a great deal of this work will revolve around the evaluation of the system's convergence properties. That is to say, whether or not the controller is able to reach the desired value given the network configuration, its power gain and the various restrictions placed on both the state and control variables. It becomes essential then that we execute a thorough analysis of the impact each of these aspects has on the performance of the controller, as to define a suitable control strategy for the regulation of DERs in heavily clustered sections of the LV distribution network.

2.2.2 Algorithm Convergence Criteria

By combining equations (9.1), (9.2) and (10), we can surmise the voltage update formula for the local control process as:

$$V^{k+1} = ([I] - [R][k])V^k + ([R][k])V^* \quad (11)$$

where $[I]$ is a n -by- n identity matrix and $[k] = [k_p] + x_{or}[k_Q]$, which we will designate as the *overall gain matrix*. We can evaluate the convergence of this update formula through the eigenvalues of the matrix that serves as the coefficient for the last obtained iterative term V^k , which we will designate as:

$$[A] = [I] - [R][k] \quad (12)$$

Per [16], the stability conditions for such process are met *iff the absolute values of the eigenvalues of $[A]$ are all less or equal to one*. Furthermore, if said values are also non-negative and real the system will converge in a non-oscillatory manner, returning to its steady state through exponential decay of the error. As an illustrative example, in Table IV we showcase the eigenvalues for each of the fourteen models of Table I and II with an unitary gain matrix ($[k] = [I]$):

Table IV
Eigenvalues and Error Behavior for each Study Model with Unitary Gain

Model #	Eigenvalues of $[A]$	Error Behaviour
1	{0 ; 0 ; 0.6}	<i>Overdamped</i>
2	{-0.3123 ; 0 ; 0.5123}	<i>Oscillatory</i>
3	{-0.5 ; -0.1372 ; 0.4372}	<i>Oscillatory</i>
4	{-0.6745 ; 0 ; 0.4745}	<i>Oscillatory</i>
5	{-1 ; -0.3464 ; 0.3464}	<i>Oscillatory</i>
6	{-0.7683 ; -0.2121 ; 0.3804}	<i>Oscillatory</i>
7	{-1.0891 ; -0.3360 ; 0.8252}	<i>Unstable</i>
8	{-1.6593 ; 0.2418 ; 0.8175}	<i>Unstable</i>
9	{-1.2215 ; -0.0731 ; 0.6946}	<i>Unstable</i>
10	{-0.9886 ; -0.0368 ; 0.8254}	<i>Oscillatory</i>
11	{-1.3568 ; -0.3390 ; 0.6958}	<i>Unstable</i>
12	{-0.8965 ; 0.2699 ; 0.8267}	<i>Oscillatory</i>
13	{-1.1506 ; 0.2470 ; 0.7036}	<i>Unstable</i>
14	{-2.1567 ; 0.6857 ; 0.8710}	<i>Unstable</i>

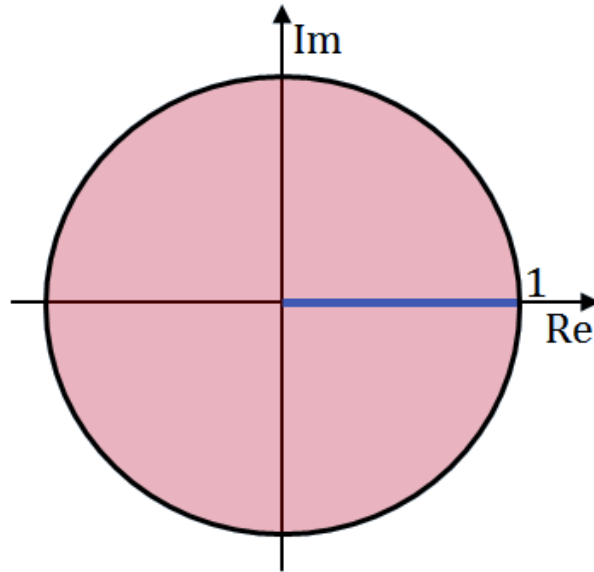


Fig. 2.4 Plane representation of the stability criteria for the control system. If the eigenvalues of $[A]$, $\lambda(A)$, are all contained within the pink area the system will be able to converge. Furthermore, this convergence will be non-oscillatory iff all eigenvalues are contained within the blue line segment.

As we can see, based on the above Table and Figure, only one of the models currently satisfies both the stability and the non-oscillation clause, and almost half of them are unstable altogether, all of which refer to unevenly phase-distributed models. This last fact is our first clue that the allotment of more than one generator per phase, as we will likely encounter in a real-life scenario for DG, contributes greatly to a system's lack of stability. Mathematically and matrix-wise, this is seen by the presence of positive non-diagonal terms in $[R]$, which become negative in $[A]$, with values closer to those of the diagonal ones, which causes the observed greater dispersal between eigenvalues in the later examples, as it'll be discussed in further detail ahead. Therefore, much of the goal concerning the guaranteeing a system's stability will revolve around diminishing the influence these terms have in the eigenvalues of $[A]$, which in practice means decreasing the clout each DER has on its neighbors through the controller's power gain k .

With the obtained eigenvalues, we can judge that, in its current state, the algorithm will not converge to its voltage set-point in an admissible manner for nearly all of the network schemes, regardless of any given initial conditions. Therefore, in order to mitigate this vulnerability, it becomes necessary for the algorithm to update the power injections more conservatively through an attenuation factor, thus enabling its convergence. As $[R]$ is an inherently fixed value, it falls upon the overall gain matrix $[k]$ to act as the attenuating coefficient, allowing us to reduce the difference between the power values in-between consecutive iterative steps. The larger this attenuation (that is the smaller the terms of $[k]$ get), the lesser the weight of the resistance matrix product will be over $[A]$, which will tend towards the identity matrix, and thus a set of eigenvalues closer to one. However, while lowering the power gains will help stabilize the system, they will also make the corrective process slower which, as stated before, can also be detrimental. As such, we must strive to find a compromise between speed and robustness of the local control process.

2.2.3 Instability and Oscillation Power Gain Threshold

Taking this mindset into account, we will discuss and study the various formats $[k]$ can take in order to find the composition that will best suit our intended goal. Of our particular interest, will be determining the limit power gain of the system, that is to say, from which set of k_i does the system error begins behaving in a non-convergent manner and, to a lesser degree, begins experiencing oscillations. In mathematical terms, with $\lambda(A)$ referring to the eigenvalues of $[A]$, one needs to find the respective $[k_{stb}]$ and $[k_{osc}]$ so that $Max|\lambda(A([R.k_{stb}]))| = 1$, and $Min(Real(\lambda(A([R.k_{osc}])))) = 0$ with $Imag(\lambda(A([R.k_{osc}])))) \equiv 0$. These eigenvalues are obtained through the determinant of the matrix:

$$[A] - \lambda[I] = \begin{bmatrix} 1 - k_1 R_{11} - \lambda & -k_2 R_{12} & -k_3 R_{13} \\ -k_1 R_{12} & 1 - k_2 R_{22} - \lambda & -k_3 R_{23} \\ -k_1 R_{13} & -k_2 R_{23} & 1 - k_3 R_{33} - \lambda \end{bmatrix} \quad (13)$$

which will result in the third degree polynomial equation:

$$\lambda^3 + a([R.k])\lambda^2 + b([R.k])\lambda + c([R.k]) = 0 \quad (14)$$

with its coefficients being equal to:

$$a([R.k]) = k_1 R_{11} + k_2 R_{22} + k_3 R_{33} - 3 \quad (15.1)$$

$$b([R.k]) = k_1 k_2 R_{11} R_{22} + k_1 k_3 R_{11} R_{33} + k_2 k_3 R_{22} R_{33} - k_1 k_2 R_{12}^2 - k_1 k_3 R_{13}^2 - k_2 k_3 R_{23}^2 - 2a([R.k]) - 3 \quad (15.2)$$

$$c([R.k]) = k_1 k_2 k_3 (R_{11} R_{22} R_{33} + 2R_{12} R_{13} R_{23} - R_{11} R_{23}^2 - R_{22} R_{13}^2 - R_{33} R_{12}^2) + a([R.k]) - b([R.k]) - 1 \quad (15.3)$$

Writing the overall gain matrix as $[k] = \alpha[K]$, where $[K]$ is the *controller specific power gain*, individual to each DER generator, and α the *common gain factor*, equal throughout the system, we can transform (14) into:

$$\lambda^3 + (a_1 + \alpha a_2([R.K]))\lambda^2 + (b_1 + \alpha b_2([R.K]) + \alpha^2 b_3([R.K]))\lambda + (c_1 + \alpha c_2([R.K]) + \alpha^2 c_3([R.K]) + \alpha^3 c_4([R.K])) = 0 \quad (16)$$

Given its composition, (16) can factorized into the general expression:

$$\prod_{i=1}^n (\lambda_i - \Delta_i([R, K]) \alpha - B_i) = 0 \quad (17)$$

which allows us to conclude that the eigenvalues of $[A]$ are linearly dependent of the common gain factor α , with a gradient Δ_i solely dependent on the controller gain $[K]$ and the reduced resistance matrix $[R]$. Moreover, we can determine the value of B_i by applying $\alpha = 0$ to (16), the former resulting in $\lambda^3 - 3\lambda^2 + 3\lambda - 1 = 0$, which yields $\lambda_i = 1$, and with (17) we get that $\lambda_i(\alpha = 0) = B_i = 1$, serving as the corollary that a large enough attenuation will always bring the system into stability. Incidentally, from these results, we can additionally derive that $[k_{stb}] = 2[k_{osc}]$.

Expanding upon (14), if we are to replace λ with $\lambda = \Delta \alpha + 1$, we will obtain another third degree polynomial general equation, equal to:

$$\Delta^3 + a_{\Delta}([R, K])\Delta^2 + b_{\Delta}([R, K])\Delta + c_{\Delta}([R, K]) = 0 \quad (18)$$

whose coefficients are given by:

$$a_{\Delta}([R, K]) = K_1 R_{11} + K_2 R_{22} + K_3 R_{33} \quad (19.1)$$

$$b_{\Delta}([R, K]) = K_1 K_2 R_{11} R_{22} + K_1 K_3 R_{11} R_{33} + K_2 K_3 R_{22} R_{33} - K_1 K_2 R_{12}^2 - K_1 K_3 R_{13}^2 - K_2 K_3 R_{23}^2 \quad (19.2)$$

$$c_{\Delta}([R, K]) = K_1 K_2 K_3 (R_{11} R_{22} R_{33} + 2R_{12} R_{13} R_{23} - R_{11} R_{23}^2 - R_{22} R_{13}^2 - R_{33} R_{12}^2) \quad (19.3)$$

By calculating the roots of the polynomial (18), we will attain the gradient for each eigenvalue, which in turn allows us to determine the $[k_{stb}]$ through:

$$[k_{stb}] = \frac{2}{\text{Max}|\Delta_i([R, K])|} [K] \quad (20)$$

It can be said with confidence then that, we can comparatively measure a system's robustness basing ourselves on this value, and thus the choice of which $[K]$ is the most suitable for the power controller chiefly revolves around it. Namely, we should strive to minimize $\text{Max}|\Delta_i([R, K])|$, while simultaneously maximizing $[K]$, as we will want the algorithm to have the highest possible speed while still maintaining its stable behavior.

Chapter 3

Limits to Fully Decentralized Voltage Control

3.1 Approaches to the Controllers' Power Gain

Next, we will be looking at several arrangements for each individual controller's power gains, to get a better understanding of $[R]$'s and $[K]$'s influence, now that we are aware of their theoretical weight on the general behavior of the system, and so that we can define a strategy for future study.

3.1.1 Common Network Gain

The first, and most basic, approach to the question pertaining the magnitude of the DER controller power gain will be to apply an equal value throughout the entire network. In other words, make it that $[K] = [I]$, and as a result, that $[k] = \alpha[I]$. The example showcased in the below graphs and table refer to such a case, where $\alpha = 1$, exhibiting the two robustness factors, $\Delta_i([K, R])$ and $[k_{stb}]$.

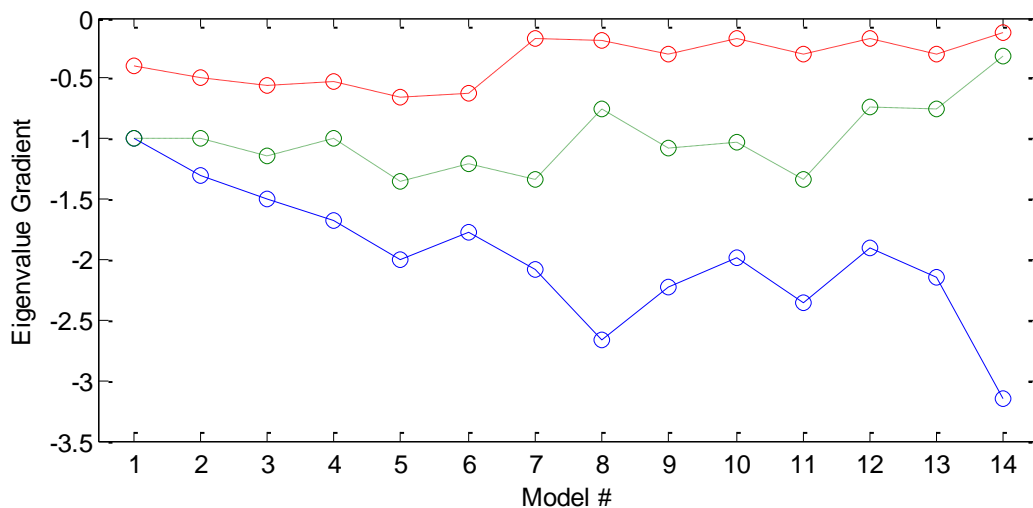


Fig. 3.1 Eigenvalue gradients Δ_i for the different study models, with $[k] = \alpha[I]$. Note that the colors are NOT indicative of the DERs themselves, as was the case in Table I and II.

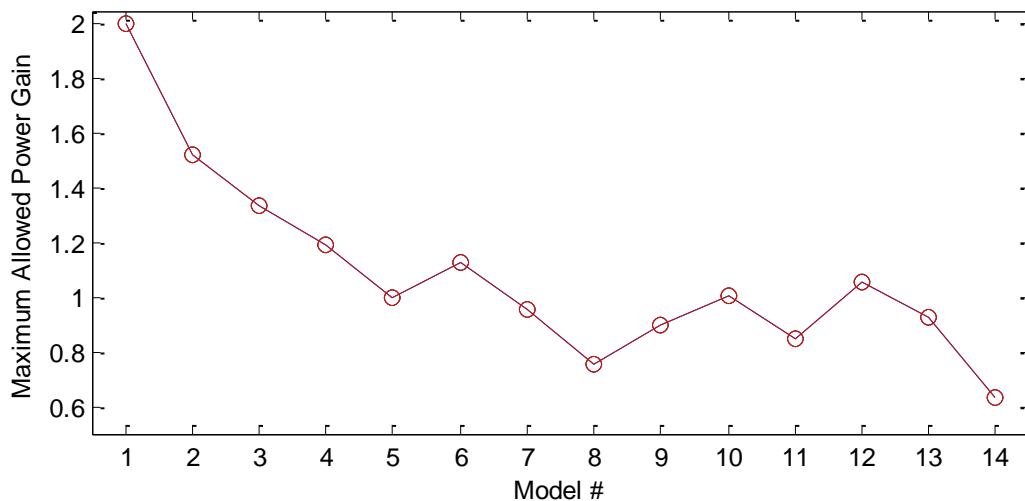


Fig. 3.2 Diagonal terms of $[k_{stb}]$ for the different study models, with $[k] = \alpha[I]$.

Table V
Eigenvalue Gradients and Maximum Allowed Power Gains with $[k] = \alpha[I]$

Model #	$\Delta_i([K.R])$	$diag([k_{stb}])$
1	$\{-1; -1; -0.4\}$	$\{2; 2; 2\}$
2	$\{-1.3123; -1; -0.4877\}$	$\{1.526; 1.526; 1.526\}$
3	$\{-1.5; -1.1372; -0.5628\}$	$\{1.334; 1.334; 1.334\}$
4	$\{-1.6745; -1; -0.5255\}$	$\{1.196; 1.196; 1.196\}$
5	$\{-2; -1.3464; -0.6536\}$	$\{1; 1; 1\}$
6	$\{-1.7683; -1.2121; -0.6196\}$	$\{1.132; 1.132; 1.132\}$
7	$\{-2.0891; -1.3360; -0.1748\}$	$\{0.958; 0.958; 0.958\}$
8	$\{-2.6593; -0.7582; -0.1825\}$	$\{0.754; 0.754; 0.754\}$
9	$\{-2.2215; -1.0731; -0.3054\}$	$\{0.902; 0.902; 0.902\}$
10	$\{-1.9886; -1.0368; -0.1746\}$	$\{1.006; 1.006; 1.006\}$
11	$\{-2.3568; -1.3390; -0.3042\}$	$\{0.85; 0.85; 0.85\}$
12	$\{-1.8965; -0.7301; -0.1733\}$	$\{1.056; 1.056; 1.056\}$
13	$\{-2.1506; -0.7530; -0.2964\}$	$\{0.93; 0.93; 0.93\}$
14	$\{-3.1567; -0.3143; -0.1290\}$	$\{0.634; 0.634; 0.634\}$

As expected, the configurations where phase distribution is uneven (models 7 through 14) have the worst response to a controller's power gains, as seen by the higher absolute values for the maximum gradients that in turn translate into lower overall gains for the stability threshold. More important, however, is that the above figures allow us to visualize that a slight change in the system's configuration can seriously compromise its health. Looking specifically between models 1 and 2, we see that the rearrangement of a single generator to the next downstream bus (see Table I) causes quite the considerable drop in $[k_{stb}]$, from 2 to 1.526. These values continue to decrease the more we concentrate DG on downstream buses, further away from the DER closest to the source bus.

To better assess the effects these alterations accrue in the value of the limit power gain, we can check the difference between two even-phase (1 through 6) models limit power gains, with said models differing only by the positioning of a single DER further downstream. Ordering model transition by the value of the drop in $[k_{stb}]$, we get: 1 \rightarrow 4 (0.804); 1 \rightarrow 2 (0.474); 2 \rightarrow 6 (0.394); 2 \rightarrow 4 (0.330); 3 \rightarrow 6 (0.202); 4 \rightarrow 5 (0.196); 2 \rightarrow 3 (0.192); 4 \rightarrow 6 (0.064). As it can be observed, the steepest declines occur in situations where the increase in the difference between the impedances of the generator closest to the source and the one farthest is the largest. Specifically, the worst observed case is a result of a DER jumping two busses downstream while the remainder stay at the most upstream (1 \rightarrow 4) or, if we put it matrix-wise, with $R_{11} = R_{22} = 0.8$ and $R_{33} = 0.8 \rightarrow R_{33} = 1.6$. While not negligible, it appears that moving a DER between the two delimiting generators has much less impact on the value of $[k_{stb}]$ than the prior. This phenomenon can also be observed in the remaining study cases as well, though they generally possess a much lower tolerance than the first six, likely a result of the uneven distribution of DG through the three phase-lines of the feeder grid.

Regardless, it's obvious that the relative arrangement of the connected DERs plays a fundamental role in determining the range of common network power gain each controller can operate on without putting the convergence of their algorithm in jeopardy. Any change, however minor, to the positioning of the generators can have unforeseen consequences, and variations on the latter should not be made without careful consideration. As it can easily be discern by the equations in the previous chapter, we already know that $[k_{stb}]$ will be inversely proportional to the bus-to-bus line impedance z , as such factor can be folded into the common gain factor α . Another aspect we can measure the effect of on $[k_{stb}]$ is the distance of the whole three generator cluster to the source bus 0, as shown by Fig 3.3 where we increase the distance (that is the, line impedance) between latter and the most upstream DER.

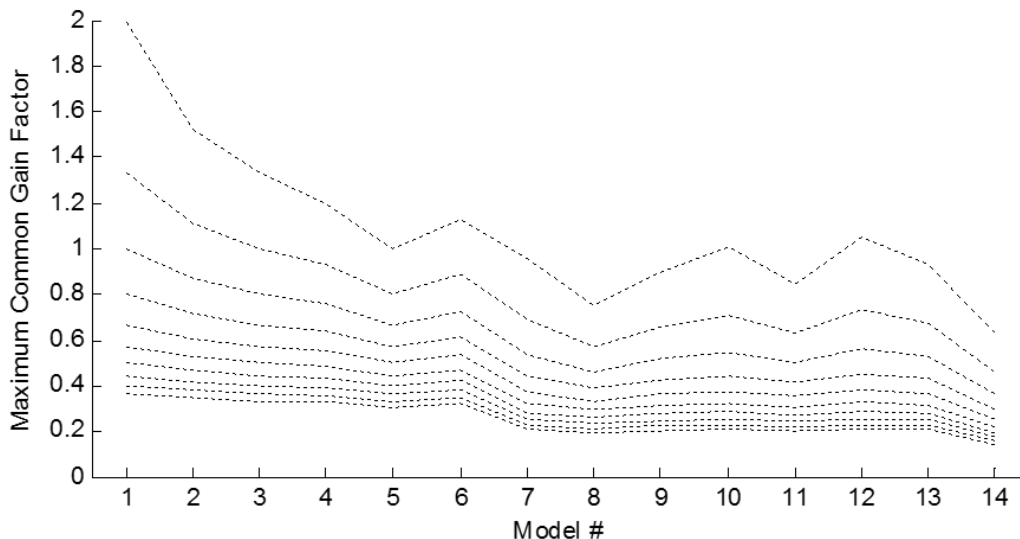


Fig. 3.3 Effects of distancing (i.e. adding more impedance) the DG cluster from the source bus on the maximum α . The topmost line represents the same example as Fig 3.2, with each subsequent line below representative of an gradual increase in the loop impedance between the cluster and the source. In matrix terms, this amounts to a $R_{ii} + 2z = R_{ii} + 2 \times 0.2$ increment when compared with the line immediately above.

Unlike an overall increase of the line impedance z throughout the entire grid, this distancing does not decrease $[k_{stb}]$ in an inversely proportional like manner. We can observe that as the graph lines progresses further down, the disparity between the $[k_{stb}]$ for the evenly distributed models is lessened, and the same goes between those spread between two phases. Eventually, with enough distance, this difference would become insignificant, resulting in a step graph where each step would represent a different distribution of the generators through R , S and T . This means that, the further the cluster is downstream, the less susceptible it will be to changes in configuration, as long as they don't pertain to its phases.

Nevertheless, as it has been made patent above, distance of any kind has an adverse repercussion on the overall system's stability when considering a single fixed value for all controllers' power gain. Further taking into account real-life implications for micro-producers, especially seeing they have little to no say on the distance to the provider and between one another, it makes this strategy less than practicable. Thus, to help mitigate these issues, the more sensible approach to take will then be for the gains to be somehow reflective of the distance their respective DERs are from the source bus.

3.1.2 Gain through Inverse Impedance

One parameter we can employ to add dynamism to the power gains is the very numerical reflection of distance, that being the terms of resistance matrix $[R]$ itself. In an ideal situation, with centralized control, every controller would be capable of communication with the rest of the network, and thus able to report any changes in its DER power injection so the others could compensate appropriately. Algorithmically, the overall gain matrix $[k]$ would be made equal to the inverse resistance matrix $[R]^{-1}$, resulting in $[A] = [I] - [R][R]^{-1} = 0$, whose eigenvalues are naturally null as well. As a consequence, $[k] = [k_{osc}]$, meaning that the voltage error behavior would always be critically damped. However, as stated in an earlier chapter, $[k]$ has to invariably be a diagonal matrix, as to reflect each controller's inherent lack of information about the impedances "seen" by other DERs in decentralized control. Still, we can take this ideal scenario into account by approximating $[K]$ to $[R]^{-1}$. Instead of the full inverse matrix each controller will only operate with inverse of their respective loop resistance R_{ii}^{-1} , which put together form what we will designate as the inverse diagonal resistance matrix $[R_I]$. As before:

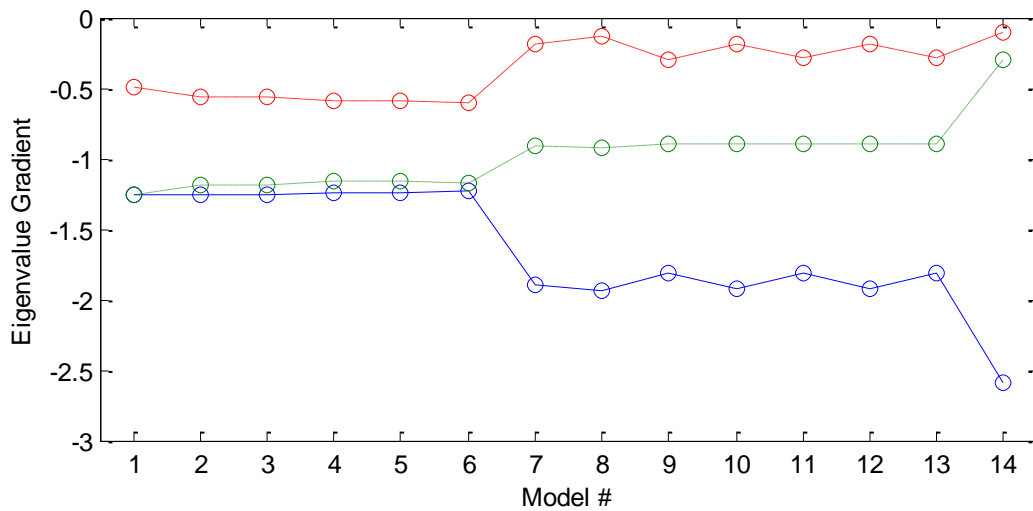


Fig. 3.4 Eigenvalue gradients Δ_i for the different study models, with $[k] = \alpha[R_I]$. Note that, again, the colors are NOT indicative of the DERs themselves, as was the case in Table I and II.

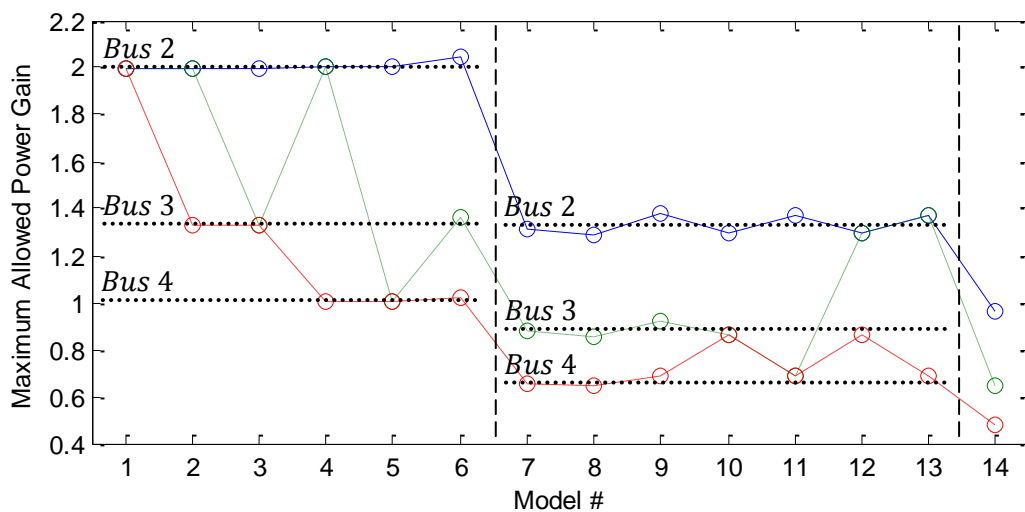


Fig. 3.5 Diagonal terms of $[k_{stb}]$ for the different study models, with $[k] = \alpha[R_I]$. The colors ARE indicative of the DERs and we see that, for the same phase distribution, the terms of $[k_{stb}]$ are consistent per their positioning.

Table VI
Eigenvalue Gradients and Maximum Allowed Power Gains with $[k] = \alpha[R_i]$

Model #	$\Delta_i([R, K])$	Diag($[k_{stb}]$)
1	$\{-1.25; -1.25; -0.5\}$	$\{2; 2; 2\}$
2	$\{-1.25; -1.1896; -0.5604\}$	$\{2; 2; 1.333\}$
3	$\{-1.25; -1.1896; -0.5604\}$	$\{2; 1.333; 1.333\}$
4	$\{-1.25; -1.1545; -0.5955\}$	$\{2; 2; 1\}$
5	$\{-1.25; -1.1545; -0.5955\}$	$\{2; 1; 1\}$
6	$\{-1.223; -1.1758; -0.6013\}$	$\{2.044; 1.363; 1.022\}$
7	$\{-1.9023; -0.9153; -0.1825\}$	$\{1.314; 0.876; 0.657\}$
8	$\{-1.9430; -0.9235; -0.1335\}$	$\{1.287; 0.858; 0.643\}$
9	$\{-1.8156; -0.8916; -0.2928\}$	$\{1.377; 0.918; 0.689\}$
10	$\{-1.9277; -0.8902; -0.1821\}$	$\{1.297; 0.865; 0.865\}$
11	$\{-1.8186; -0.8927; -0.2888\}$	$\{1.375; 0.687; 0.687\}$
12	$\{-1.9277; -0.8902; -0.1821\}$	$\{1.297; 1.297; 0.865\}$
13	$\{-1.8186; -0.8927; -0.2888\}$	$\{1.375; 1.375; 0.687\}$
14	$\{-2.5949; -0.2970; -0.1081\}$	$\{0.963; 0.642; 0.482\}$

The first noticeable aspect is the fact that very little variation is observable between the eigenvalue gradients for models with a similar allocation of DER through the network's three phases. Indeed, the lines of Fig 3.4 are almost approximate to a step graph, not at all unlike to what was witnessed in Fig 3.3 with a progressive distance increase between the cluster and the source. With this approach, the relative positioning between each connected generator does not affect the system's susceptibility to the common gain factor α as it did when he had $[k] = \alpha[I]$. One only was to look at the discrepancy between the Δ_i of models 1 and 5 for both strategies to appreciate this difference in results. Moreover, this also extends to limit gains $[k_{stb}]$, whose main contributing factor for their values appears to be the distance to the source R_{ii} and the number of connected DERs per phase, rather than their relative positioning. The topmost line (blue) in Fig 3.5, indicative of the most upstream generator and thus with a fixed distance to the source, more or less only experiences changes in its power gain due a shift in the *RST* configuration, again unlike what occurred in the beforehand strategy.

To obtain a better perception of the contrast between a common network gain and one based on the inverse of the loop resistance, we can repeat the same experience we've displayed on Fig 3.3, where we measure the outcome of moving the DG cluster downstream. A proper comparison point would be their common gain factor α for $[k_{stb}]$, which is dependent on the maximum absolute value of the gradients Δ_i , both of which are presented in Fig 3.6. On that note, whereas $[k_{stb}]$ was inversely proportional to z in the first method, in the second it will remain constant since, due the inverse nature of $[K]$ in the latter, equations (18.1-3) are independent from the line impedance.

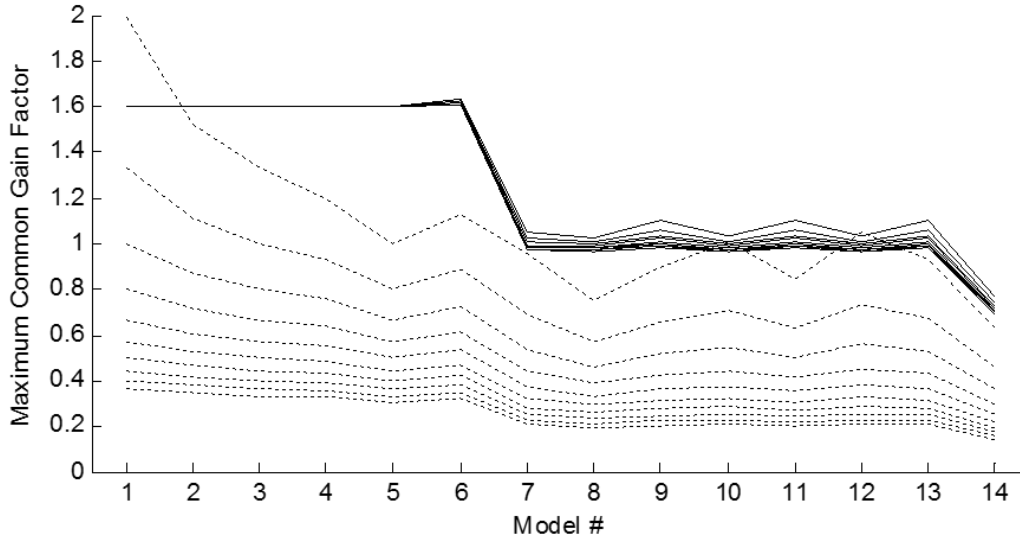


Fig. 3.6 Comparison of the effects of distancing the DG cluster from the source bus with a common network (dotted lines) and an admittance based (full lines) power gain on the maximum α . As in Fig 3.3, the topmost line represents the same example as Fig 3.2, with each subsequent line below representative of an gradual increase in the loop impedance between the cluster and the source. In matrix terms, this amounts to a $R_{ii} + 2z = R_{ii} + 2 \times 0.2$ increment when compared with the line immediately above.

As demonstrated in the above graph, the dislocation of the DG cluster does not have nearly the same amount of influence it has on $[k_{stb}]$ as it had in the previous case arrangements for the power gains. This means that, maintaining the same common gain factor α , we can reasonably make the guarantee that the magnitude of the terms in the resistance matrix $[R]$ will not adversely affect the system's stability by applying this strategy. For example, we can assure that the algorithm will preserve its convergence for every model from 1 to 6 should $\alpha \leq 1.6$. Overall, the distance, or in other words the feeder resistance seen by each DER, will play a much less important role when it comes to factoring in into the system's stability, as it was intended when devising this method. This reasoning is not only applicable to the source-to-cluster distance but also the distances between the generators inside the cluster, as we've adjudged from Fig 3.4 and Fig 3.5. Consequently, the crux of the matter now towards the ramifications of a unbalanced phase distribution in the feeder network, and whether or not we can mitigate its effects.

3.1.3 Alternative Strategies

Segueing from the last section, we can propose several different approaches for the defining a DG cluster's overall gain matrix $[k]$. As we mentioned beforehand, the core issue pertaining to the stability of a decentralized control scheme revolves around the influence between the various DERs connected throughout a feeder grid and an inherent lack of information available to their controllers. The former is mathematically reflected by the non-diagonal terms of $[R]$, and the latter by the diagonal aspect of $[k]$. Looking at the makeup of matrix $[A]$, the most straightforward solution to lessen the influence of other generators' injected power is simply eliminate its non-diagonal terms altogether. Specifically, make it so that only one k_{ii} is non-null, which will produce a triangular matrix $[A]$, as seen by (21). Characteristically, its eigenvalues will be equal to its main diagonal, which in this case would be $1 - R_{ii}k_{ii}$ with the remainder being 1s. In practice, this entails that each individual controller be updated one at a time, subsequently generating a $[k_{stb}]$ with terms comprised of $2R_{ii}^{-1}$, which is incidentally the highest collective set of values for the overall gains.

$$[A] = \begin{bmatrix} 1 & 0 & R_{1i}k_{ii} & 0 & 0 \\ 0 & 1 & \vdots & 0 & 0 \\ 0 & 0 & (1 - R_{ii}k_{ii}) & 0 & 0 \\ 0 & 0 & \vdots & 1 & 0 \\ 0 & 0 & R_{ni}k_{ii} & 0 & 1 \end{bmatrix} \quad (21)$$

Simulations corroborate this conclusion. Considering the diagonal of $[k]$ in a $\alpha[1 \ x \ y]$ format, their results determined that to maximize the possible common gain factor α , or in other words to minimize $Max|\Delta_i([R.K])|$, the x and y variables would have to be null. This applies to every study model and regardless of the terms' arrangement. Tangentially, they've also concluded that the highest possible α is attained solely with either x and/or y lower than zero, unusable as power gains since it would lead to a positive feedback for the state variable error. It's easy to see however that this method can become too time-consuming, as the more generators are connected to a grid, the longer the average wait will be for a correction for a voltage deviation to occur, which in certain cases may prove damaging to the network's infrastructure. There's also the question of organizing a time schedule for an entire group of incommunicable DERs, which will be subject to variations with each newly installed or uninstalled generator, making a perfect synchronization of their controller's an overly complex problem to handle.

Though not an ideal alternative, this approach can be used as a basis to find one that might. One way to avoid these (potently crippling) time delays would be to trigger each DER controllers in groups dependent of certain criteria, rather than individually. This could either be bus-by-bus, though that would still retain most of the same problems in spread-out clusters, or timing the adjustment based on the connected phase. The latter would narrow the interval between updates to a fixed amount, independent of the number of DERs, and take advantage of the fact that two or more generators connected to the same phase can mutually assist one another in correcting a potential overvoltage. However, practical issues continue to persist with any timestamp activation, chief among them pertaining to coordination within the DG cluster and slowness when compared with $[k] = \alpha[R_I]$.

Taking inspiration from the second approach, one twist that could be added to its principle leading to another possible proposition, that being the utilization of phase-specific gain factors. Let us assume that the diagonal of $[k]$ is written as $[\alpha_1 R_{11}^{-1} \alpha_2 R_{22}^{-1} \alpha_3 R_{33}^{-1}]$, α_{1-3} being the new coefficients, should generator i and j be connected to the same phase then $\alpha_i = \alpha_j$. Again through simulations, we've determined that, for our study models, such a configuration produces a higher average gain than with a inverse diagonal resistance matrix $[R_i]$. Its one major drawback is that to acquire the various α_i , a study of the feeder network makeup would be necessary, an inconvenient (and ultimately an impediment) for an autonomous control solution whose main purpose is to avoid such exercise.

Regardless of conjectures, what both theory and simulation have allowed to conclude is that the negative effect on the system's stability originating from multiple generators' influence, especially marked in an unbalanced distribution through RST , lie in the simultaneity of their power controllers' operation. Thus, the best course of action to guarantee the safety of the convergence process is to eliminate this concurrence altogether. Though we've discussed the drawbacks of applying such measures, later ahead we'll be proposing a different methodology for voltage control that allows to implement this rationale without sacrificing on the subject of prolonged time delays or synchronization between DERs.

3.2 Limitations on Injected Power

In theory alone, the described voltage dependent power controller could resolve any deviation in a network’s voltage profile, so long as the stability criteria pertaining to the eigenvalues of the iterative algorithm are met. However, as often is the case, in reality the physical characteristics of the electrical equipment, in conjunction with existing environmental conditions, will invariably place restrictions on the maximum power available to the system at any given time. Thus, the magnitude of the voltage spike (or drop) that triggers the controller’s activation and the values of the control variables at the start of the iterative sequence will now have to be weighed in, since the calculated power adjustment might be simply beyond the machine’s capabilities.

3.2.1 Generator Operational Area

The first inhibiting factor to consider, and also the most evident, is that of the quantity of sunlight available to a DER to convert into electrical energy. A photovoltaic cell’s power output will entirely depend on weather conditions, whose patterns tend to vary from region to region and may hinder the collection of solar radiation. Mathematically, the available active power P_A to a PV cell is a product between its surface area, the solar irradiance ($SI: W.m^{-2}$), and its overall energy conversion efficiency, with a recorded maximum of 46% in laboratory conditions, and between 11 – 15% in practical conditions [17]. As an example, in the Greater Lisbon area we have an average Global Horizontal Irradiance of around $194 W.m^{-2}$, meaning a $1x1$ meter solar panel is be able to produce $29.1 W$ on average, supposing a 15% efficiency.

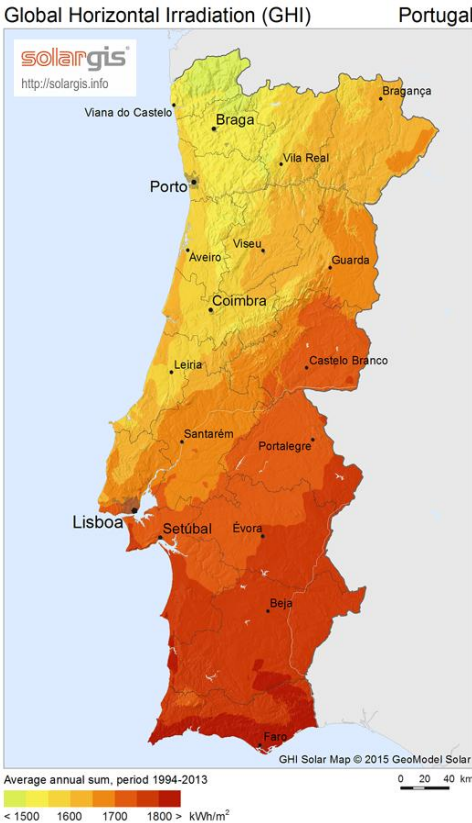


Fig. 3.7 Global Horizontal Irradiation values for Continental Portugal. Source: Solargis, GHI Solar Map © 2015.

Besides its active component, restrictions also exist relating to the injection of reactive power by a DER. A generator is commonly rated with a maximum apparent power output, specified for a rated voltage and power factor PF . Thus, during its operational periods, a DER's capability to inject reactive, and by association active, power into the grid will also be limited by a VA cap. This value is defined by three main aspects: the armature current limit, the field current limit, and the end region heating limit [18]. Together, they'll define the operational area for the generator, that, for the sake of not adding any unnecessary complexity, we will define as a semi-circle in a $[P, Q]$ plane, with the maximum apparent power S_M as its radius.

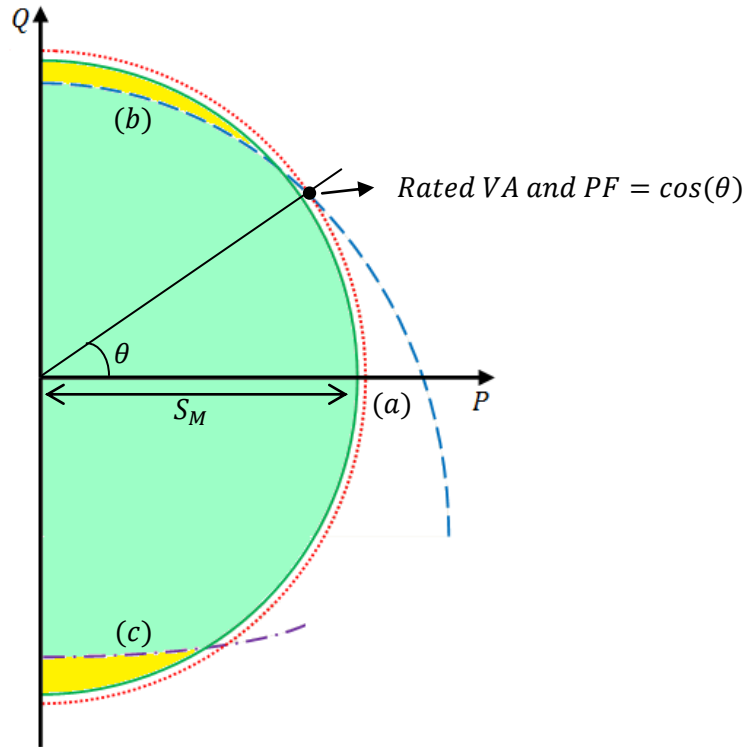


Fig. 3.8 $[P, Q]$ plane representation of the maximum apparent power S_M (green semi-circumference) and the operational area of a generator (light green area), assuming $S_M \leq P_A$. (a), (b) and (c) denote the restrictions imposed on the system by the armature current, the field current, and the end region heating limit, respectively. Yellow areas represent the zones within S_M where the injected power violates the last two provisions. We opted to define S_M towards the rated VA as that limit will be more pertinent for cases of voltage spikes.

Per the defined area of operation, S_M will impose the following stipulation upon the controller:

$$S_M^2 \geq P_G^2 + Q_G^2 \quad (22)$$

whereas P_G has to be greater than zero, seeing a generator cannot receive active power from the grid, and less or equal than the available active power P_A .

Because of these operational breakdown thresholds, there is now the tangible possibility that the controlling algorithm's state variable may not be able to reach the intended set-point. It becomes necessary then to ascertain if it's possible to find a solution within the acceptable range of values from any given set of initial conditions. To do so, we hearken back to (10). If we define V^0 , p^0 and q^0 as the state and control variables at the onset of the controller's activation and V^* , p_f and q_f as their respective values at the end of a successful correction, we obtain:

$$V^* = V^0 + [R]((p_f - p^0) + x_{or}(q_f - q^0)) \quad (23)$$

considering additionally that the system became bounded to the limit curve defined by S_M , we'll have that $S_M^2 = p_f^2 + q_f^2$. Reducing all initial conditions and system presets to a single variable C_0 :

$$C_0 = ([R]^{-1}(V^* - V^0) + p^0) x_{or}^{-1} + q^0 \quad (24)$$

We can then solve (23) for p_f , getting:

$$(1 + x_{or}^{-2})p_f^2 - (2C_0 x_{or}^{-1})p_f + (C_0^2 - S_M^2) = 0 \quad (=)$$

$$p_f = \frac{C_0 x_{or}^{-1} \mp \sqrt{(1 + x_{or}^{-2})S_M^2 - C_0^2}}{(1 + x_{or}^{-2})} \quad (25)$$

And as p_f must be a real number, we come to the conclusion that:

$$(1 + x_{or}^{-2})S_M^2 - C_0^2 \geq 0 \quad (=)$$

$$\left[\sqrt{(1 + x_{or}^{-2})S_M^2} - |[R]^{-1}(V^* - V^0) + p^0 + x_{or} q^0| \right]_i \geq 0 \quad (26)$$

If the above inequality is valid, in addition to the previously stated restrictions for the active power $\min\{p_{f1}, p_{f2}\} \leq P_A$, then the system state variable for i will be fully capable of converging to the intended value V^* , as a set of coordinates $[P_G, Q_G]$ exists within the established boundaries. From the acquired expression, we can also perceive how the system's ability to handle deviations is directed correlated to the initial and preset values. A system with a higher x_{or} and S_M , will accommodate for a higher discrepancy between V^0 and V^* , in concurrence with an opposite signal p^0 and q^0 .

3.2.2 Power Coordinates Solution Line Set

Moreover, from (25) we can determine that there are two points in the limit curve where the value of p_f , and consequently q_f , satisfy the needed corrective shift. With these two sets of coordinates, we can trace a line in the $[P, Q]$ plane, whose equation is derived from (23):

$$q_f(p_f) = C_0 - x \circ r^{-1} p_f \quad (27)$$

It stands to reason then that all points contained within the area defined by the S_M radius semi-circle, the plane delimited by the maximum and minimum allowed active power, and line (27) are all valid solutions to correct the given voltage deviation $V^* - V^0$.

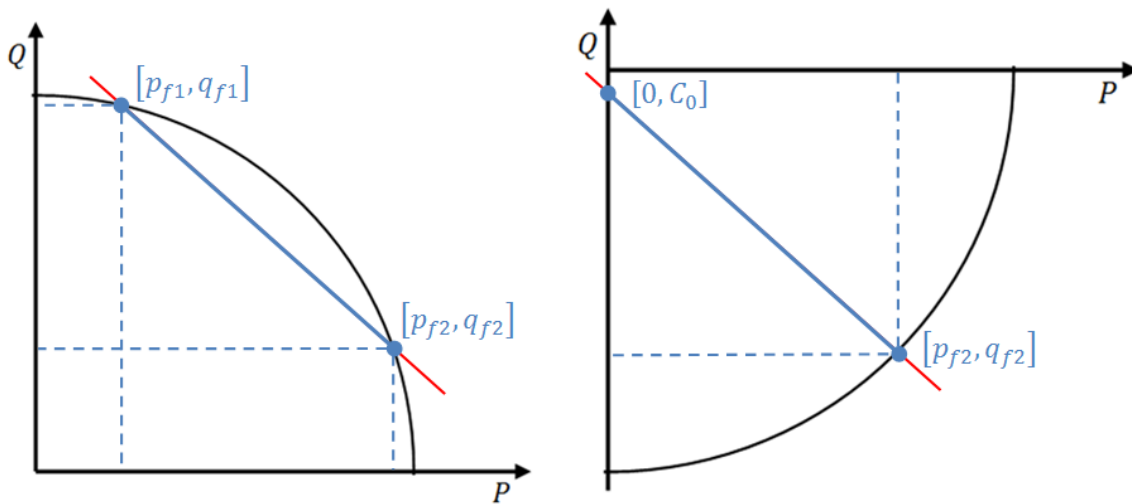


Fig. 3.9 $[P, Q]$ plane hypothetical representations of (27), assuming that $p_{f2} \leq P_A$ for demonstrative purposes. The highlighted blue line segment contains all the possible solutions for active and reactive power. Two scenarios are shown; in the first the leftmost abscissa is positive while in the second its null due to the set restrictions. In a situation where (26) is equal to zero, (27) will be tangent to the semi-circumference.

Equation (27) allows for some significant leeway when controlling each generator's power output, seeing that the network's voltage profile will remain undisturbed so long as the injected power coordinates "travel along" their corresponding blue line, as exemplified in Fig. 3.9. For instance, this feature becomes useful in situations where there's a sudden drop in P_A (e.g. from a sudden shift in luminosity) as it lets a controller readjust its DER's output without triggering the activation of its counterparts in the DG cluster, as a consequence of the voltage disturbances it would incite otherwise. Another benefit would be if we desire to set the machine to a specific PF , though this would only be possible if the blue line crosses paths with the one defined by the angle θ (see Fig. 3.8). What's more, application of this property only entails the use of the equations slope value, itself easily obtainable through reactance-to-resistance ratio, while C_0 can be calculated once the algorithm reaches any point in the line segment.

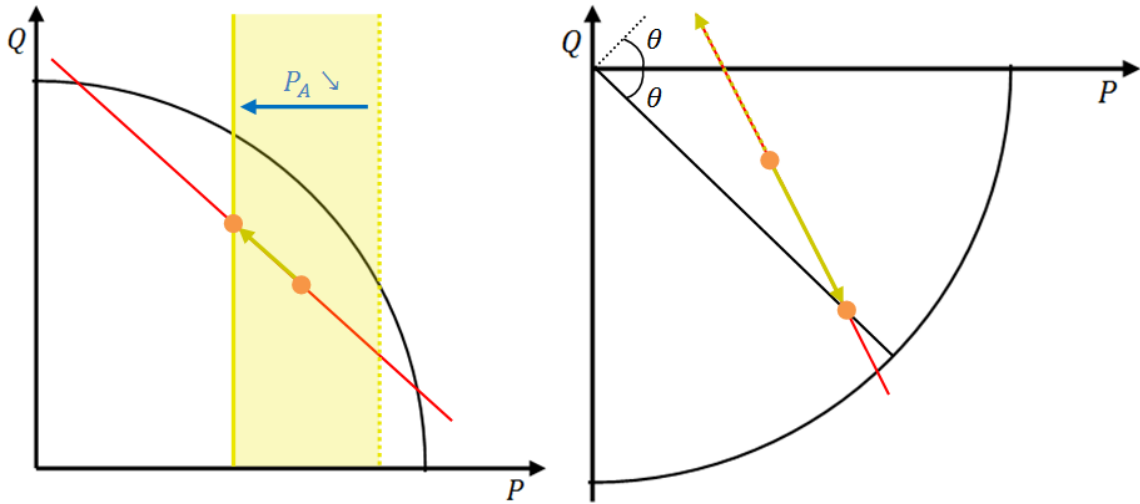


Fig. 3.10 $[P, Q]$ plane hypothetical representations of the possible applications of the inherent properties of (27). In the leftmost, we see how the system would handle an unexpected drop in available active power P_A , and in the rightmost how it would fix the power coordinates to a specific $PF = \cos(\theta)$. In both cases, the network's voltage profile would remain unchanged despite the variation in the injected active and reactive power.

We can also gauge that any line with a $-x \circ r^{-1}$ slope contains all the power coordinates corresponding to one specific voltage profile. Based on the initial values for the network's nodal voltage and power injected by the generators, with each iterative step, we consecutively jump between several of these parallel lines, progressively closing in on the one that holds the set of the latter that can fix the former to the desired set-point. Starting from any staging point, a shift to a right line represents an increase in the nodal voltage, while to the left will cause a decrease.

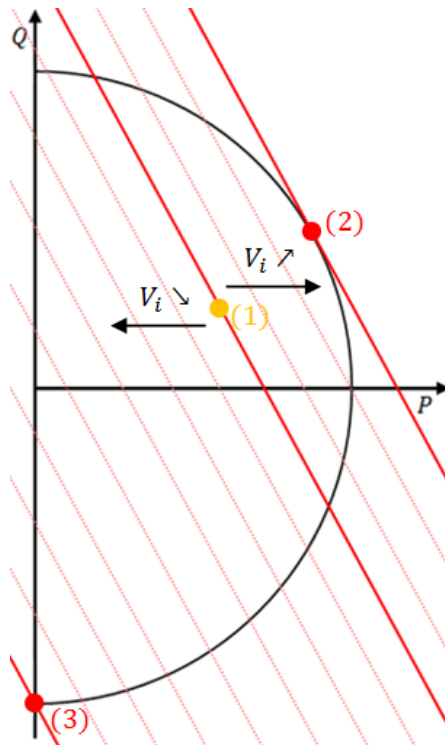


Fig. 3.11 Examples of possible power coordinates solution sets in a $[P, Q]$ plane, with each hypothetical line corresponding to a specific voltage profile, and (2) and (3) defining the generator's operational range.

In the above figure, point (1) depicts any staging point the algorithm might find itself in at a given time, be it the initial, final or anywhere in between. (2) and (3) relate to the power coordinates that will produce the highest attainable positive and negative shift in the DER's voltage respectively. We can thus define the range of operation for the controller using the points where line (27) is tangent with the limit semicircle, those being $[p_f = S_M (1 + x \circ r^2)^{-1/2}, q_f = x \circ r S_M (1 + x \circ r^2)^{-1/2}]$, resulting in $C_0 = S_M x \circ r^{-1} (1 + x \circ r^2)^{1/2}$, and $[p_f = 0, q_f = -S_M]$, resulting in $C_0 = -S_M$. In relates to these expressions, and in tandem with (26), the inequality:

$$S_M x \circ r^{-1} (1 + x \circ r^2)^{1/2} \geq [C_0]_i \geq -S_M \quad (28)$$

also needs to be valid for the algorithm to successfully reach a solution, seeing as, otherwise, the correspondent line (27) will not overlap with the operational area of the generator.

3.3 Updated Controller Algorithm

Given the limitations imposed by maximum available active power P_A and the maximum apparent S_M , it's evident that the control algorithm describe in length in Table III will have to suffer several modifications to take in account these two new restricting parameters to its operation. The former is reasonably straightforward to implement, making so that for every i : $p^{k+1} = \min \{p^k + [k_p](V^* - V^k), P_A\}$. The latter issue requires more consideration, as we'll need to carefully juggle between the two types of voltage dependent power controller, $P(V)$ and $Q(V)$, seeing that we'll want to avoid exceeding the bounded limit (22). In essence, the core of the subject matter invariably revolves around the handling of the controller's two distinct power gains $[k_p]$ and $[k_q]$. We've identified two possible strategies for defining the exact values of $[k_p]$ and $[k_q]$, based on the previously obtained overall gain matrix $[k]$.

Both these strategies involves using only one type of voltage dependent control at any given time. This means that, for each individual iterative step, we'll either have $[k] = [k_p] + 0$, for an active power shift, or $[k] = 0 + x \circ r [k_q]$, for a reactive power shift, alternating between them as necessary by setting the opposite gain as zero. Seeing that the most numerous, and most detrimental, instances of voltage deviation are cases of overvoltage, entailing a corrective drop in the injected power, and it's in our interest to avoid a decrease in the DER's active power output whenever possible, it was decided that $Q(V)$ will take precedence over its counterpart. Thus, when the autonomous controller is springs into action, it'll first try to correct the voltage difference by adjusting the generator's Q_G with (9.2), while keeping P_G unchanged, until it either eliminates the discrepancy by itself or the apparent power surpasses the limit dictated by S_M . Upon the latter occurrence, $P(V)$ will then trigger, curtailing the active power to correct the violation, until $Q(V)$ is allowed to continue its operations. How the controller acts when it reaches the limit curve is also subject to two different methodologies.

3.3.1 Bounded to the Maximum Apparent Power Limit Curve

As a first option, we can simply ensure that whenever the reactive power variation infringes (22), an additional adjustment is done to P_G , so that the set of power values remains bounded to the limit curve until one of the possible solutions is reached.

Table VII
Logical Steps of a Voltage Dependent Alternating Q(V)/P(V) Power Controller with Q(V) precedence – Bounded

Step 1	Compare set-point V^* and actual voltage to obtain error $\Delta V_i = V^* - V_i$;
Step 2	Compute power-shift ΔQ_i based on ΔV_i and gain $\Delta Q_i = [k_Q]_{ii} \Delta V_i = x^{\sigma r^{-1}} [k]_{ii} \Delta V_i$; Check if $S_M^2 \geq P_i^2 + (Q_i + \Delta Q_i)^2$
Step 3	If True \rightarrow continue to Step 4; Else \rightarrow Compute power-shift ΔP_i so that: $S_M^2 = (P_i + \Delta P_i)^2 + (Q_i + \Delta Q_i)^2$;
Step 4	Update V_i based on the new values of P_i and Q_i $V_i = f([P_i, Q_i]) = V^0 + [R]((P_i - p^0) + x^{\sigma r}(Q_i - q^0))$;
Step 5	Check if $V_i \neq V^*, \forall_i$ If True \rightarrow return to Step 1; Else \rightarrow stop;

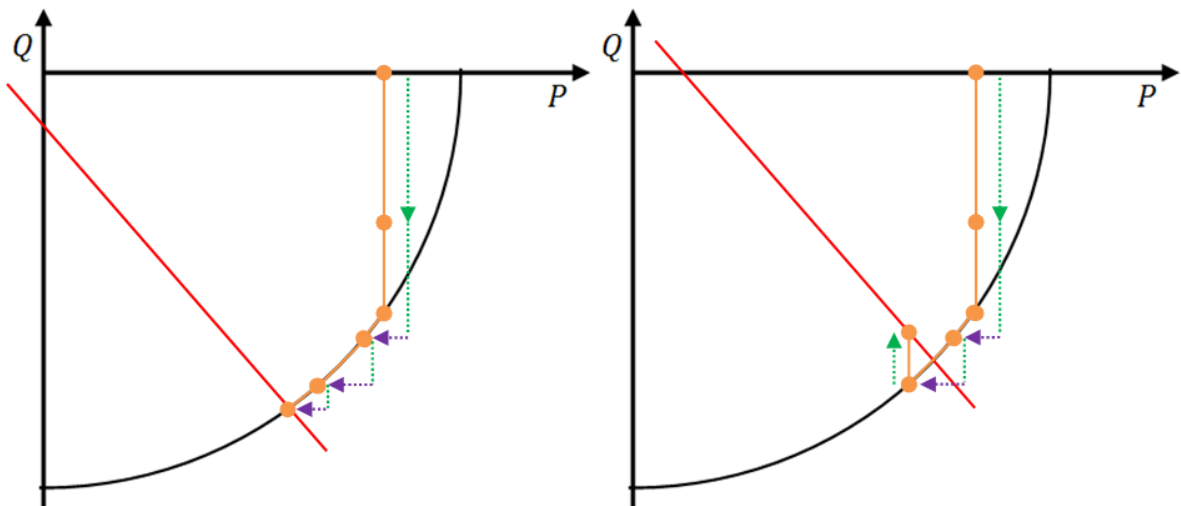


Fig. 3.12 [P, Q] plane hypothetical representations the logical steps taken by the controller when correcting an instance of nodal voltage deviation, when using the S_M bounded strategy. Green vertical arrows represent $Q(V)$, purple horizontal arrows $P(V)$ and the red line the solution set of values per (27).

3.3.2 Active Power Shift by Foresight

Alternatively, we can introduce some degree of foresight to the controller. Rather than constantly fixing the apparent power to its allowed maximum, it can detect beforehand if the next shift in reactive power will carry the coordinate set beyond the boundaries of the S_M semi-circle. When such situation occurs, it'll instead make use of an active power shift, and will continue to do so until a subsequent reactive shift is possible again. In essence, we make use of $P(V)$ to unblock $Q(V)$'s path.

Table VIII
Logical Steps of a Voltage Dependent Alternating $Q(V)/P(V)$ Power Controller with $Q(V)$ precedence – Foresight

Step 1	Compare objective V^* and actual voltage to obtain error $\Delta V_i = V^* - V_i$;
Step 2	Compute power-shift ΔQ_i based on ΔV_i and gain $\Delta Q_i = [k_Q]_{ii} \Delta V_i = x^{or-1} [k]_{ii} \Delta V_i$; Check if $S_M^2 \geq P_i^2 + (Q_i + \Delta Q_i)^2$
Step 3	If True \rightarrow continue to Step 4; Else \rightarrow Compute power-shift ΔP_i based on ΔV_i and gain $\Delta P_i = [k_P]_{ii} \Delta V_i = [k]_{ii} \Delta V_i$, and <i>discard</i> Step 2's ΔQ_i ;
Step 4	Update V_i based on the new values of P_i or Q_i $V_i = f([P_i, Q_i]) = V^0 + [R]((P_i - p^0) + x^{or}(Q_i - q^0))$;
Step 5	Check if $V_i \neq V^*, \forall_i$ If True \rightarrow return to Step 1; Else \rightarrow stop;

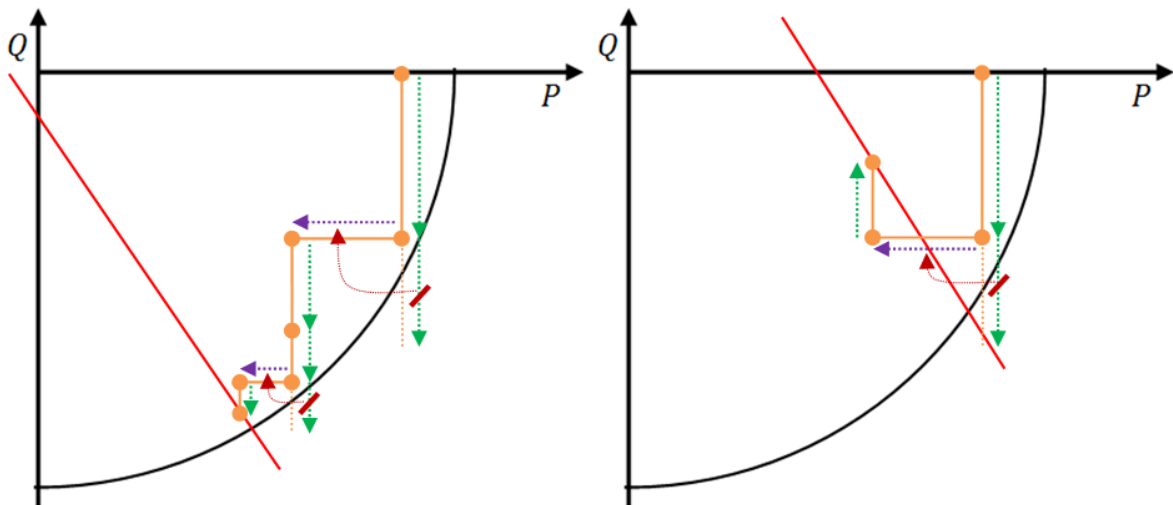


Fig. 3.13 $[P, Q]$ plane hypothetical representations the logical steps taken by the controller when correcting an instance of nodal voltage deviation, when using an the foresight strategy. Green vertical arrows represent $Q(V)$, purple horizontal arrows $P(V)$ and the red line the solution set of values per (27).

If we are to compare these two solutions, it appears that the second option is the more preferable. For one, the number of corrective power adjustments, active and reactive, in the first case is invariably going to be larger, as moving along the limit curve inevitably entails the use of both types. Discerning the stability of this process also becomes exceedingly difficult due to the introduction of a squared factor for the update equation (10), that adds a fair amount of complexity to the calculations. The interchangeability between $Q(V)$ and $P(V)$ in terms of convergence, as $[k]$ remains constant regardless of which is used, means that both the algorithm speed and voltage error behavior are the same if we were to have no power related restrictions. Moreover, that we avoid skirting too close to the S_M , as fluctuations in both state and control variables naturally tend to occur, is another factor in the latter's favor. Finally, through additional simulations, we've appraised that the bounded option often behaves poorly with an uneven distribution of DERs through the phases, a very high likelihood in a real life scenario.

Chapter 4

Simulation Results

With all the necessary theoretical groundwork laid down, we now move to testing stage of this work, as to corroborate the suppositions made in the previous chapters and to better understand the effects a decentralized controller has on the evolution of a network's voltage profile. All practical studies are realized through computer simulations running with MATLAB programming language, and compiled with the eponymous PC software. The results are divided into two separate sections, each pertaining, correspondingly, to the evolution of the voltage error and the injected power throughout the controller's process. As mentioned in Chapter 3, given the interchangeability between $Q(V)$ and $P(V)$ in terms of convergence, the behavior of the nodal voltages is independent of the type of combination between the two types of power adjustment. In short, its error response will be the same regardless of the initial conditions for active and reactive power, plus S_M , provided that (26) and (28) hold true. As such, we can study these two aspects in separate sections, so we can dedicate more of our focus onto either the control and state variables at a time.

All MATLAB code used for these simulations is fully detailed in Annexes A through F.

4.1 Establishing the Initial Voltage Error

Before beginning commencing the study itself, we'll first need to establish a set of initial values for the nodal voltages of each grid configuration presented in Chapter 2. Given the different positioning of the generators, it's natural to assume that a voltage rise phenomenon will result in equally different values for the voltage deviation in each DER, relative to one another. Thus, as we'll want these values to represent a more or less realistic scenario that could be encountered in any practical feeder network, we made use of a simple power-flow code to calculate a satisfactory set of values for the initial conditions of the state variable. Any subsequent alteration to the initial voltages V^0 , as to gauge the system's response to small alterations, will have a basis in these settings, that range on average between a 1% and 4% deviation (max. 10%) in relation to the predetermined V^* .

The following two tables present the results yielded by the simulation of the power flow for the feeder grid in Fig 2.3.

(For network models number 1 through 6, the generated voltage for each of the three DERs, being respectively {0.9615; 0.9601; 0.9651}, remains constant. Number 7 through 13, we add a 0.1 factor to the corresponding DERs that share the same phase, as to represent their mutual generation effect. For model 14, this addition is increased to 0.2, given that all three are connected in line. This choice was also made so that (26) and (28) remain valid for the chosen p_0 and q_0 described in the injected power part of this chapter, with $S_M = 1.035$.)

Table IX
Initial Voltage Values for Evenly
Distributed per Phase Models

Model #	V^0 [pu]
1	{1.1147; 1.1200; 1.1185}
2	{1.1240; 1.1254; 1.1049}
3	{1.1145; 1.1132; 1.1084}
4	{1.1256; 1.1269; 1.1226}
5	{1.1115; 1.1286; 1.1239}
6	{1.1174; 1.1126; 1.1227}

Table X
Initial Voltage Values for Unevenly
Distributed per Phase Models

Model #	V^0 [pu]
7	{1.1166; 1.1102; 1.1247}
8	{1.1213; 1.1528; 1.1646}
9	{1.1179; 1.1135; 1.1252}
10	{1.1187; 1.1140; 1.1095}
11	{1.1168; 1.1264; 1.1229}
12	{1.1218; 1.1256; 1.1140}
13	{1.1207; 1.1260; 1.1296}
14	{1.1006; 1.1350; 1.1463}

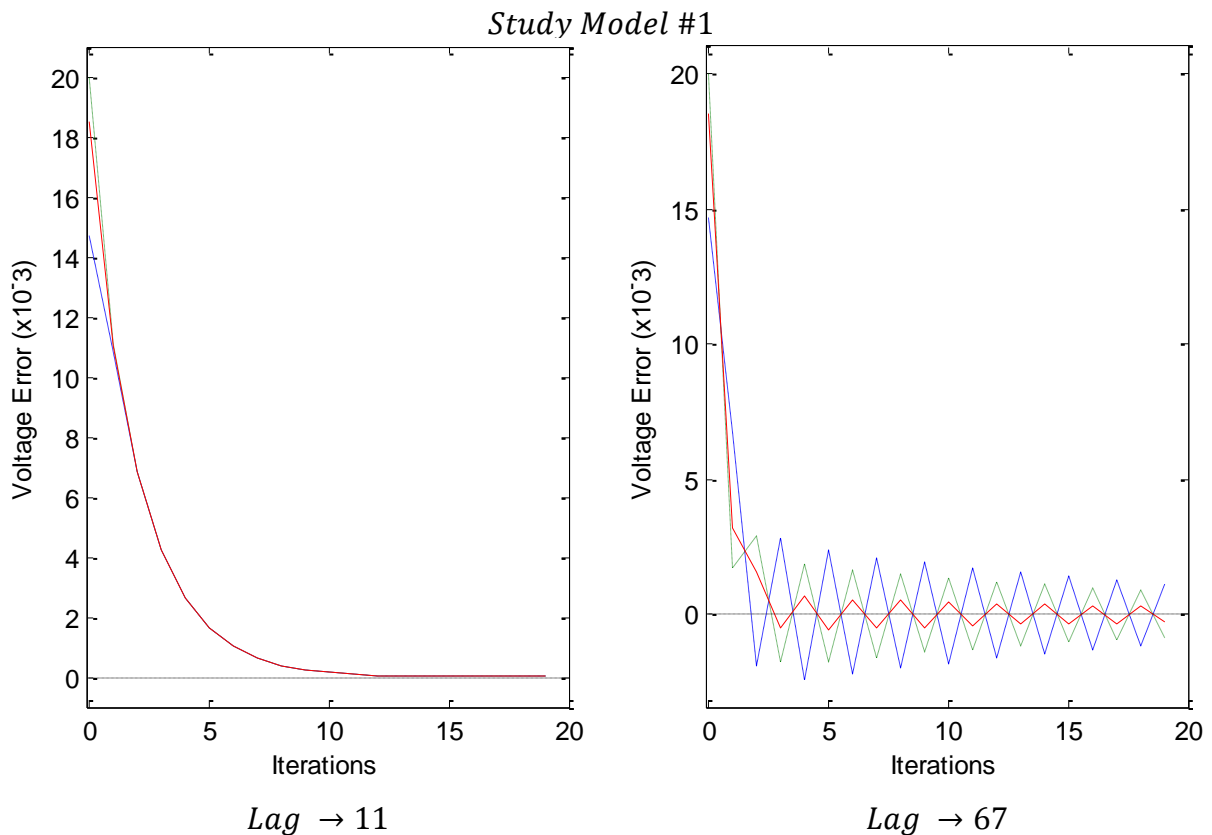
As a superficial glance of the results can tell, the incremental effects resulting from voltage rise tend to be more pronounced the more DERs are clustered together. Looking at the figures from Table IX, and judging by the total difference in relation to the set-point V^* , we see that the least severe errors occur in models where less generators are connected to the same bus. In the same vein, reducing the distance between both ends of the cluster, and concentrating the DERs on its downstream end, also contributes towards a lower voltage deviation. For Table X, we witness a similar situation, though the average error tends to be greater due to the addition of a mutually induced increase for same-phase nodal voltages.

There is, however, an unusually high discrepancy for model 8, when compared with the other figures. From what can be surmised, this seems to stem from the fact that, unlike the other cases from 7 to 13, the two same-phase generators are positioned further downstream than in the other models. This inference is corroborated by reconfiguring the algorithm's code, as to add additional distance between the cluster and the source bus, and an increase in the line impedance. The new results show that an increment in either parameter aggravates the magnitude of the voltage spikes for the DERs that share a phase with another. The contrary occurs to those that are alone, where we see an alleviation of the overvoltage for the same generated voltage.

A further analysis of the code and results seems to suggest that another reason behind this discrepancy may stem from the lack of generation in one or two of the phases. As the nodal voltage in these empty lines progressively decreases (the decay of which accelerates the further the cluster is from the source and with the line impedance), the amplitude of the voltage in the remaining phases will inevitably rise, as expounded in Chapter 2. It is yet another attestation of the substantial impact simple DER distribution on a feeder network has on the system's viability. This, in particular, is an aspect that will be further delineated upon when we move to study a full-grid.

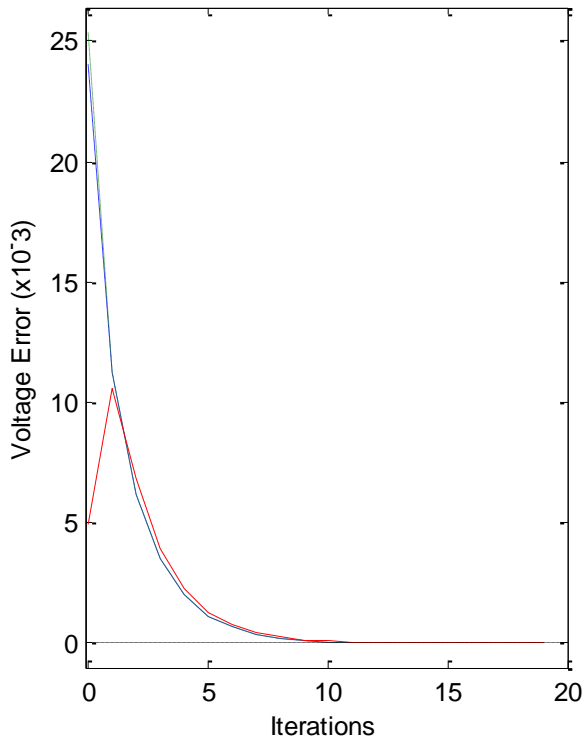
4.2 Voltage Error Behavior and System Performance

For a first behavior study, we'll have the preset values so that the algorithm only has to employ $Q(V)$ to reach the set-point voltage, here $V^* = 1.1$. For that, we'll simply start with a S_M and P_A high enough that $P(V)$'s activation won't be necessary. Furthermore, as to compare the error's overdamped and oscillating behavior respectively, we'll have one instance where $[k] = 0.95[k_{osc}]$ and another where $[k] = 1.95[k_{osc}]$. We'll also note the speed of the algorithm, that is the number of iterations it takes for the maximum voltage error to drop below a certain value, in this case 10^{-4} , even if it's beyond the displayed 20 iterations. Finally, the results are once more divided, between the evenly and unevenly distributed models, to underline the differences between the two situations. The leftmost graphs display the overdamped error behavior, and the right ones the oscillatory.

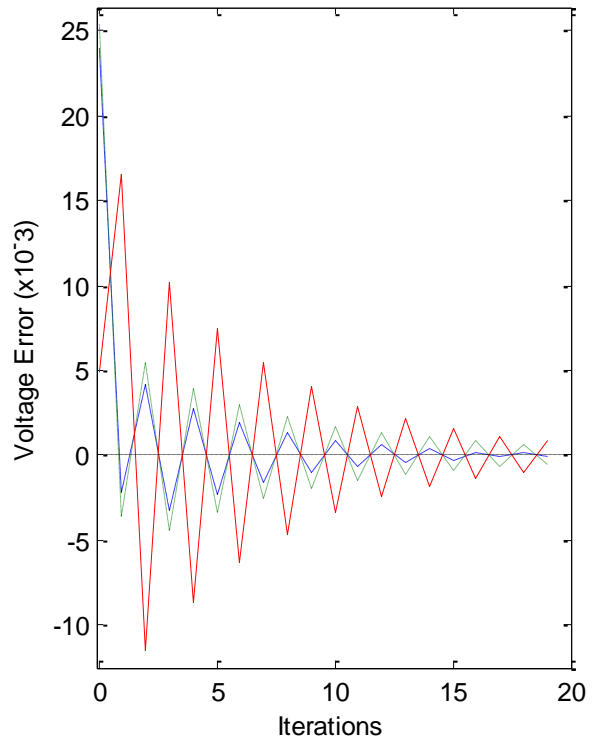


Figs. 4.1 and 4.2 Evolution of the state variable error for the evenly-distributed per phase study model 1, with $[k] = 0.95[k_{osc}]$ (left) and $[k] = 1.95[k_{osc}]$ (right), up to twenty iterations.

Study Model #2



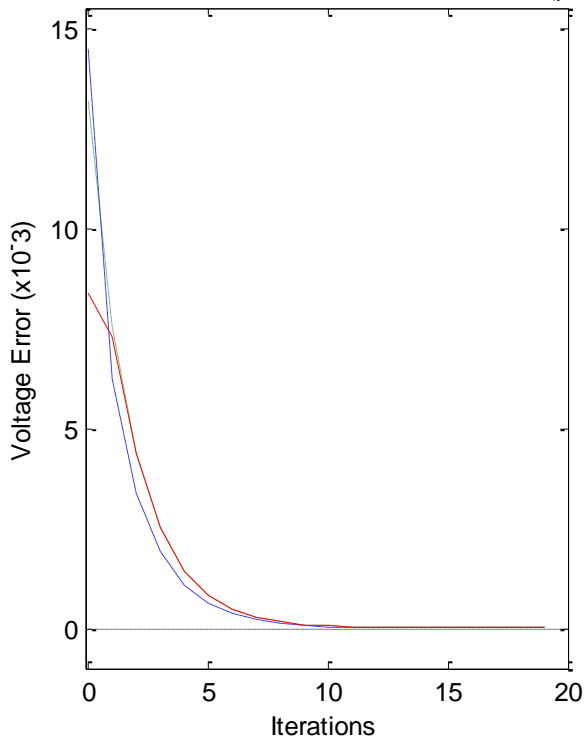
Lag → 10



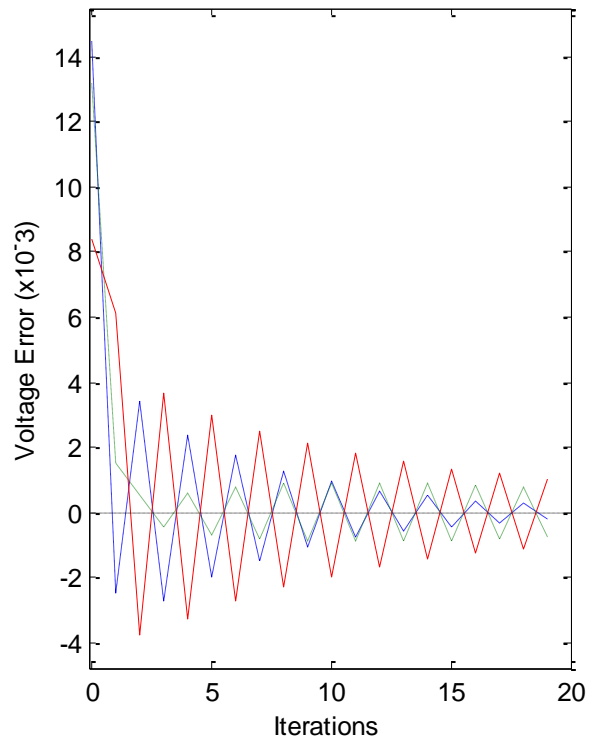
Lag → 41

Figs. 4.3 and 4.4 Evolution of the state variable error for the evenly-distributed per phase study model 2, with $[k] = 0.95[k_{osc}]$ (left) and $[k] = 1.95[k_{osc}]$ (right), up to twenty iterations.

Study Model #3



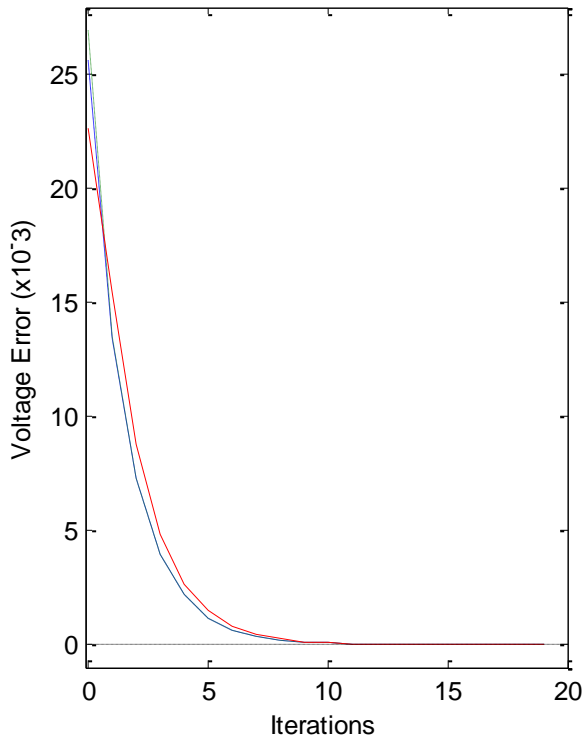
Lag → 9



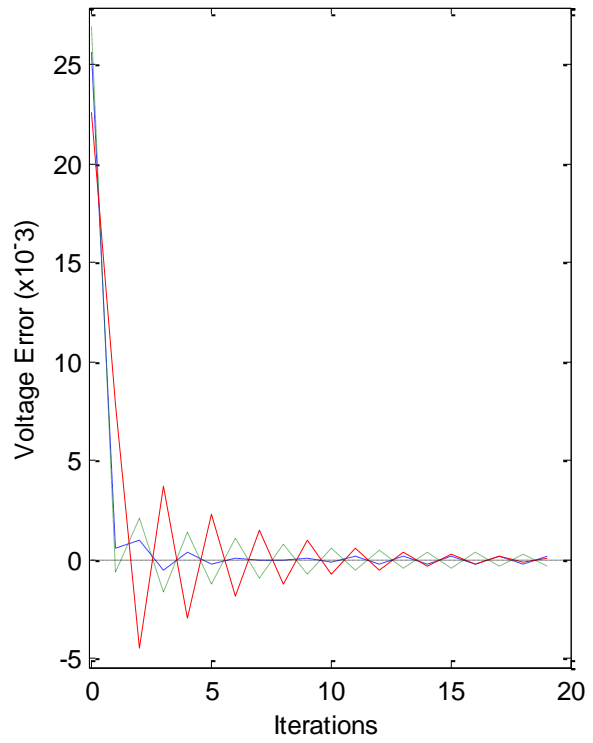
Lag → 62

Figs. 4.5 and 4.6 Evolution of the state variable error for the evenly-distributed per phase study model 3, with $[k] = 0.95[k_{osc}]$ (left) and $[k] = 1.95[k_{osc}]$ (right), up to twenty iterations.

Study Model #4



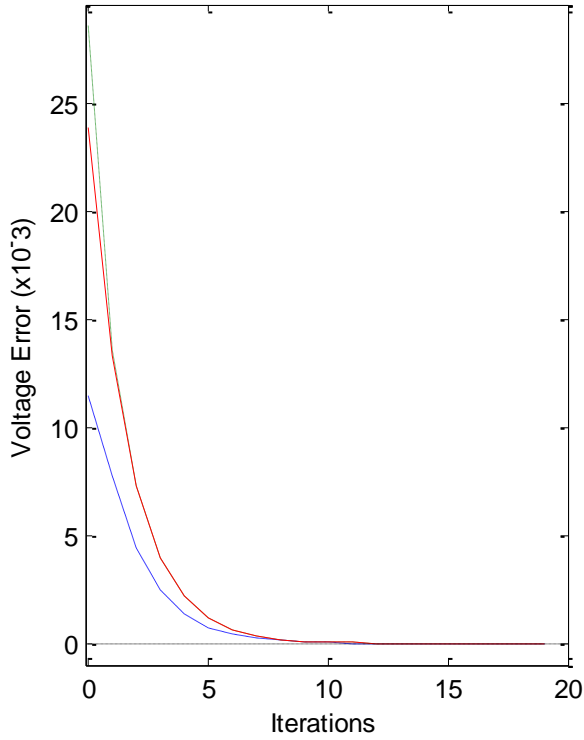
Lag \rightarrow 10



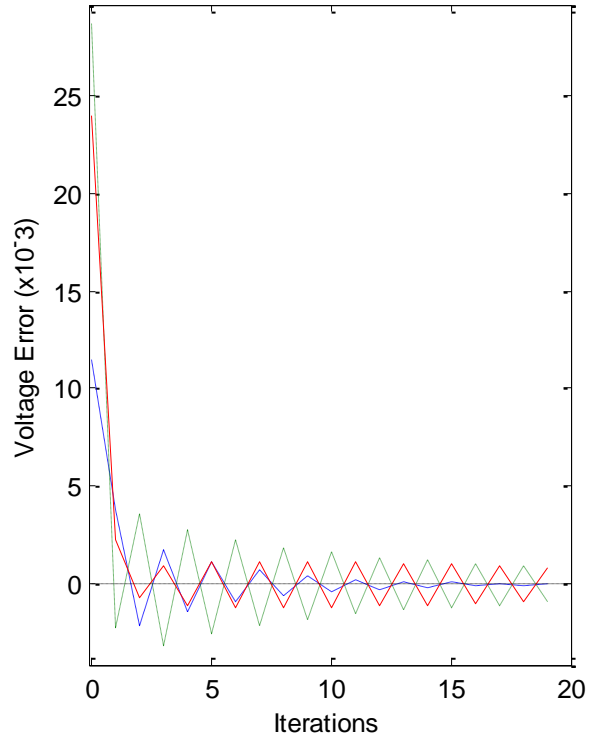
Lag \rightarrow 37

Figs. 4.7 and 4.8 Evolution of the state variable error for the evenly-distributed per phase study model 4, with $[k] = 0.95[k_{osc}]$ (left) and $[k] = 1.95[k_{osc}]$ (right), up to twenty iterations.

Study Model #5



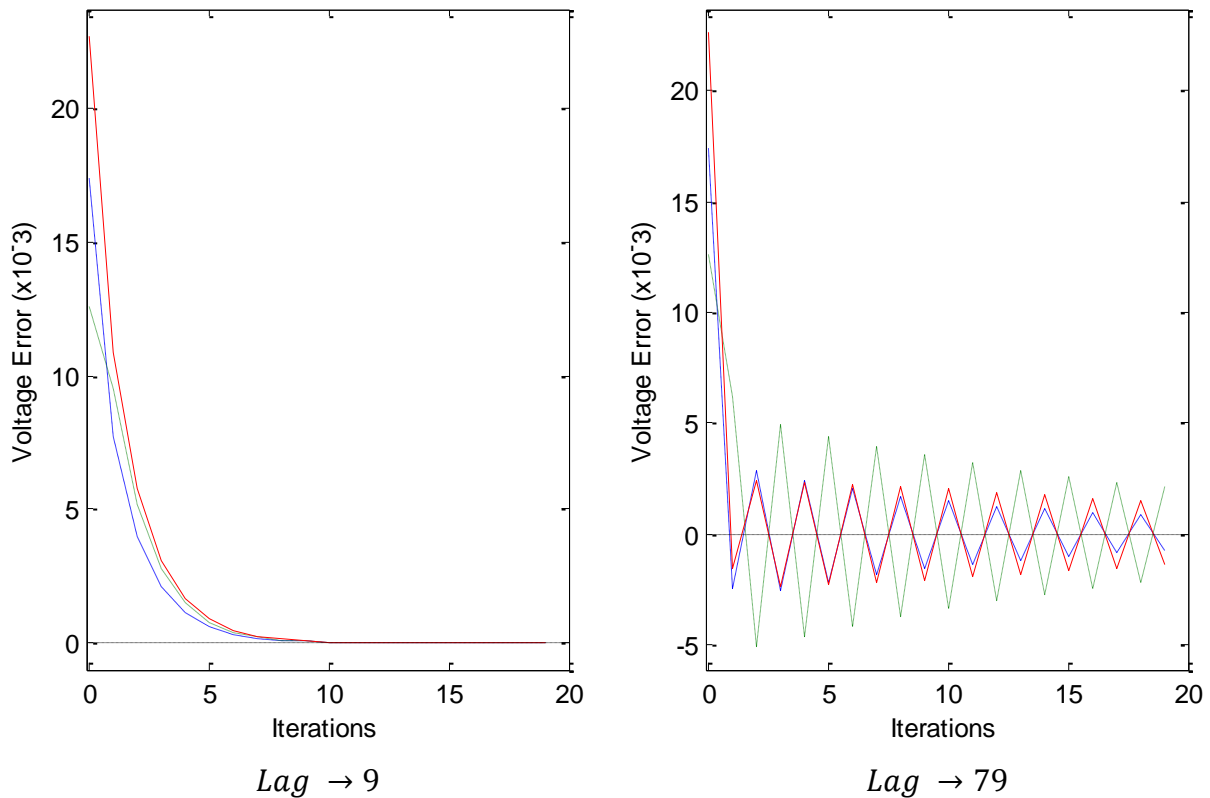
Lag \rightarrow 10



Lag \rightarrow 62

Figs. 4.9 and 4.10 Evolution of the state variable error for the evenly-distributed per phase study model 5, with $[k] = 0.95[k_{osc}]$ (left) and $[k] = 1.95[k_{osc}]$ (right), up to twenty iterations.

Study Model #6



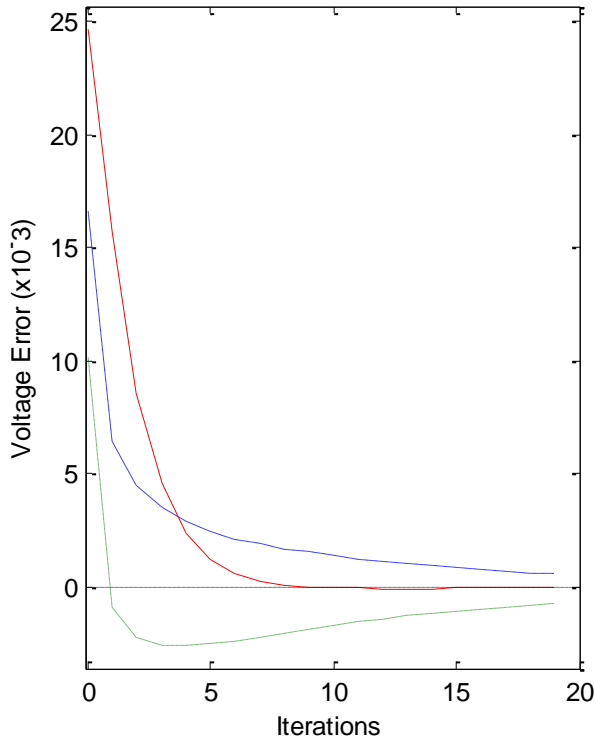
Figs. 4.11 and 4.12 Evolution of the state variable error for the evenly-distributed per phase study model 6, with $[k] = 0.95[k_{osc}]$ (left) and $[k] = 1.95[k_{osc}]$ (right), up to twenty iterations.

The Lag below each graph refers to the number of necessary iterations until $\max|V_i - V^*| \leq 10^{-4}$ and, to reiterate, the graphs colors refer to each of the generators as presented in Tables I and II.

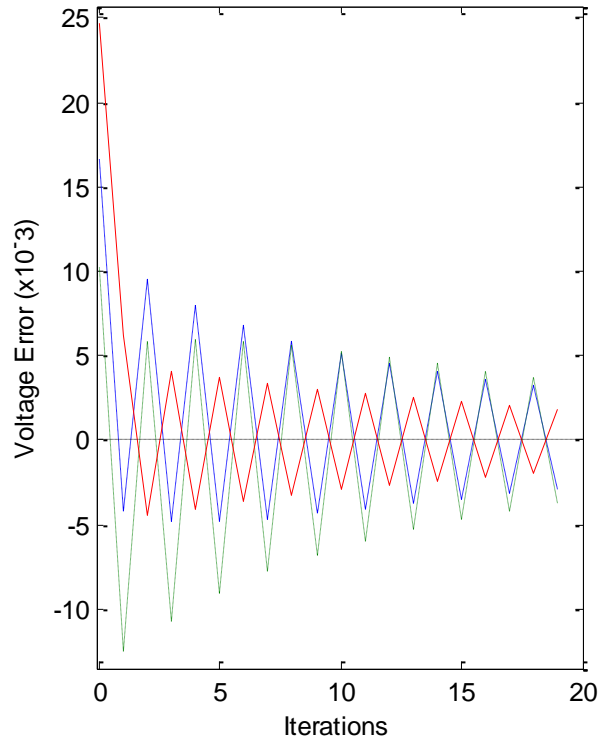
As predicted, with each given overall power gain, all the generators connected to the grid managed to successfully correct their own voltage deviation, relying solely on their own autonomous control system. From the left graphs, we immediately notice that when the system is overdamped, and despite the dissimilar initial voltage values, all error curves tend to coalesce together, approaching V^* at the same rate after the first few iterations. This can also be verified for system's where one or more of the initial voltages start below V^* . The algorithm's lag is near constant for $[k] = 0.95[k_{osc}]$, likely owing its slight differences to the disparity in V^0 for each model. For $[k] = 1.95[k_{osc}]$, the speed with which the error amplitude decays is visibly more distinct for each studied configuration. Though certainly dependent on the relative positioning of the DERs, unlike with was the case with the voltage rises, it seems that there's no pattern from which we can infer how the configuration itself affects the speed. However, as we can see in the oscillating wave graphs, two of the errors invariably become in phase opposition to the remaining third. Moreover, the total sum of these three errors rapidly tends towards zero, well within the 20 iterations.

Moving to the unevenly distributed models:

Study Model #7



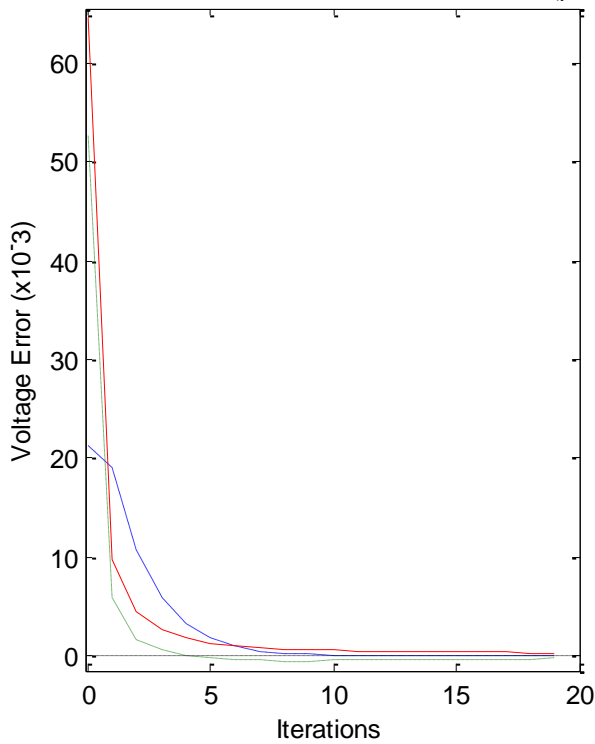
Lag \rightarrow 40



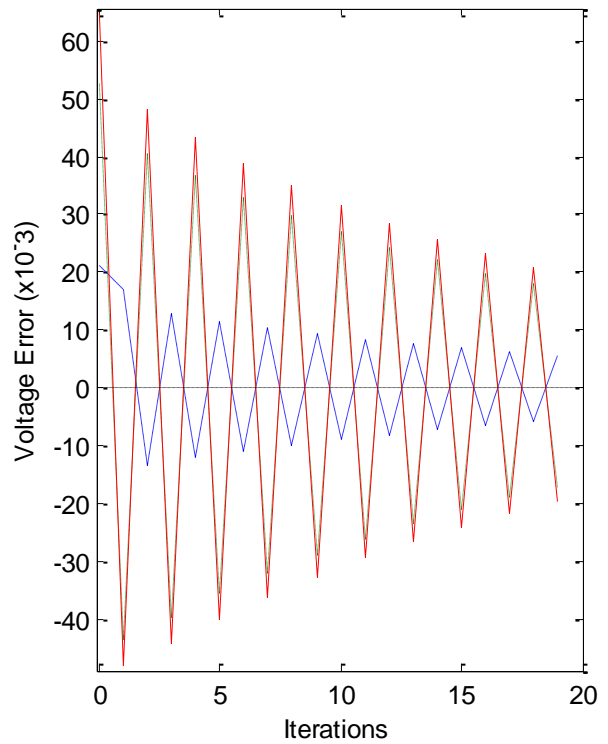
Lag \rightarrow 90

Figs. 4.13 and 4.14 Evolution of the state variable error for the unevenly-distributed per phase study model 7, with $[k] = 0.95[k_{osc}]$ (left) and $[k] = 1.95[k_{osc}]$ (right), up to twenty iterations.

Study Model #8



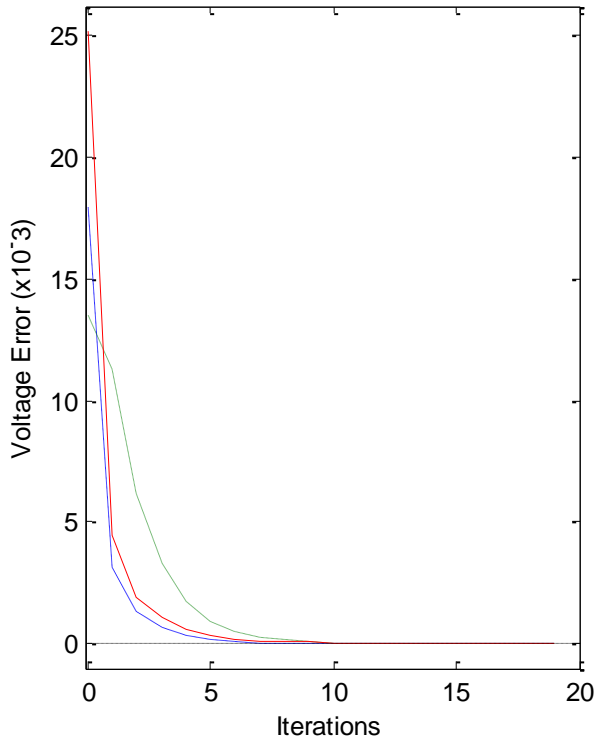
Lag \rightarrow 36



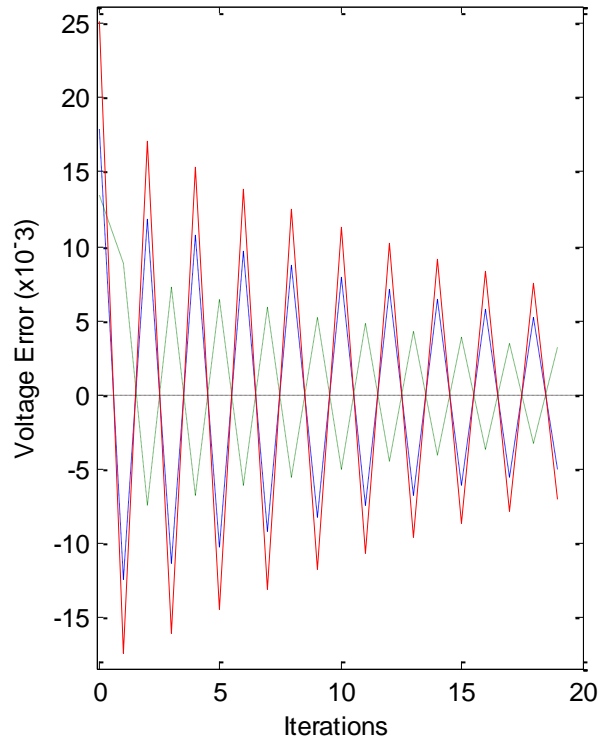
Lag \rightarrow 123

Figs. 4.15 and 4.16 Evolution of the state variable error for the unevenly-distributed per phase study model 8, with $[k] = 0.95[k_{osc}]$ (left) and $[k] = 1.95[k_{osc}]$ (right), up to twenty iterations.

Study Model #9



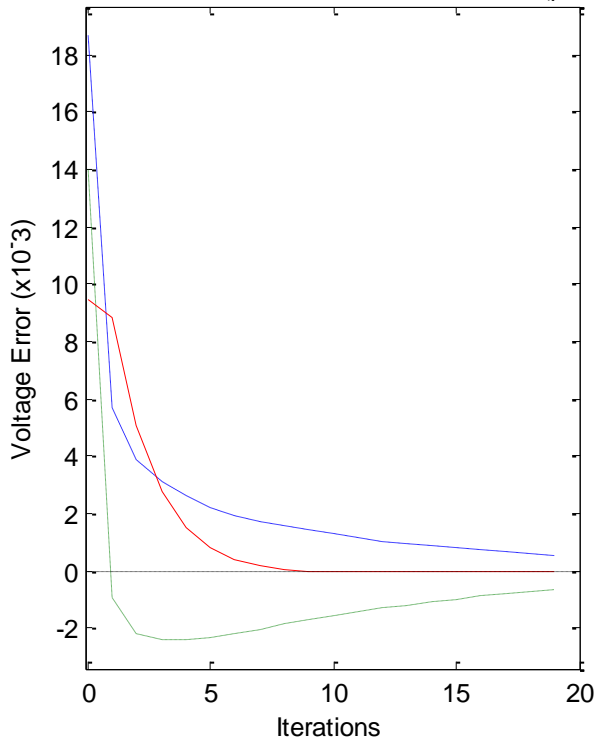
Lag → 9



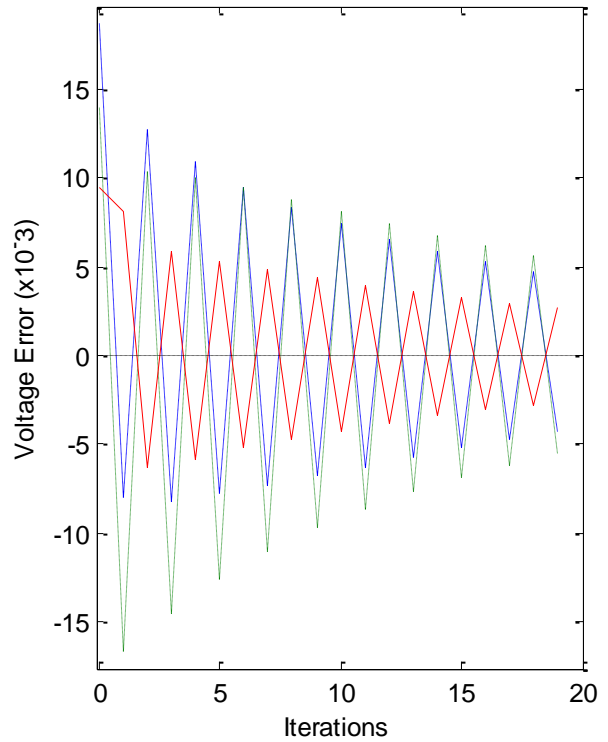
Lag → 103

Figs. 4.17 and 4.18 Evolution of the state variable error for the unevenly-distributed per phase study model 9, with $[k] = 0.95[k_{osc}]$ (left) and $[k] = 1.95[k_{osc}]$ (right), up to twenty iterations.

Study Model #10



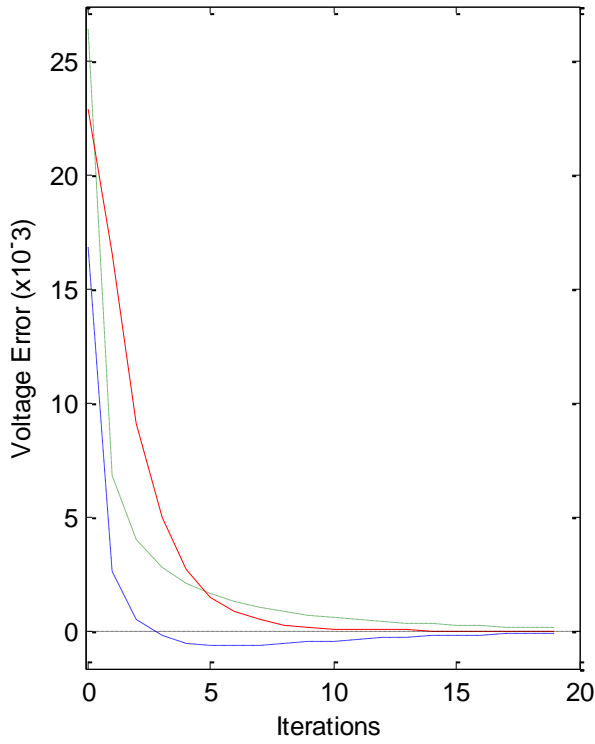
Lag → 40



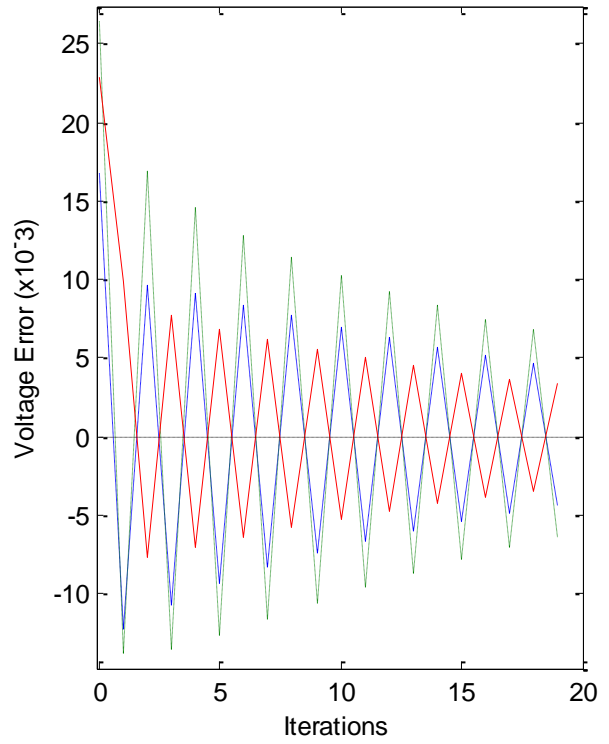
Lag → 97

Figs. 4.19 and 4.20 Evolution of the state variable error for the unevenly-distributed per phase study model 10, with $[k] = 0.95[k_{osc}]$ (left) and $[k] = 1.95[k_{osc}]$ (right), up to twenty iterations.

Study Model #11



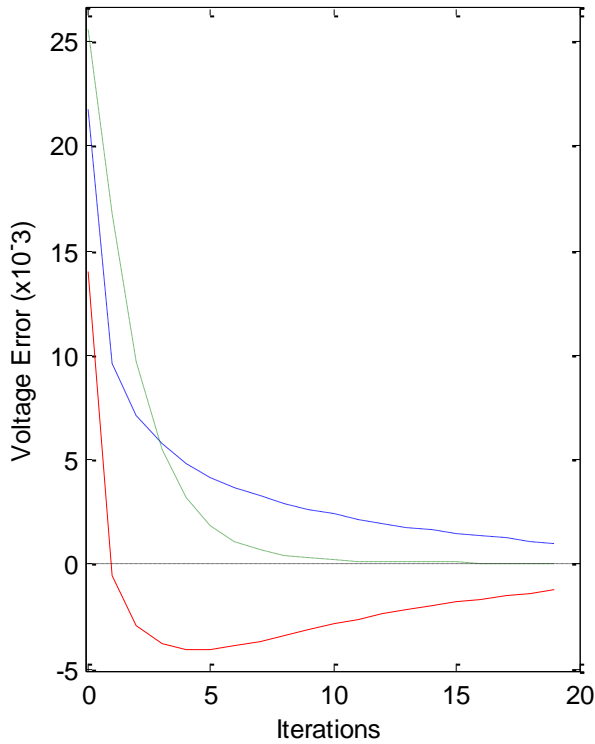
Lag \rightarrow 21



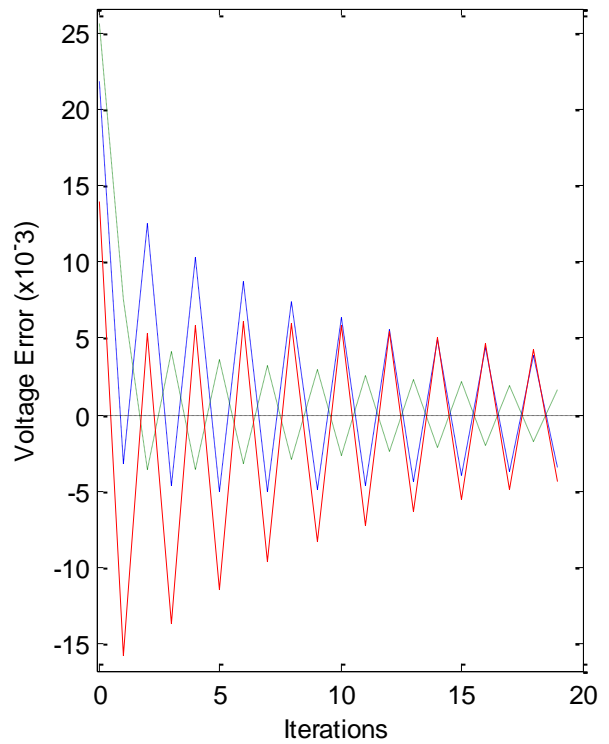
Lag \rightarrow 101

Figs. 4.21 and 4.22 Evolution of the state variable error for the unevenly-distributed per phase study model 11, with $k = 0.95[k_{osc}]$ (left) and $k = 1.95[k_{osc}]$ (right), up to twenty iterations.

Study Model #12



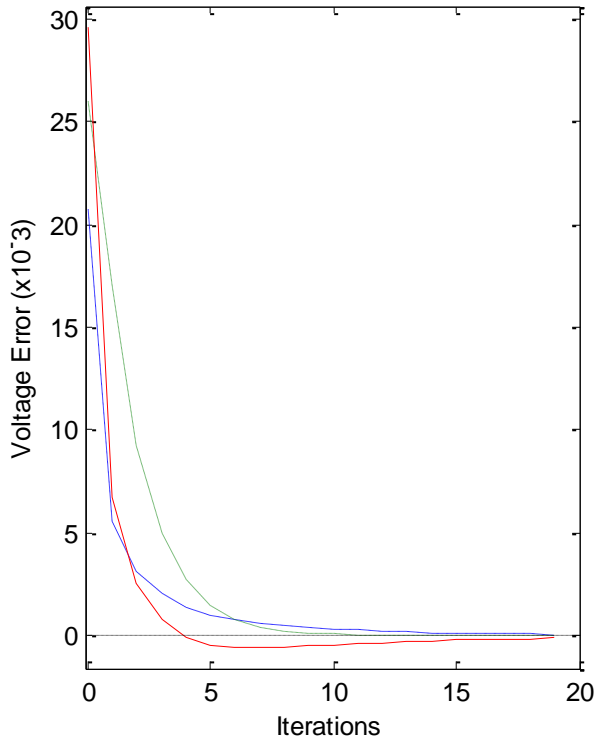
Lag \rightarrow 46



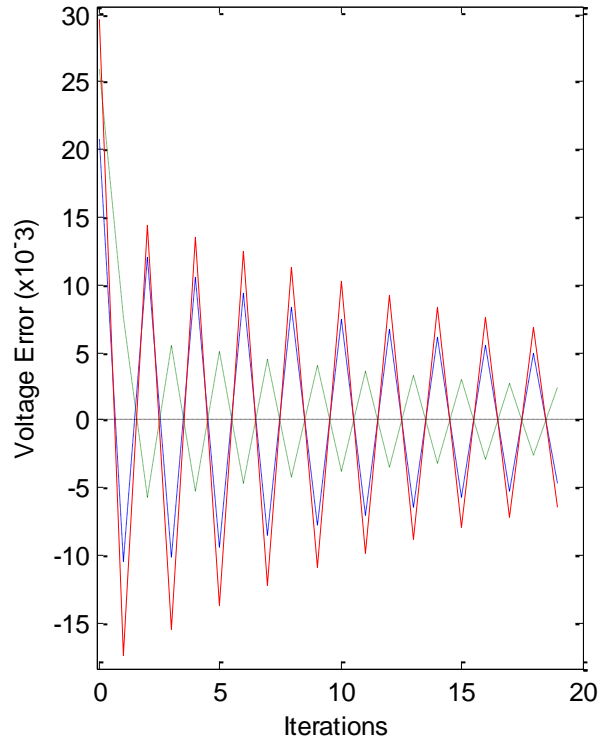
Lag \rightarrow 93

Figs. 4.23 and 4.24 Evolution of the state variable error for the unevenly-distributed per phase study model 12, with $k = 0.95[k_{osc}]$ (left) and $k = 1.95[k_{osc}]$ (right), up to twenty iterations.

Study Model #13



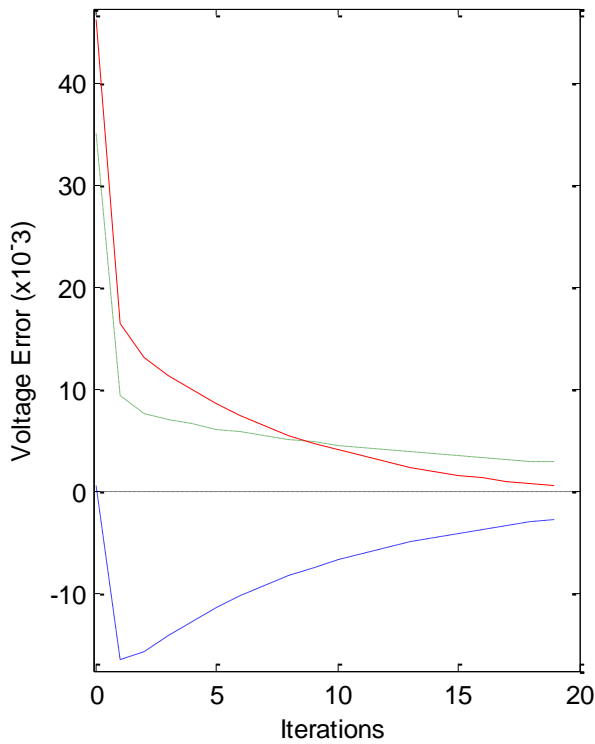
Lag \rightarrow 20



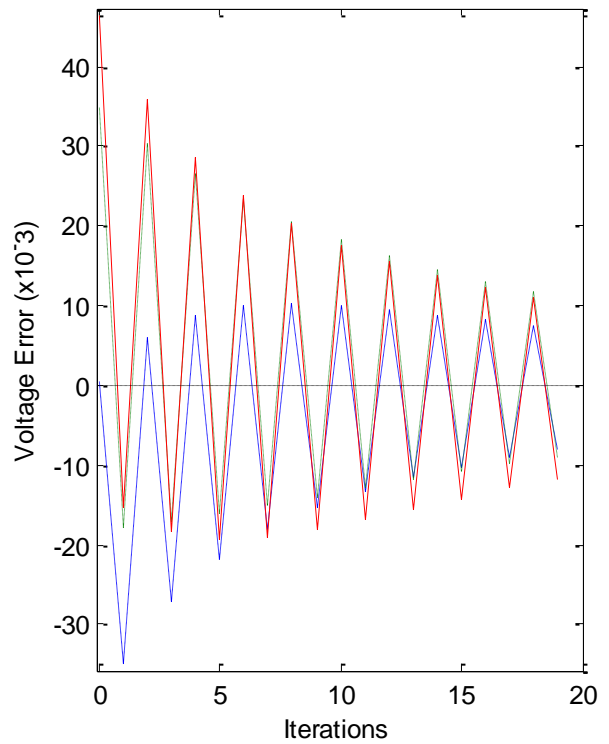
Lag \rightarrow 101

Figs. 4.25 and 4.26 Evolution of the state variable error for the unevenly-distributed per phase study model 13, with $[k] = 0.95[k_{osc}]$ (left) and $[k] = 1.95[k_{osc}]$ (right), up to twenty iterations.

Study Model #14



Lag \rightarrow 98



Lag \rightarrow 111

Figs. 4.27 and 4.28 Evolution of the state variable error for the unevenly-distributed per phase study model 14, with $[k] = 0.95[k_{osc}]$ (left) and $[k] = 1.95[k_{osc}]$ (right), up to twenty iterations.

As it was to be expected, with an unbalanced distribution of the DERs through the three phases, it takes a greater amount of time for the algorithm to correct the voltage deviation, in both instances. In addition, the error curves for the under-oscillation gain no longer tend to a single exponential arc, and the speed throughout the models lacks the consistency it had. The pattern of two nodal voltages being in phase opposition to a third is however present still, given the reciprocal nature for DERs' voltage when connected to the same phase. The sole exception is logically 14, where all three generators are coupled to the same line and, thus, all in phase. One conclusion we can arrive at is that, speed-wise, putting as much distance possible between same phase connected generators improves the algorithm's performance significantly, as exemplified by models 9, 11 and 13 when compared with the remainder.

In matrix terms, this is seen by the diagonal terms of the downstream generators being superior to their non-diagonal counterparts, that's to say those in the same line, by an additional margin. For example, the sole difference between models 12 and 13 is that the latter's R_{33} is 33% greater than the former's. However, this seemingly minute difference results in the process's speed being cut in more than half, despite 13 having a larger set of initial voltages. (For test purposes, the same was simulated by giving both the same initial deviation, and this observation still holds.)

In succinct, the greater the difference between the (absolute) values of a matrix's diagonal and the sum of their respective non-diagonal terms, be it of its row or column, the faster the algorithm will be able to correct the voltage error for the corresponding configuration. That is to say, the closer $[A]$ is to a diagonally dominant matrix the more the system's performance will be improved. This is in line with our previous conclusion that the algorithm's efficiency is directly correlated with the influence each DER exerts on one another: the lesser the better.

4.3 Power Gains and Optimal Performance

Figures 4.1 through 4.28 are representative of the voltage error behavior for a power gain close to its respective thresholds for oscillation (left) and instability (right). It becomes clear when comparing both sides, that $[k]$ plays a major influence in determining the speed with which the algorithm can eliminate the given discrepancy. One can then ask the question which specific $[k]$ can provide the best speed for each system, and whether or not we can determine an universal value for it, applicable to all configurations. Again making use of the previously used MATLAB code, through trial and error, we've managed to find the range of gains that produce the shortest lag:

Table XI
Optimal Gains for Evenly
Distributed per Phase Models

Model #	$\alpha[k_{osc}]$	Lag
1	1.31 – 1.60	7
2	1.32 – 1.51	6
3	1.25 – 1.56	6
4	1.29 – 1.61	6
5	1.47 – 1.48	5
6	1.20 – 1.51	6

Table XII
Optimal Gains for Unevenly
Distributed per Phase Models

Model #	$\alpha[k_{osc}]$	Lag
7	1.65 – 1.78	22
8	1.56 – 1.70	21
9	1.21 – 1.37	6
10	1.64 – 1.77	22
11	1.46 – 1.66	13
12	1.73 – 1.78	24
13	1.46 – 1.63	12
14	1.84 – 1.86	49

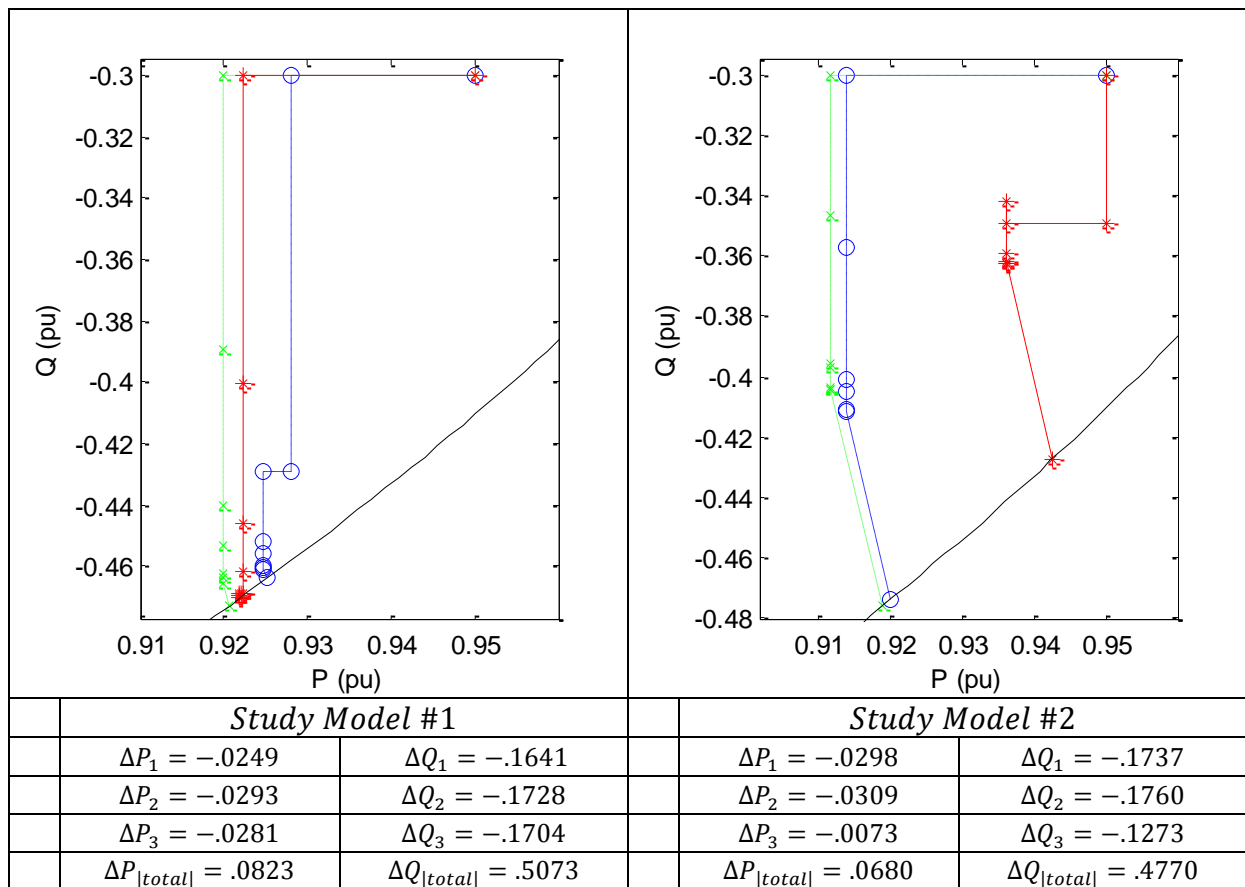
Again, as we've seen so far, both the best achieved speeds and the range of gains that allow them follow the same logic as they did when we studied the results illustrated in the graphs above. A more even and spaced-out distribution of the DERs results in a more rapid resolution of the deviation, with a lower percentage of $[k_{osc}]$ needed. (Case in point, we notice that model 9's speed is identical to most evenly-distributed models, and his initial range is also similar, reinforcing the previously made statement.) While the optimal percentage of $[k_{osc}]$ rises the higher the difference between V^0 and V^* , we can still define the best overall gain based on the typical range of values we can expect for instances of voltage rise. Based on the obtained initial values and the above factors, setting α to 1.5 appears to be the best compromise, should we need to pick a gain to apply it for all configurations. In relation to the inverse diagonal matrix $[R_I]$ this is an approximate factor of 1.2 for models 1 through 6, 0.8 for 7 through 13 and 0.6 for 14. Should we want to avoid any form of oscillation, $[k] = [k_{osc}]$ is then the best possible power gain.

Having witnessed the behavior of the nodal voltage in each connection node, we now move to the study of the algorithm's control variables, that is the injected active P and reactive power Q , during the same iterative process seen above. Aside from the graphical evolution of both variables, we'll take a vested interest in the required variation of injected power necessary to achieve the intended goal of eliminating the same presented instance of overvoltage. Unlike the case with the voltage study, where p_0 and q_0 only determined if it was possible for the algorithm to converge on V^* per (26) and (28), due to the presence of the limiting factors of S_M and P_A these initial values will affect the final outcome of the process, in both behavior and final value.

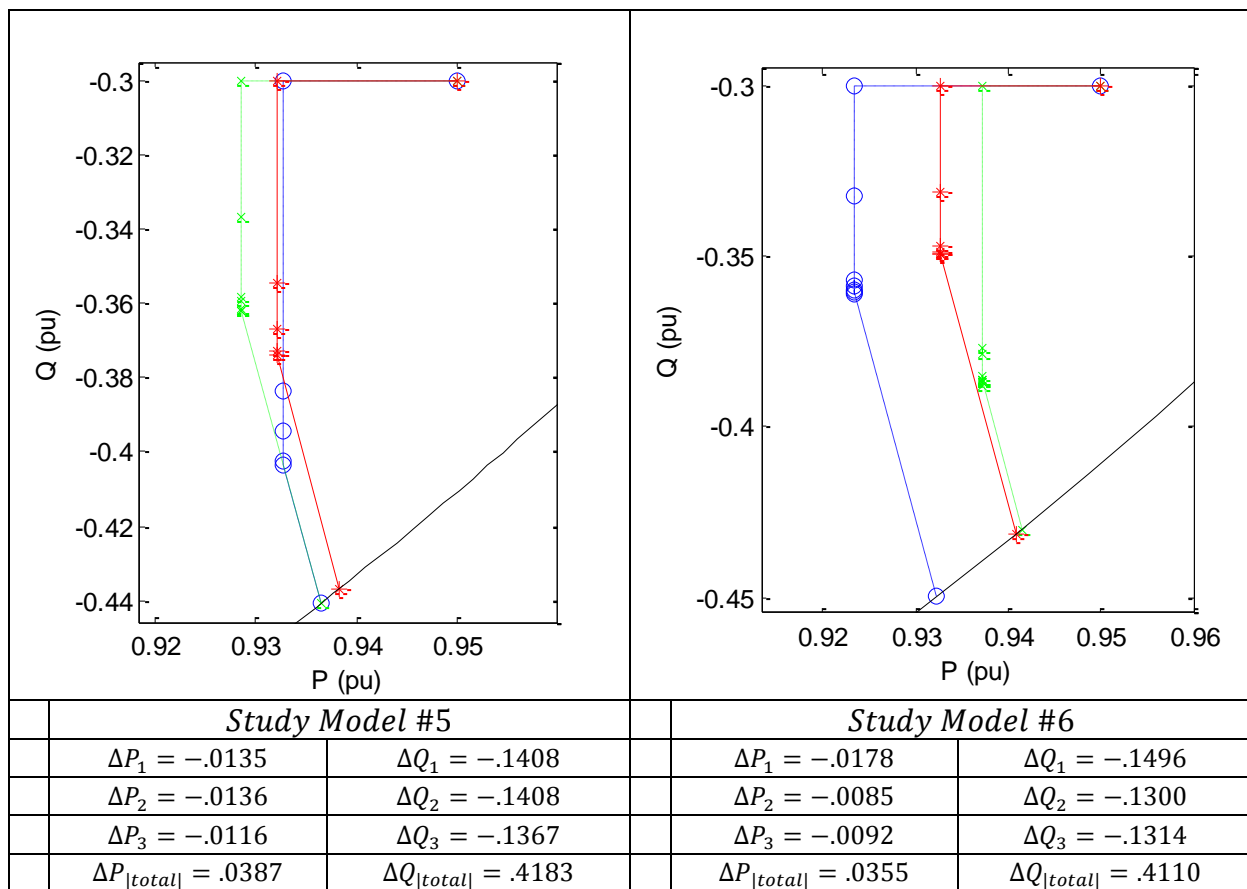
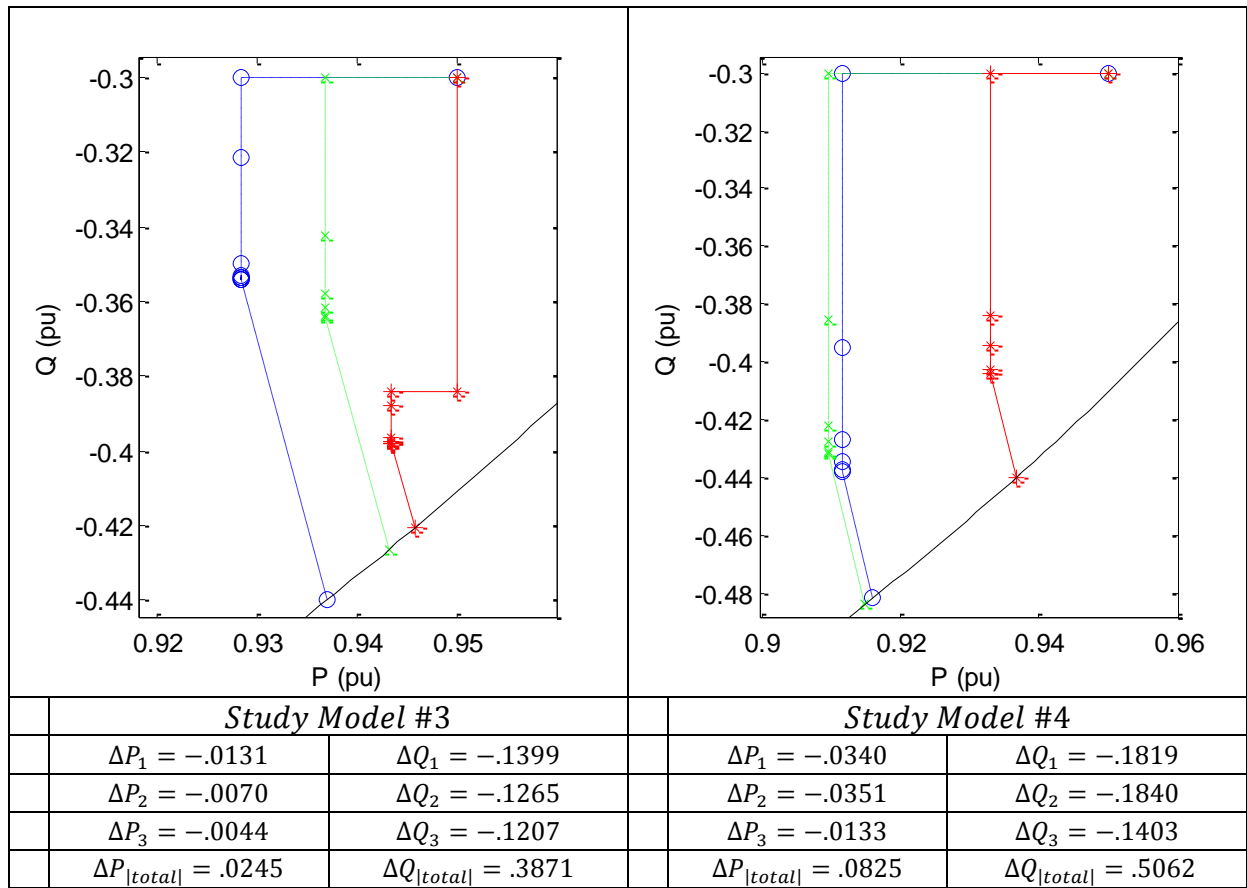
4.4 Active and Reactive Power Curtailment

The chosen controller power gain will have an effect on the difference between the yielded and initial values, ΔP and ΔQ seen in (8), as well. However, seeing that C_0 is independent of $[k]$, the solution line is ultimately the same regardless of the chosen value for overall gain, or even the logical steps the algorithm takes. This means that $[k]$ only determines where in line (27) will the controller lead a DER's $[p, q]$ set to, and as such we can always readjust the coordinates to fit any criteria we wish. This can be done with each iteration, as moving along a $-x \circ r^{-1}$ slope line does not change the voltage profile, or at the very end of the process. To demonstrate this property of (27) type lines, we've showcase the latter option in the graphs below, using the already determined $[k] = 1.5[k_{osc}]$. As we'll want to curtail the drop in active power first and foremost, the final shift is focused on obtaining the lowest possible ΔP . Therefore, each value below the graphs represent the minimal variations of active power necessary to correct the deviation for each model case, along with the sum of their absolute values.

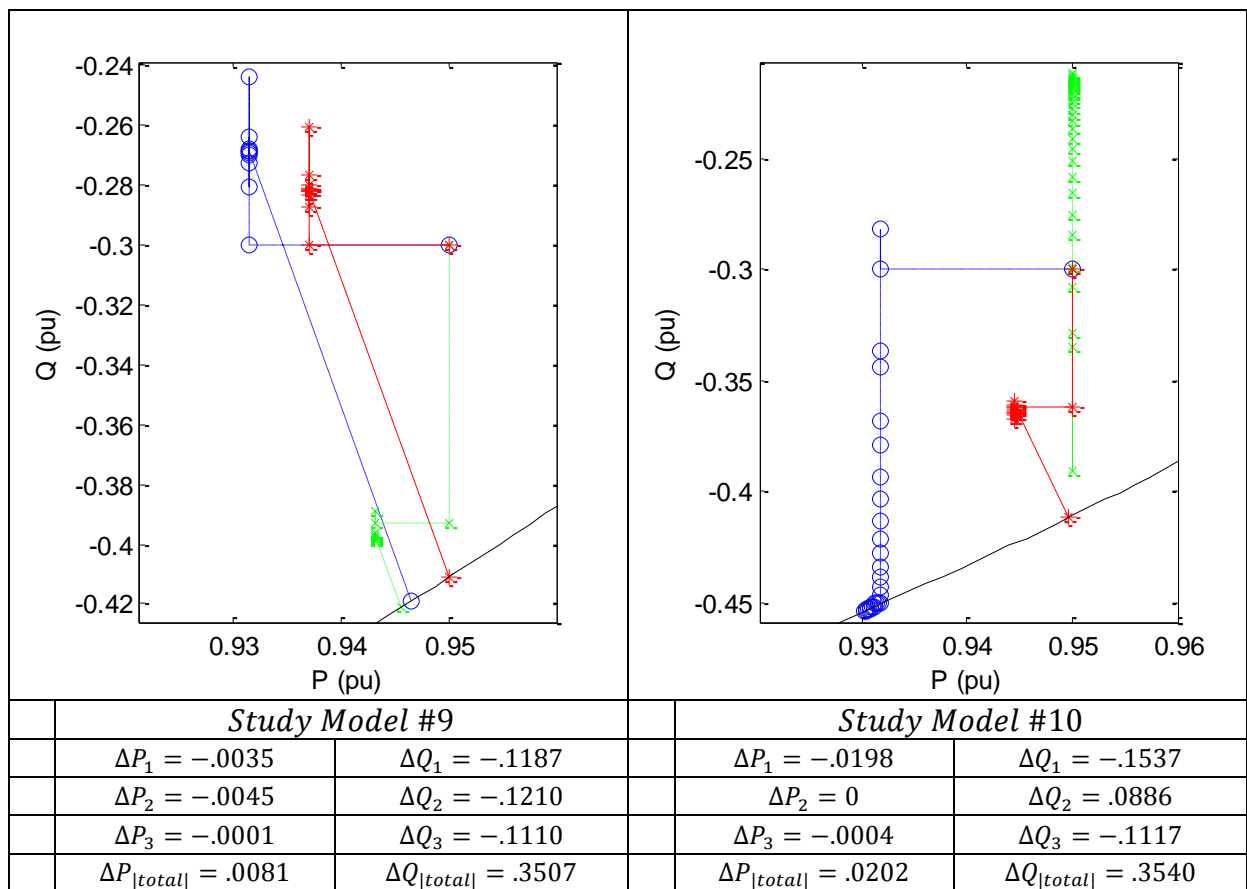
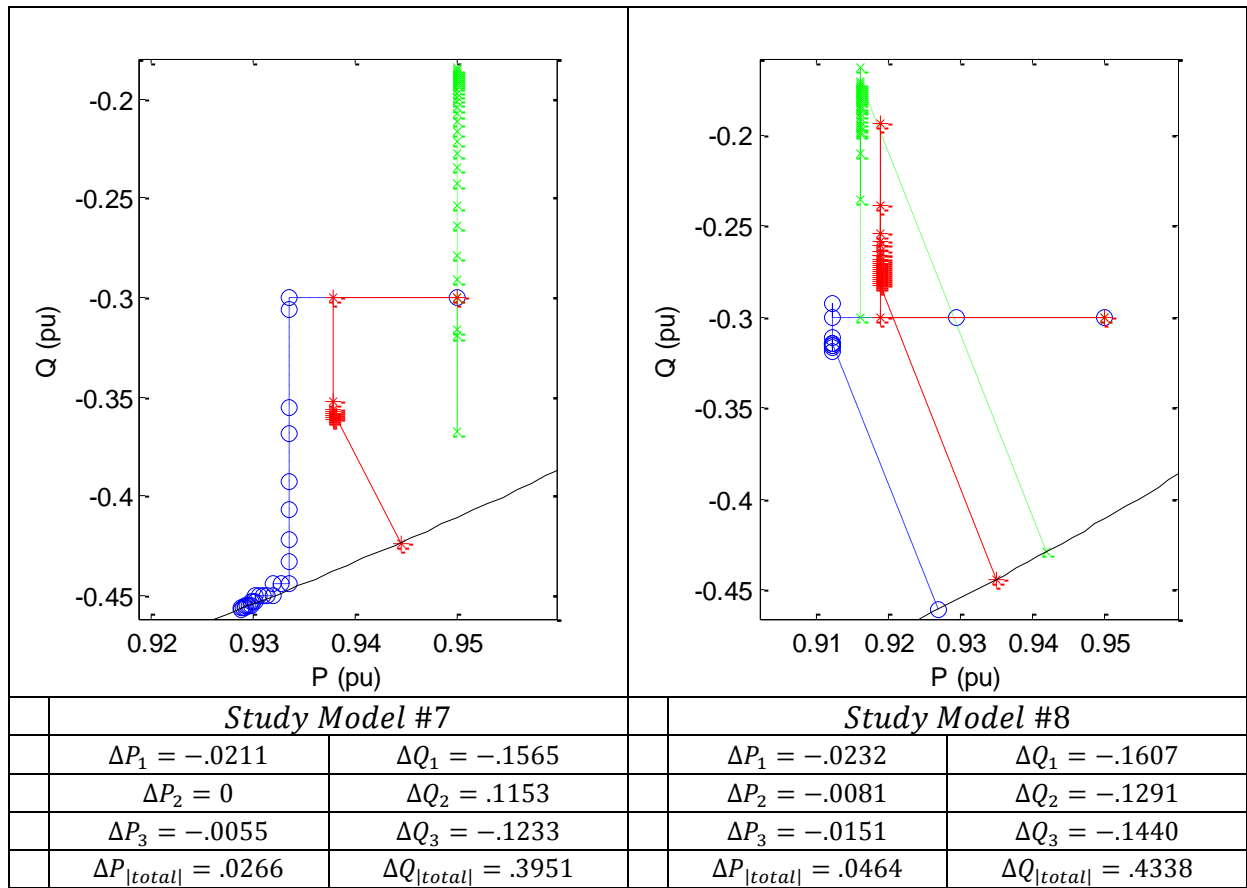
For every generator, again color coded according to Tables I and II, we've picked a $p_0 = 0.95$ and $q_0 = -0.3$, while V_0 is the same as in the voltage error study (Tables IX and X). Below each graph is the variation of active and reactive power at the end of the iterative process, for each generator and the absolute total, after a readjustment along the respective solution line set (27) as to minimize ΔP .



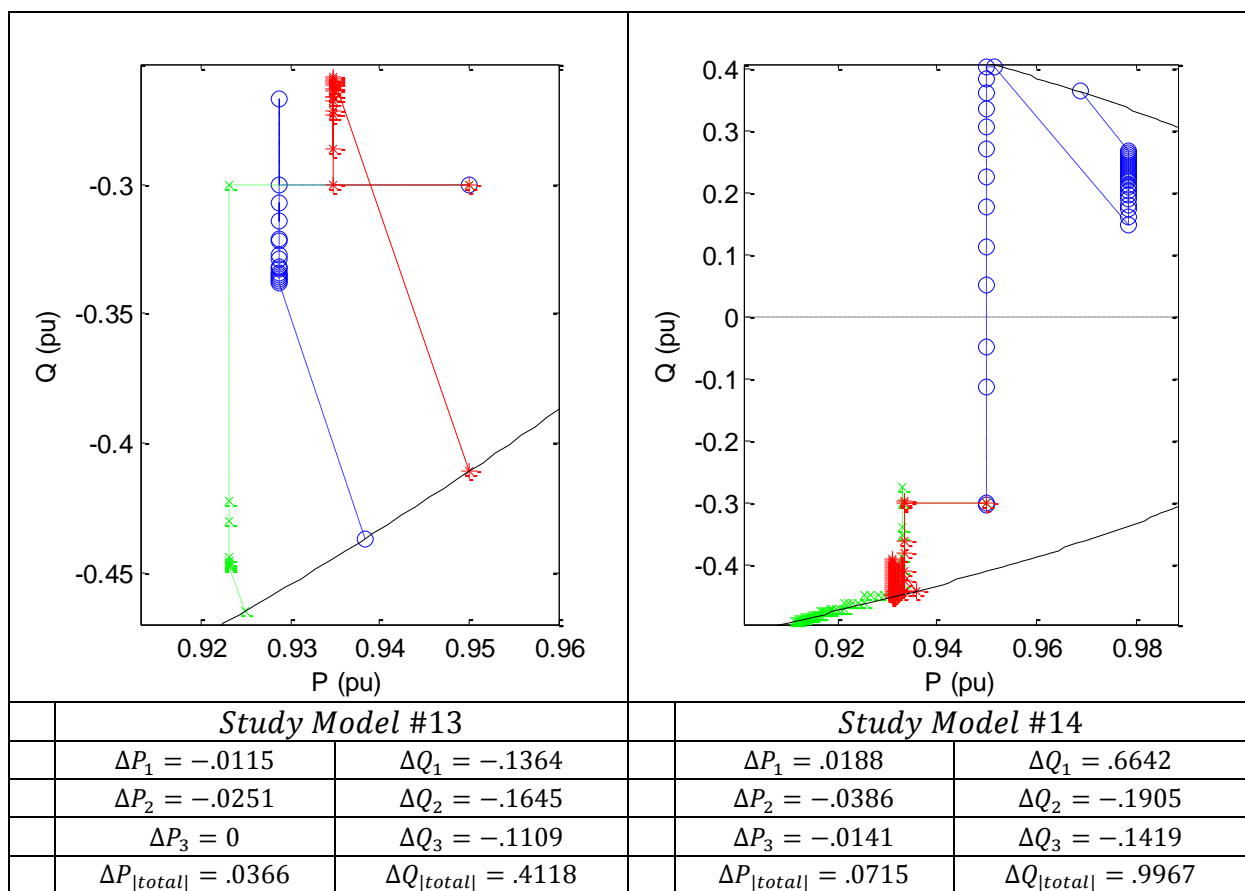
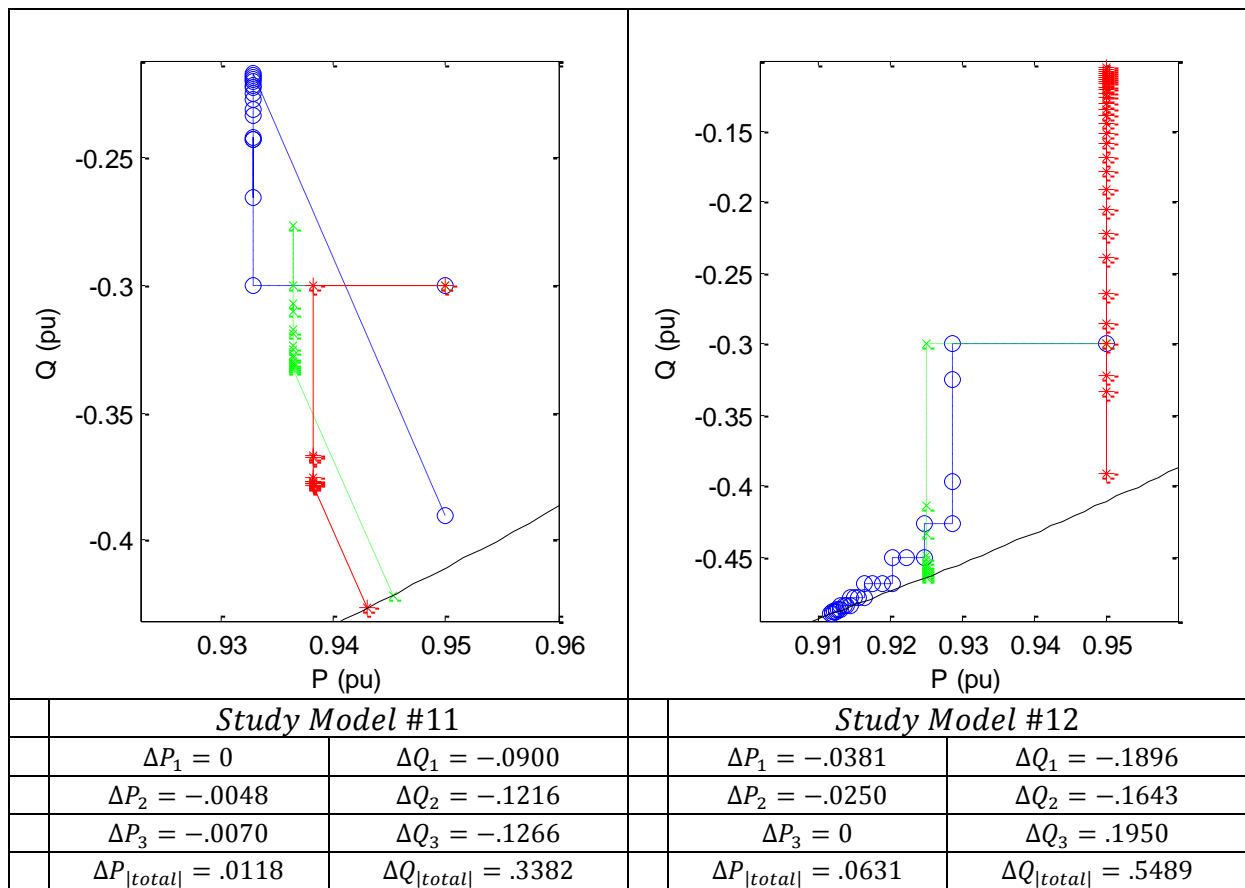
Figs. 4.29 to 4.30 Evolution of the control variables for the studied models 1 and 2, with $[k] = 1.5[k_{osc}]$, up to a hundred iterations.



Figs. 4.31 to 4.34 Evolution of the control variables for the studied models 3 through 6, with $[k] = 1.5[k_{osc}]$, up to a hundred iterations.



Figs. 4.35 to 4.38 Evolution of the control variables for the studied models 7 through 10, with $[k] = 1.5[k_{osc}]$, up to a hundred iterations.



Figs. 4.39 to 4.42 Evolution of the control variables for the studied models 11 through 14, with $[k] = 1.5[k_{osc}]$, up to a hundred iterations.

We can see that, for the schemes with more than one generator per phase (7 through 14), $\Delta P_{|total|}$ is, on average, less than that required when there's only one DER per phase, even when the general initial voltage error for the former is greater or roughly equal than the latter's. This occurs due to the fact that, as explained in Chapter 2, any change in the nodal voltage of a DER, rise or fall, will produce an identical response along the line. Thus, because of the way the DG network is configured, same phase-connected generators will mutually help each other eliminating their overvoltage, lessening the needed decrement in injected power for each one. In turn, this also abates the induced voltage hike in the other two-phases, allowing for a similarly smaller power shift to correct the deviation as the controller no longer has to compensate as much for said increase. The differences between each model's various ΔP are also mirrored by the obtained ΔQ .

However, this can also work against the system. As when those two error signals become opposite, causing the controllers to start working against each other, one increasing the injected power to rise the nodal voltage to V^* , and the other doing the opposite. This can lead to situations (such as in 10, 12 and 14) where the final difference for certain generators is positive, and the sum total is higher compared with the other cases. This means that a DER ultimately ended up having to injected *more* power to correct a rise in its nodal voltage, which can naturally be problematic given the set restrictions. This incongruity is all more the detrimental during the first iterations, where the error amplitude is greater, and, because of it, is more serious when the $V^0 - V^*$ values, and to a lesser degree those of the next iterations, are in signal opposition. Indeed, for model 14, a small decrement of 0.01 in V_1^0 is enough to cause a violation of (26) and (28).

Aside from this, the other significant aspect we can detect is the diagonal shifts that occur at the end of the process, as a result of the readjustment through (27). In all cases the network's voltage profile remains unchanged, similarly as to those exemplified in Fig. 4.1 to Fig. 4.28. The trace it leaves allows to ascertain the relative positioning of each generators' solution set for the given initial parameters. It also permits a more accurate gauging of the relative shifts in active power, independent of the chosen gain, as it will always lead to the same results regardless of $[k]$. Moreover, using the properties of (27) we can also manipulate the injected power to suit our needs, whether it be to minimize ΔQ instead, fix Q/P to a certain ratio, or even the set a desired power factor.

4.5 Additional Alteration to the Algorithm

Another poignant detail, and again for 14, we notice that there are two diagonal shifts in the graph. The reason for this is, due to the way it was programmed, the algorithm became ‘stuck’ if it needed to increase either the injected active or reactive power, but couldn’t because of the placed restrictions. Thus, we needed to add an extension to the code as to ‘unstuck’ it. With the chosen method, should the algorithm detect that a shift in active power will go over the limit (either S_M or P_A), the power coordinates will shift down a $-x \circ r^{-1}$ slope line, settling in the midway point between the two points where it intercepts the limit semi-circumference. Seeing as this line has the same slope as (27), the voltage throughout this readjustment also remains the same, while freeing up the highest ‘breathing space’ available for the controller to operate on. In MATLAB, this is achieved through an additional function in the algorithm. What we see in the graph for 14 is a consequence of this, the leftmost line being the mid-process shift, and the other the one to minimize ΔP .

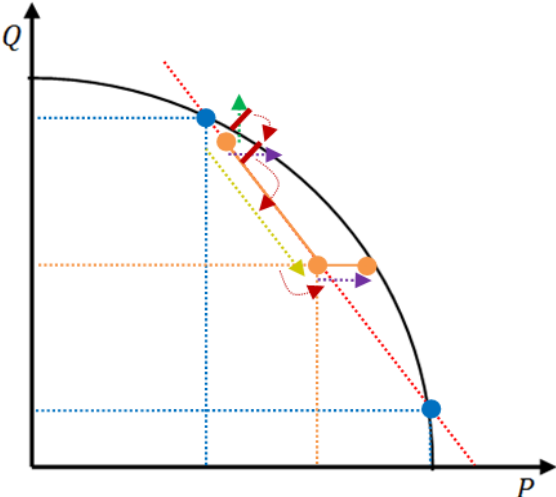


Fig. 4.43 $[P, Q]$ plane hypothetical representations the logical steps taken by the controller when applying the abovementioned function, represented by the dashed yellow arrow. The dotted red line represents the $-x \circ r^{-1}$ slope line. Note that both purple arrows, depicting the active power shift, have the same length.

Chapter 5

Expanding the Study Model

As observed in the previous section, through MATLAB simulations we've managed to obtain a theoretical result demonstrating the potential feasibility of the proposed decentralized voltage control strategy. Despite a lack of communication between the connected DERs, we've determined that with a proper power gain value $[k]$ we're able to correct instances of voltage rise in the connection nodes. However, at the same time, we've also ascertained how the initial conditions for voltage (V^0) and injected power (p^0 and q^0) can affect this process, possibly even precluding it. Namely, though the system may be able to converge, the physical limitations of the equipment (mainly P_A and S_M) can potentially hinder this correction. Moreover, up until this point, all the work realized has been based on a 3bus-by-3phase grid model with only 3 DERs connected to it. It's well within reasonable expectation that any feeder network in a real life scenario will have a higher number of generators injecting power into it at any given time. As such, it becomes imperative for our study to expand the LV circuit model, the objective being to analyze the impact on the behavior of the control and state variables as the resistance matrix $[R]$ gradually morphs and, more crucially, the viability of the autonomous control scheme as it does.

Therefore, this chapter is dedicated to examining the impact these additions will produce on the autonomous system model. To begin with, we'll be making use of the same 3bus-by-3phase grid, to appraise the effects of concentrating DERs within the same area, then expanding it beyond, into a 3-by- n network, for the purposes of studying the consequences of spacing out clusters of generation. The main objective will be to evaluate how these changes influence the stability of the system, by again evaluating the previously discussed assessment criteria of using the eigenvalues of $[A] = [I] - [R][k]$, and its capability given the limitations on power output.

5.1 Concentration of Distributed Generation

Our first step will be to evaluate what occurs when we gradually 'fill' the nine node circuit grid described in Chapter 2, until we connect an equal number of DERs. To assess the relative stability between each case, we'll again gauge the eigenvalue gradients Δ_i and the diagonal terms of the maximum stability overall gain matrix $[k_{stb}]$. Due to the number of possible combinations for generator distribution throughout the network, we elected to pick the worst possible cases for each, those being the distribution that generates the highest possible $|\lambda_i|$.

5.1.1 Effects on Stability

Retreading the same steps seen in Chapter 2, particularly (20), by first obtaining the eigenvalues with a common gain factor $\alpha = 1$, we can then acquire their gradients and, subsequently, the $[k_{stb}]$ with their highest absolute value.

Table XIII
Maximum Eigenvalue Gradient and respective Common Gain Factor

Number of DERs	Max $ \Delta_i([R, K]) $	$\alpha = k_{stb_{ii}}/K_{ii}$
1	1	2
2	1.8662	1.0717
3	2.5949	0.7707
4	2.6843	0.7451
5	2.8798	0.6945
6	3.2436	0.6166
7	3.2436	0.6166
8	3.2436	0.6166
9	3.2436	0.6166

It is not at all surprising to observe that a higher number of connected DERs invariably leads to a necessary decrease in the overall gain to assure the system's stability, yet another indication of its precariousness in relation to the generators. This decrease results from the overarching algorithm struggling to juggle and consolidate the power flow of more generators in order to maintain an adequate voltage profile. It's also worth mentioning that, as we've seen with the 3 generator study models, the combinations that originate the worst results in terms of the eigenvalues of $[A] = [I] - [R][k]$ are those that concentrate more DERs in one phase, in lieu of distributing them more evenly through RST. For example, with six generators, a balanced 2-per-phase distribution results in a more robust system than 3-per-phase (with one being empty), and any combination in between. Additionally, their placement relative to the source bus also impacts the stability, though to a lesser degree than that of the phase distribution. Interestingly, it also seems that maximum gradient caps off when two of the phases are completely filled, starting with upwards of six DERs, and it should be noted that with a full grid two of the gradients have the listed value.

Having seen how the concentration of DERs influences the inherent stability of the autonomous system, we move on towards discussing what implication exist in relation to the initial values of its variables.

As seen in Chapter 3, p^0 , q^0 and V^0 play an important role in determining whether or not the system is physically able to correct its voltage profile due to the generator's limitations, represented chiefly by S_M and P_A . The initial value for the state variable is in itself mostly dependent on the configuration of the DERs, due to the aforementioned phenomenon of voltage rise that occurs in three-phase LV grids. One of the first conclusions we can arrive at is that a fuller, but still balanced, grid results in a more uniform voltage profile. That is, there's a lessening discrepancy between the various V_0 as we connect more generators, provided there's an equal distribution through RST , much like what was witnessed in Chapter 4.

The issue pertaining to the magnitude of the voltage deviation is mostly tied with p_0 and q_0 . Whether over or under V^* , a successful correction is dependent on whether there's enough 'room' for the system to maneuver the two variables in, given the existing caps. This was seen in Chapter 3 with (28). Instances of a nodal voltage dropping below the desired value (mainly as a result of a voltage rise in another phase and/or a drop somewhere in the same phase) are thus more prejudicial to the system than it spiking, as that would entail an increase in that DER's injected power to counteract it. Due to the abovementioned limits in power output, which given its typical values while on operation are more likely to hinder the system as P_G approaches S_M or P_A , this might prove difficult to accomplish.

Moreover, on account of these induced drops in nodal voltage, there will be situations where some nodal voltages are below V^* while the remainder are still above it. This lends another layer of complexity as one section of the individual controllers tries to compensate the deviation by increasing its power output while the other by decreasing it. As we've seen for model 14, this might even result in a positive change in active power for one or more generators, even though all of its initial voltage values were higher than the desired value. The inclusion of more DERs ultimately means more possible grid configurations, which in turn means more ways that each generator play off each other, exacerbating all of these concerns as we strive predict what kind of ripple effects might originate from such scenarios.

5.1.2 Effects on the Initial Voltage Error

One of such issues pertains to the system's performance. As stated before, it's in our interest that our autonomous control strategy be able to resolve any occurrences of overvoltage to avoid degradation of the associated electrical equipment, and potentially endangering the network's integrity. As the system juggles with an increasing number of DERs, and thus an equally growing number of added elements to the network's power flow, it's natural to assume that the speed with which it can resolve any of these deviation will tend to lower, as seen by the decreasing α in Table XIII. However, one only needs to look at the results presented in Chapter 4 to see that such assumption is not as straightforward as it may appear initially.

There are numerous factors that come into play when influencing with which speed the system acts can act upon any deviations of its voltage profile, not least of which being the magnitude and disparity between the initial voltage values. Both factors are influenced by the DERs' distribution on the grid, which will also determine the weight of the diagonal members in the resistance matrix $[R]$. The multitude of elements derived from the network's configuration alone makes it hard to trace a reliable model based solely on the number of connected generators. To showcase this intrinsic complexity, we've realized similar simulations as those in Table XIII, this time with the intent of obtaining the number of iterations the system requires so that $\max|V_i - V^*| \leq 10^{-4}$, for $\alpha = 0.3$ ($[k]$ near $[k_{osc}]$) and $\alpha = 0.6$ ($[k]$ near $[k_{stb}]$).

Table XIV
Initial Values for the Nodal Voltage and subsequent System Performance

Number of DERs	V^{0*} [pu]	lag	
		$\alpha = 0.3$	$\alpha = 0.6$
1	{ ; 1.1200; }	15	6
2	{ ; 1.1114; 1.1286}	107	52
3	{1.0933; 1.1277; 1.1390}	122	60
4	{1.1030; 1.1363; 1.1493} { ; 1.0913; }	114	57
5	{1.0978; 1.1226; 1.1303} { ; 1.1180; 1.1313}	102	50
6	{1.1032; 1.1217; 1.1351} {1.1045; 1.1226; 1.1330}	80	37
7	{1.1193; 1.1257; 1.1355} {1.1207; 1.1267; 1.1336} { ; 1.0783; }	126	63
8	{1.1225; 1.1189; 1.1184} {1.1238; 1.1198; 1.1163} { ; 1.1208; 1.1195}	121	60
9	{1.1230; 1.1203; 1.1168} {1.1243; 1.1212; 1.1199} {1.1196; 1.1191; 1.1157}	96	64

*values adjusted so that $mean(V^0) = 1.12$ pu for comparative purposes

A cursory glance at the results indicates that, while do we notice a change in the system's performance with incremental DG, such change in lag does not appear to be proportionally related with the amount of generators connected to the feeder grid. As we suspected, it's not the actual number of DERs that influences the speed with which the controlling algorithm can correct disturbances in the network's voltage profile. And, once more in line with conclusions taken in Chapter 4, we can also immediately conclude that a better performance (i.e. speed of correction) is achieved through an oscillatory error response. Still, though we failed to find any proof of causality between performance and the number of DERs, Table XIV nonetheless provides some insight as to how the former is affected by the latter's presence.

The speeds between each setup seem to own their dissimilarity to a variety of factors, not least of which being the initial values for the nodal voltage, both in magnitude and in disparity between one another. This also goes in tandem with the same established rule of thumb that a system acts more efficiently upon deviations of its voltage profile if the DG is balanced throughout its phases. Moreover, the presence of additional non-diagonal members in the resistance matrix $[R]$, that will influence each DER controller, also adversely affects the algorithm's speed as it adds more varying elements to the multinomial expression of the error, as stated by (10). Taking into account all of these factors, we can get situations like a fully-filled grid (9 DERs) that, despite the smaller magnitude and fewer discrepancies between its nodal voltages, remains slower than a system with two thirds of its generation (6 DERs). Yet, at the same time, the latter is also faster than that of a feeder network with only three generators. Looking at the behavior of nodal voltage error for two of the presented cases, and noting that each colored line in the below graphs represents a different DER:

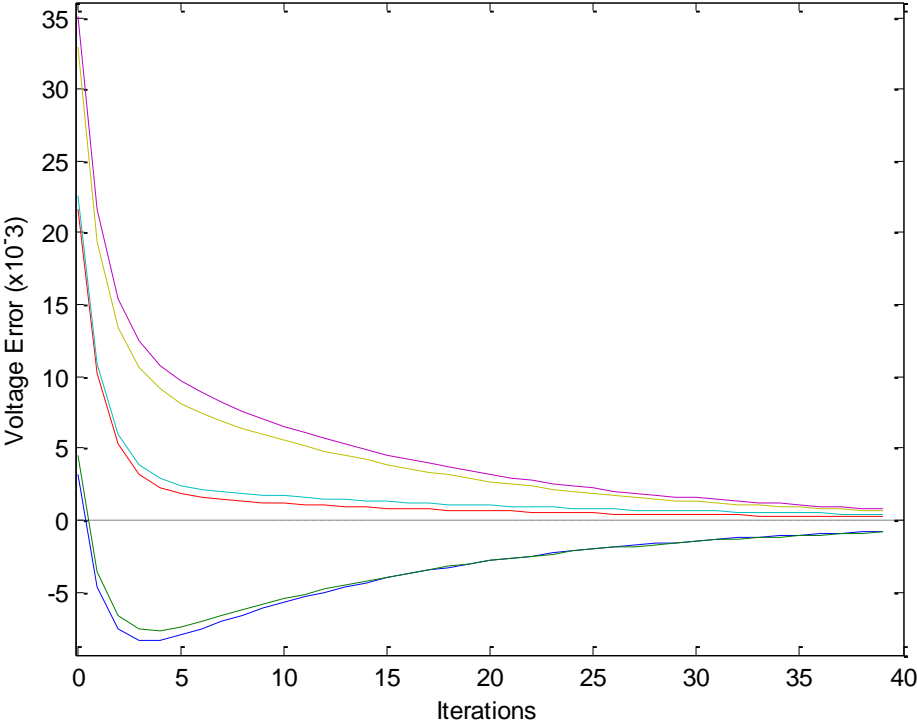


Fig. 5.1 Evolution of the state variable error with 6 DERs, for $\alpha = 0.3$, with the same initial values as the ones listed in Table XIV.

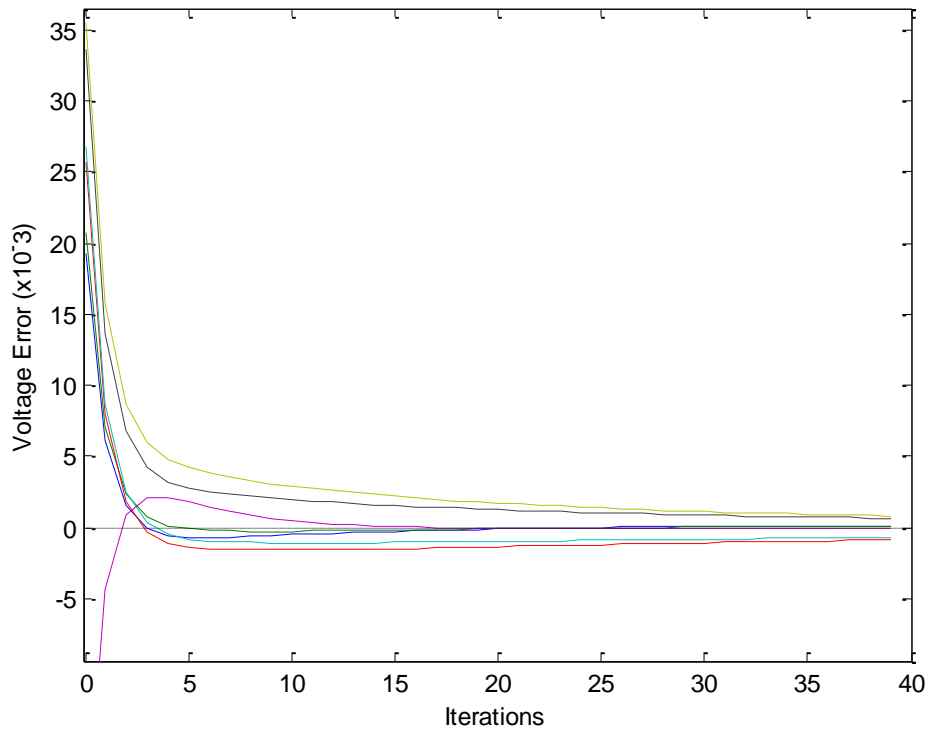


Fig. 5.2 Evolution of the state variable error with 7 DERs, for $\alpha = 0.3$, with the same initial values as the ones listed in Table XIV.

A close examination of Fig. 5.1 and 5.2 reveals that in the second graph, with approx. 20 iterations, the system (mostly) manages to correct the error in three of the seven nodes, with the remaining four generators still possessing comparatively high errors. However, it would still take a hundred or so more iterations (126 in total) of the algorithm before the error on all nodes is considered successfully curtailed while in the first case, where the error decays at a similar ratio for every DER, it would only take 80 iterations. Another way by which we can inspect it is by tallying the individual lags, where in the former it takes only 15 iterations (out of 126) for one of the controller to drop its absolute error below the 10^{-4} margin while, in the latter, 59 iterations (out of 80) are necessary.

5.2 Anchoring

From the analysis of the Figs. 5.1 and 5.2, we can then infer that when the error in one or more nodes is fully eliminated or significantly reduced while that of the others remains relatively higher, the controllers pertaining to the former, in an attempt to keep their nodal voltages mostly fixed, will act as a sort of anchor for the system, thus slowing it down. Mathematically, from (11), we have that the iterative process can be summed up as $V^{k+1} = [A]V^k + B$, with B being a fixed value in the same vein as $([R][k])V^*$. Should a controller j curtail its error well ahead of its counterparts, we'd have that $V_j^{k+1} \approx V_j^k$ and, as such, $A_{ij}V_j^k$ can now also be considered a fixed term in the iterative equation $V_i^{k+1} = A_{ii}V_i^k + \dots + A_{ij}V_j^k + \dots + A_{in}V_n^k + B_i$, becoming $V_i^{k+1} = A_{ii}V_i^k + \dots + A_{in}V_n^k + (A_{ij}V_j^k + B_i)$.

In essence, from an iteration standpoint, the coefficient matrix $[A]$ is reduced from n -by- n to $(n - 1)$ -by- $(n - 1)$ as a result. That is, the system is effectively working with less DERs. Consequently, per Table XIII, reducing $[A]$ in size will typically translate into an increase for the maximum stability gain $[k_{stb}]$. This relates to another conclusion taken early from Table XIV and Chapter 4: that an oscillatory error response produces a faster response in systems with unbalanced phases distribution. If $[k_{stb}]$ were to increase then, with the same α , the optimal area of operation would be drawn away from the present controller's power gain, therefore resulting in a slower iterative process as illustrated in the below graph.

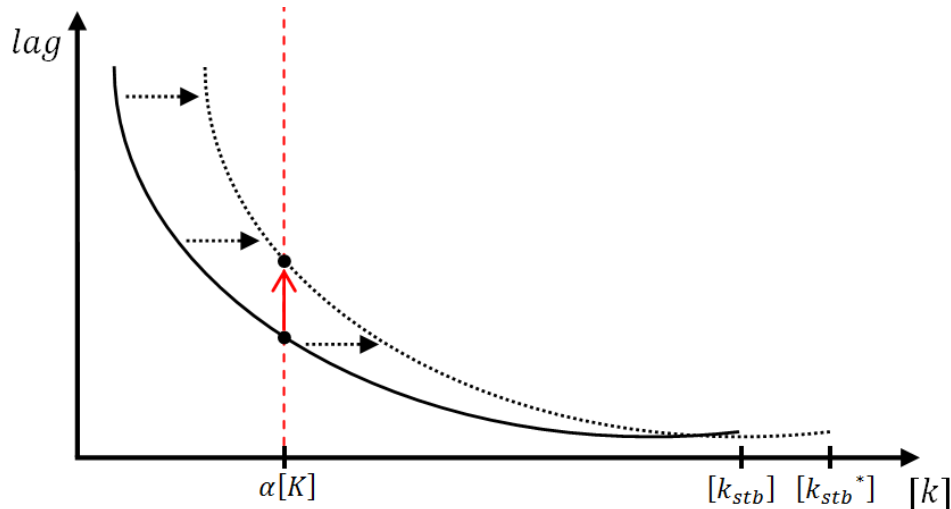


Fig. 5.3 General representation of the relation between the power gain and lag, and the shift created by the “reduction” of $[A]$. Notice how the lowest point in both curves is closer to their respective stability limit $[k_{stb}]$ rather than $[k_{osc}] = 0.5[k_{stb}]$, which is the case for most scenarios involving unbalanced DG through RST.

This *anchoring* phenomenon caused by one of the controller's reaching its end goal ahead of its companions also explains why the optimal power gains for performance are all past the oscillation threshold. The presence of oscillation would make it much more difficult for the system to find itself in a situation where $V_j^{k+1} \approx V_j^k$, thus avoiding the reduction of the iteration coefficient matrix $[A]$. In the 7 DERs example, with $\alpha = 0.6$ (for a stability limit of $\alpha = 0.6166$), only one of the errors was found to be curtailed well in advance of the others, with a resultant lag of only 63 iterations, half of those required for a non-oscillatory response.

As established in Chapter 3, a great deal of the issues that plague a decentralized control strategy derive from the simultaneity of the controllers' operation, which if centralized would lead to each individual state variable error falling at a similar, optimal rate. The key to achieve an equilibrated reduction of the error is thus having the initial conditions of the system conform with its parameters as to best emulate this situation. From (9), we know that a shift in the injected power is calculated through the product of the gain and the current error, $[k](V^* - V^k)$. A controller will have a higher power gain the further upstream it is connected, due to it being inversely proportional to R_{ii} , so in order to obtain an equal ΔP and/or ΔQ the error it acts upon should be lower to compensate for it. That is to say, higher gains should act on a smaller errors, and vice-versa, as to enable a balanced reduction of error throughout the entire network. This conclusion leaves the door open for a possible study and implementation of dynamic gains $\alpha(V^* - V^k)$, as to enhance the system's performance.

5.3 Dispersion of Distributed Generation

In the previous section, it was demonstrated how the superficially simple matter of adding an extra generator or simply readjusting one's position in the feeder grid can lead to drastic changes in both the it's controller performance and, in worst case scenario, compromise its stability altogether. This again, corroborating what was stated in previous chapters of this work concerning the fickleness of an autonomous control strategy in the face of slight changes the distribution of its DERs. As mentioned in the beginning of this section, having seen how the system responds to an increasing concentration of DG across a 3bus-by-3phase node grid, the following course of action concerns the effects of spacing said generation. That is, measuring what influence distance – the impedance $R_{ii}(1 + jx\circ r)$ seen by each individual DER and its $R_{in}(1 + jx\circ r)$ derivatives – has on the system.

Back again to Chapter 3, we observed how distancing the main generation cluster from the source bus affected the maximum common gain factor α with which the system could work (Fig 3.6), and ultimately how it influenced our choice of an admittance-based controller specific gain $[K]$. Further elaborating on that study, we shall dedicate this portion of Chapter 5 to the ramifications of creating distance, not only between the generators and the source, but also between each generating bus, in essence creating separate clusters of generation. As an initial postulation, we can say that increasing the impedance between said clusters will further isolate them from one another, likely lessening the (negative) effects that arise due to mutually induced generation and thus improving the system's overall robustness.

It's worth reiterating that varying the value of the bus-to-bus line impedance z itself does not affect the system in terms of stability as, per (17), the eigenvalue gradients are solely dependent on the product of matrix $[R]$ and $[K] = [R_I]$: any increment/decrement in R_{ii} would be met in kind by an equal decrement/increment in its inverse value K_{ii} . That said, a simulation was conducted to gauge the system's stability parameters – $\text{Max}|\Delta_i([R.K])| \rightarrow \alpha = k_{stb_{ii}}/K_{ii}$ – response to a linear increase in the distance between the generating busses, using study model 6 as a start off point.

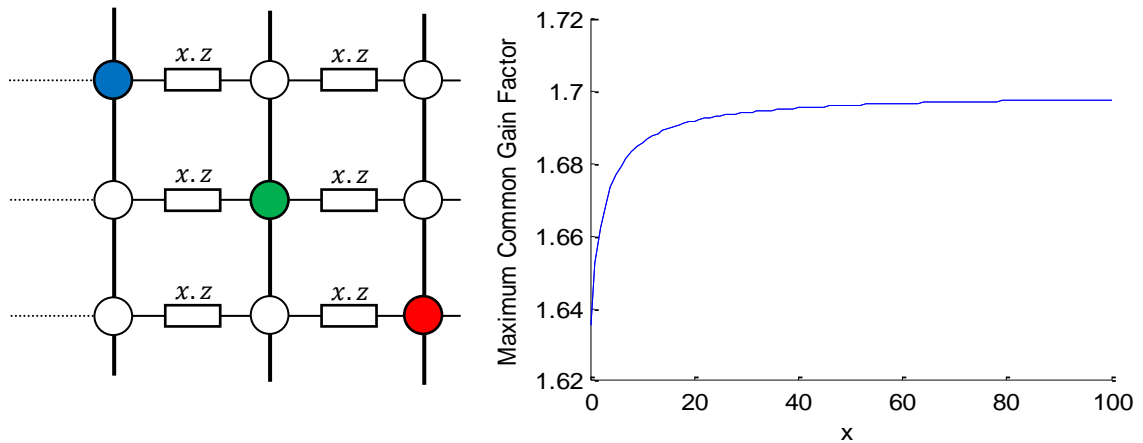


Fig. 5.4 Evolution of the Maximum Common Gain Factor for Study Model 6 in function of the line impedance coefficient x .

From $\alpha = 1.6353$ ($x = 1$), we see a growth in the maximum common gain factor growing in the form of an exponential curve, with an asymptote approximately around $\alpha = 1.7$. It is thus confirmed that placing a higher impedance between the DERs can help to improve the stability limit of the control scheme, mainly by electrically isolating the generating busses. Yet, with a hundred time the value that of the study model, one would reasonably expect that given the sheer distance (and isolation) between the generators' busses that the system would behave more similarly to a situation where each generator is by its lonesome. That is, closer to $\alpha = 2$, as seen in Table XIII. To get a more defined sense of the differences between the original and the extended network, one only has to analyze and compare matrix $[A] = [I] - [R][K]$ for both $x = 1$ and $x = 100$ (with $\alpha = 0.25$):

$$[A(x = 1)] = \begin{bmatrix} 0.75 & 0.0417 & 0.0313 \\ 0.0625 & 0.75 & 0.0469 \\ 0.0625 & 0.0625 & 0.75 \end{bmatrix} \Rightarrow [A(x = 100)] = \begin{bmatrix} 0.75 & 0.0012 & 0.0006 \\ 0.0625 & 0.75 & 0.0316 \\ 0.0625 & 0.0625 & 0.75 \end{bmatrix}$$

It's immediately perceptible that the left side of matrix $[A]$ remains unchanged, even with the increased distance between the generating busses, while the right side values decrease by an order of magnitude, with the conspicuous exception of A_{23} . These differences can be easily discerned by looking at the general composition of $[A]$ relative to each DER's distance. Its diagonal will always be equal to $A_{ii} = 1 - \alpha$, as $R_{ii}K_{ii} = 1$ regardless of the feeder network's composition. Furthermore, for this case in particular, we have that $A_{ij} = -\alpha R_{jj} K_{jj} / 4 = -\alpha / 4$, when $i > j$, which will also be independent of x . As for the right side of the matrix, R_{11} remains constant while both R_{22} and R_{33} increase, from 1.2 to 41.2 and from 1.6 to 81.6 respectively, and thus $A_{1j} = -\alpha R_{11} K_{jj} / 4 = -\alpha R_{11} / 4 R_{jj}$ decreases proportionally to the latter. It's this equivalent increment that explains why $A_{23} = -\alpha R_{22} / 4 R_{33}$ does not decrease at a similar rate to what is seen for the other two right sided values, and ultimately the reason that the asymptote in Fig 5.4 is located around $\alpha = 1.7$ and not $\alpha = 2$, as expected for an electrically isolated system.

Should all terms on the right side of the matrix scale down at a similar scale, then it could be said that $[A]$ could be approximated to a triangular matrix with an appropriately high x , and thus, owing to the properties of said matrixes:

$$[A(x \rightarrow \infty)] = \begin{bmatrix} 1 - \alpha & 0 & 0 \\ -\alpha/4 & 1 - \alpha & 0 \\ -\alpha/4 & -\alpha/4 & 1 - \alpha \end{bmatrix} \Rightarrow \lambda(A) = 1 - \alpha \Rightarrow [k_{stb}] = 2[K]$$

However, while R_{11}/R_{22} and R_{11}/R_{33} decrease at a comparable pace, R_{22}/R_{33} does not, and as a result remains in the same order of magnitude as the elements on the left of the diagonal, meaning that this generalization cannot be made. Therefore, to take better advantage of distancing generating busses, we'll have to increase the relative distance between them (4 and 5 specifically), rather than simply adding identical increments. For example, one possible solution would be to distance these two busses by a factor of x^2 instead:

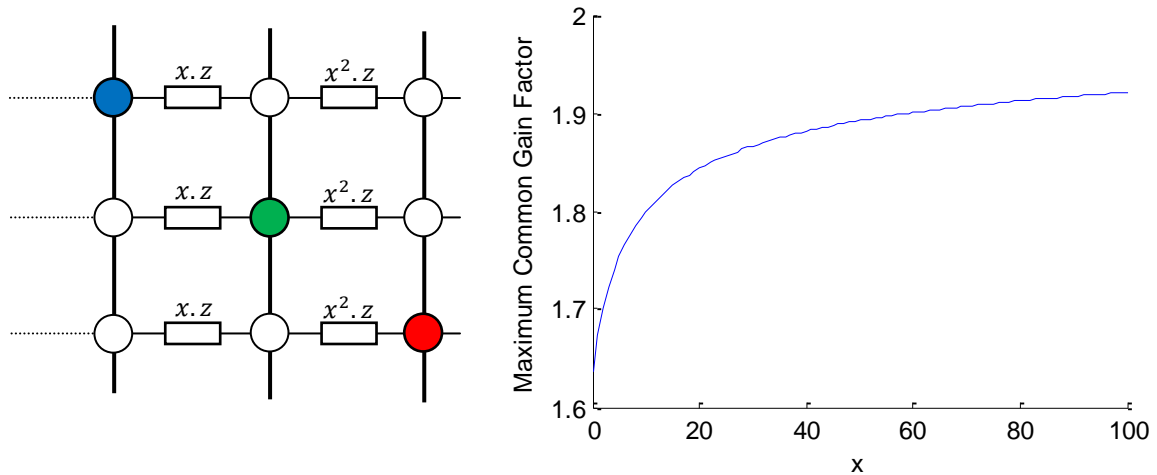


Fig. 5.5 Evolution of the Maximum Common Gain Factor for Study Model 6 in function of the line impedance coefficient x (quadratic variant).

Right away, the changes concerning the Maximum Common Gain Factor are perceptible. The graph asymptote is no longer located near $\alpha = 1.7$, but rather somewhere closer to $\alpha = 2$ (which further simulations extending the range of x corroborate). Comparatively, for the same value of R_{33} we obtain in the example demonstrated in Fig 5.4, we here obtain a $\alpha = 1.81$, in contrast to the previous case where it was (approx.) at $\alpha = 1.69$. The difference between the two above cases becomes all the more evident when we compare the decay of R_{11}/R_{22} and R_{22}/R_{33} , as illustrated in the graphs below:

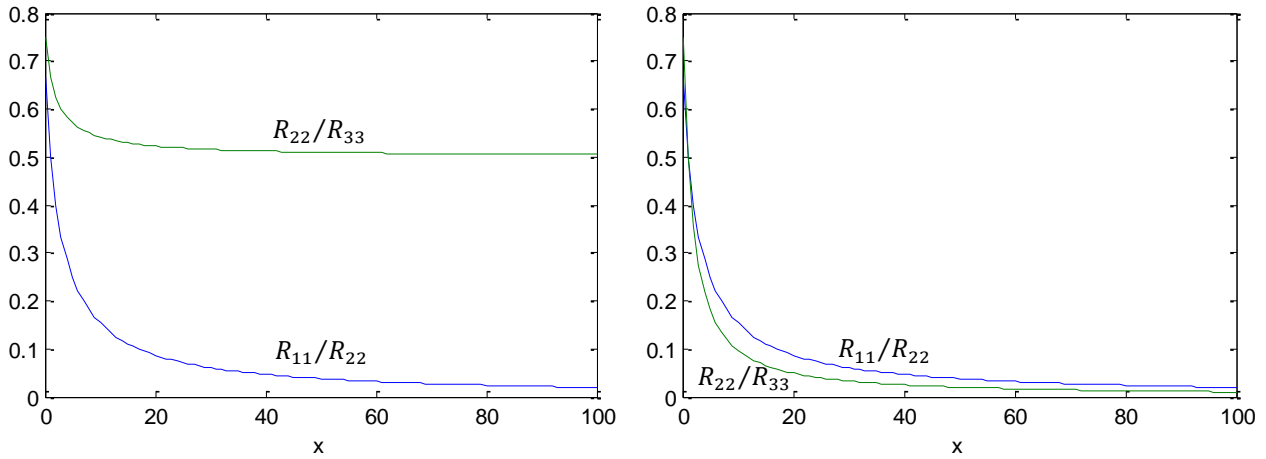


Fig. 5.6 Evolution of the R_{11}/R_{22} and R_{22}/R_{33} ratios in function of the line impedance coefficient x : left \rightarrow linear increment (Fig 5.4), right \rightarrow quadratic increment (Fig 5.5). The major difference between the two cases lies in that the R_{22}/R_{33} ratio plateaus just above 0.5 in the first case, indicating that $A_{23}(x \rightarrow \infty) = -0.25\alpha$, while in the latter it decays towards zero as x increases, similar to R_{11}/R_{22} .

As Fig. 5.6 demonstrates, in order to maximize the advantage afforded with the dispersal of DG, as to improve the system's robustness when it comes to its stability, the ratios between bordering DER busses have to tend towards zero as their distance towards the source increases. In summary, the key to better isolate the generating busses, and thus to reduce the effects originating from mutual influences between the generators, is to maximize the *relative* distance between them. The logarithmic x^2 spacing seen in Fig. 5.5 is one such instance. Another alternative, as a possible example, would be to space the busses in way so that $R_{ii}/R_{jj} = R_{11}/R_{ii}$, where $j = i + 1$ and both refer to *distinct busses*, not DERs. (In this case that would be $R_{22}/R_{33} = R_{11}/R_{22}$). Either case would ensure that the right-sided elements of matrix $[A]$ would gradually become closer to zero, allowing to approximate it to triangular matrix, with all the characteristics referenced above.

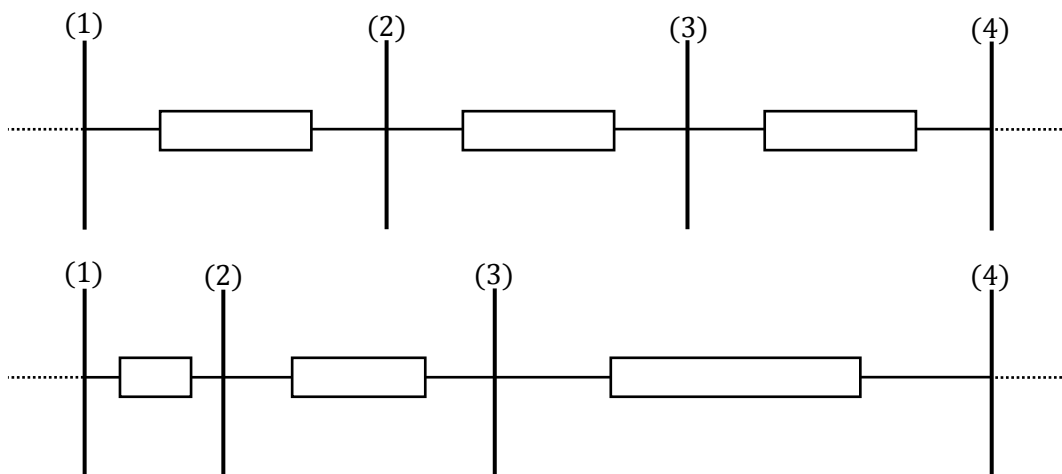


Fig. 5.7 Comparison between the two different spacing methods. As stated, the bottom bus distribution results in a higher Maximum Common Gain Factor α , though the distance between generating busses (1) and (4) remains unaltered for both cases.

These conclusions can also apply for situations where we have more than one DER connected per phase and/or per bus. The former only entails the removal of the $-1/4$ factor from some of the non-diagonal members of $[R]$, as per (6), and consequently $[A]$, and as such follows the same reasoning detailed above, which is solely dependent on the relative distance between busses. For the latter, though the presence of more than one generator per bus makes it impossible to generalize $[A]$ into a triangular matrix, the busses can still be isolated from one another. Ideally, we would get a situation similar to study model 1, where 3 DERs are connected to the same bus, with a Maximum Common Gain Factor $\alpha = 1.6$. Running the same tests for Fig 5.4 and 5.5, only with 9 DERs, we obtain:

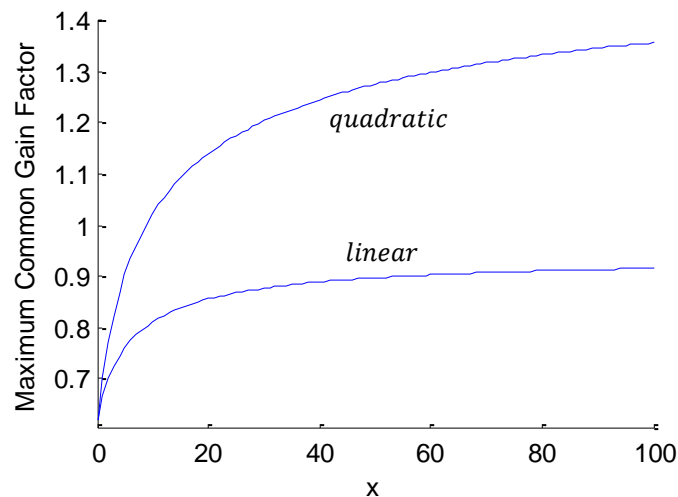


Fig. 5.8 Evolution of the Maximum Common Gain Factor for a full 3bus-by-3phase node grid (9 DERs) in function of the line impedance coefficient x , for both spacing variants.

We witness a comparable situation as when using study model 6 as a reference. A quadratic spacing results in a higher Maximum Common Gain Factor than its linear variant, with an asymptote in the vicinity of $\alpha = 1.6$. As was anticipated, this serves as evidence that as $x \rightarrow \infty$, the controllers in each of the increasingly isolated busses will start to behave like they did in study model 1. The yielded results are equally applicable for any number of generators (and busses), and their distribution throughout a feeder grid. Dispersing distributed generation has thus a somewhat noteworthy benefit in that it can provide a certain security margin when changing a network's DG profile, as with sufficient (and appropriate) distance between the connecting busses we can assure that decentralized voltage control system remains stable throughout the alteration.

Chapter 6

Voltage Error Area Integration

In all of the scenarios studied so far, it was been considered that a feeder's network voltage profile suffers alterations solely as a result of the variation in one or more of the DER's injected power. However, as seen before, real world conditions will preclude this presumption. Natural fluctuations in the node's voltage (and injected power) will invariably occur, owing to the characteristics of a LV network and a multitude of outside factors, which up until now we've neglected to properly take into consideration when simulating our chosen control algorithm. Moreover, we've also considered that the controlling algorithm operates in both an instantaneous and persistent manner for all DG, until all of the voltage deviations are corrected, not accounting for the distance induced lag between each of these nodes and their respective controller's reaction time. These influences have the potential to disrupt the algorithm's progression at an inopportune time, particularly when the system is operating with its power coordinates are near any of the imposed limits, as it can lead to a violation of clause (26) and/or (28). To showcase the impact of these fluctuations, seemingly neglectful as they might appear, can have in the performance, we repeated the simulations for study model 6 and the full grid scenario, adding a random factor to the nodal voltage, based on its initial error, at the end of each iteration.

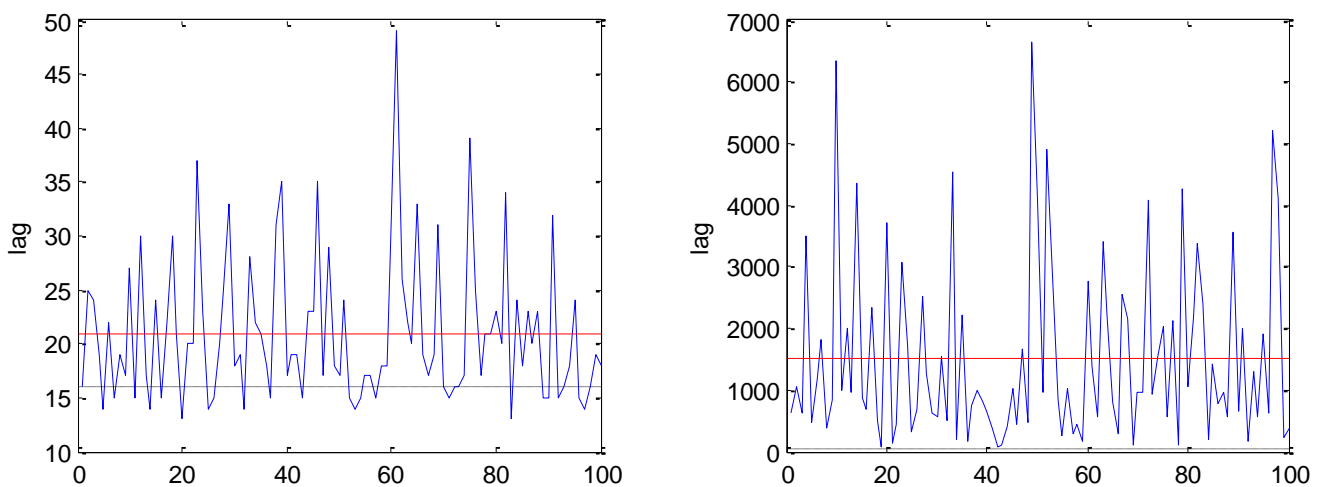


Fig. 6.1 Variation of the lag over a hundred simulations as a result of the extra term with a random value between -1% and $+1\%$ of the initial error ($V^0 - V^$), for study model 6 (left) and the full grid scenario in Chapter 5 (right). The dotted black lines represent their values without these fluctuations, and the red ones stand for the average lag.*

While the system is still able to steady the voltage profile to an acceptable level, curtailing the error below the considered threshold of 10^{-4} , its performance suffers a major hit, made all the more egregious by the presence of more DERs, as noticed when comparing the graphs side-by-side. (For the left, the worst obtained result nears 50 iterations, from the original 16, while on the right it goes beyond 6000, from 56.)

Ultimately, we can conclude that factoring in even the smallest of variations to the network voltage has resulted in a considerably larger (on average) time interval between the system's activation and suitable correction of the deviation, especially when it has to handle a higher number of generators. Another foregone inference that can be taken from this verifiable data is that a greater range of fluctuations will further exacerbate the performance deterioration.

Furthermore, the existence of these inherent irregularities in the voltage profile will make it impossible for any control scheme to fixate the nodal voltage to a predetermined value, only minimizing the absolute error below a certain limit, as seen above. This in turn requires constant updates to the injected power from the controllers, of varying degree, as each attempt to counteract these fluctuations. Moreover, if we also factor in a certain delay to the controller response, the error would've oscillated again making said adjustment either excessive or insufficient to correct the new discrepancy. Therefore, finding a more suitable criterion for triggering the voltage control process, other than simply having a non-null difference between the state variable and the intended value, becomes a necessity if we're to have an efficient voltage regulation system. This will become the focus of this section.

6.1 Voltage Error Area Correction

Thus far, the algorithm, used as the building foundation for much of our study and its conclusions, basis its operation on a discrete numerical integration of the error: with each new iteration, the control variable X^t is updated based on the current difference between the state variable Y^t and the intended set-point Y^* . The former's value is, as such, the linear combination of every previously obtained state variable error, with a set coefficient k_I here corresponding to the controller's power gains their respective nodal voltage.

$$X^t = X^0 + k_I \sum_{i=1}^t e_i \Leftrightarrow X^i - X^{i-1} = k_I e_i \text{ with } e_i = Y^* - Y^i \Rightarrow Y^i = f(X^{i-1})$$

If we were to shift to a temporal (continuous) basis, the summation in the above expression would be turned into an integral. That is, in a graphical representation, the cumulative sum of the state variable error would be translated to the total area between the voltage error curve and the x-axis, for an equivalent interval of time. It is from this integral value that we can construct our new approach for local voltage based power controller. Dividing the total area by the correspondent time interval allows us to estimate an average error for the controller to act upon, mitigating the concerns that arise due to the introduction of the aforementioned fluctuations. Not only that, this integral can also serve as the benchmark that dictates when a controller will "step in" to regulate the injected power of its DER, as opposed to its continual operation. To that effect, we can make it so that a controller acts upon a voltage deviation only when the integral area surpasses a defined limit A_X , as demonstrated in the figure below.

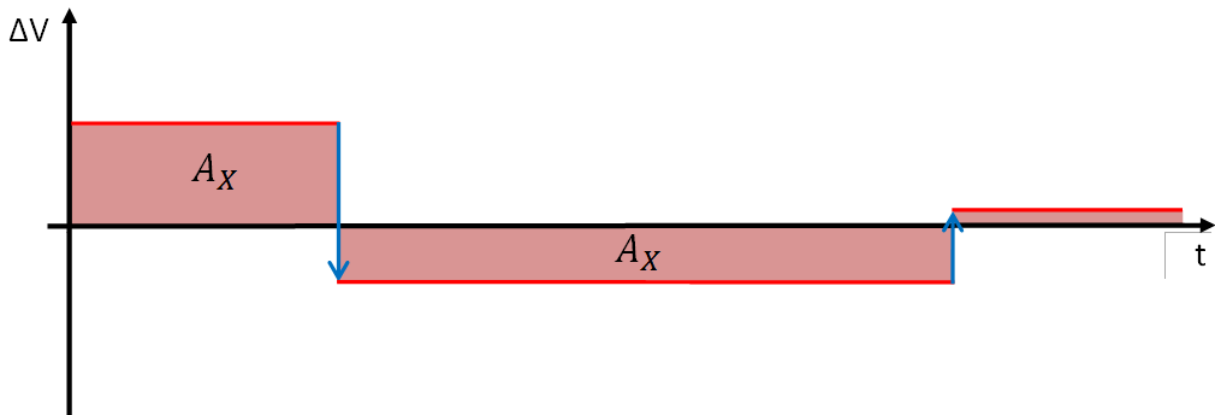


Fig. 6.2 Demonstrative example of an integral voltage error correction over a period of time. The algorithm will act upon the voltage difference only when the darkened integral area surpasses a set limit A_X .

From an electronic standpoint, the controller would function by registering the nodal voltage periodically, adding each of the (appropriately small for a better approximation) time ticks' error until the sum reaches an established maximum analogous with A_X . Upon such occasion, the corrective power shift will then be determined by averaging said error by the time interval, the algorithm using the same alternating Q(V)/P(V) logic as in the discrete process. The integral area taken into account is tallied from the last moment the error was zero, meaning the count is reset every time the error signal switches, as a consequence of any power shift or due to the natural oscillatory behavior of the state variable. Ultimately, the new control strategy's goal becomes not so much as to correct the voltage value itself but rather its average, drawing it to a point where the voltage error fluctuations gravitate around zero. However, given the previously seen influence that multiple DERs can have on the evolution of the network's voltage profile and its inherently oscillatory behavior, utilizing such average might not be ideal. Given those factors, the calculated mean error might diverge significantly from its actual value at the onset of a power shift. For the sake of making a more precise adjustment, we can have the mean error be taken solely from a fixed segment of time directly before the readjustment in the injected power, putting more weight into the latest instances.

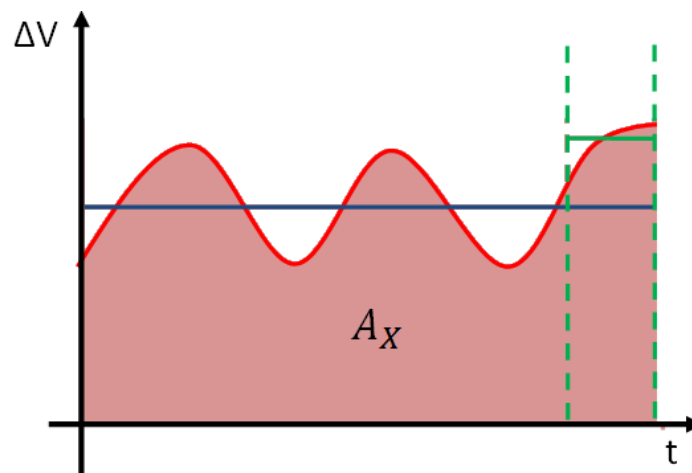
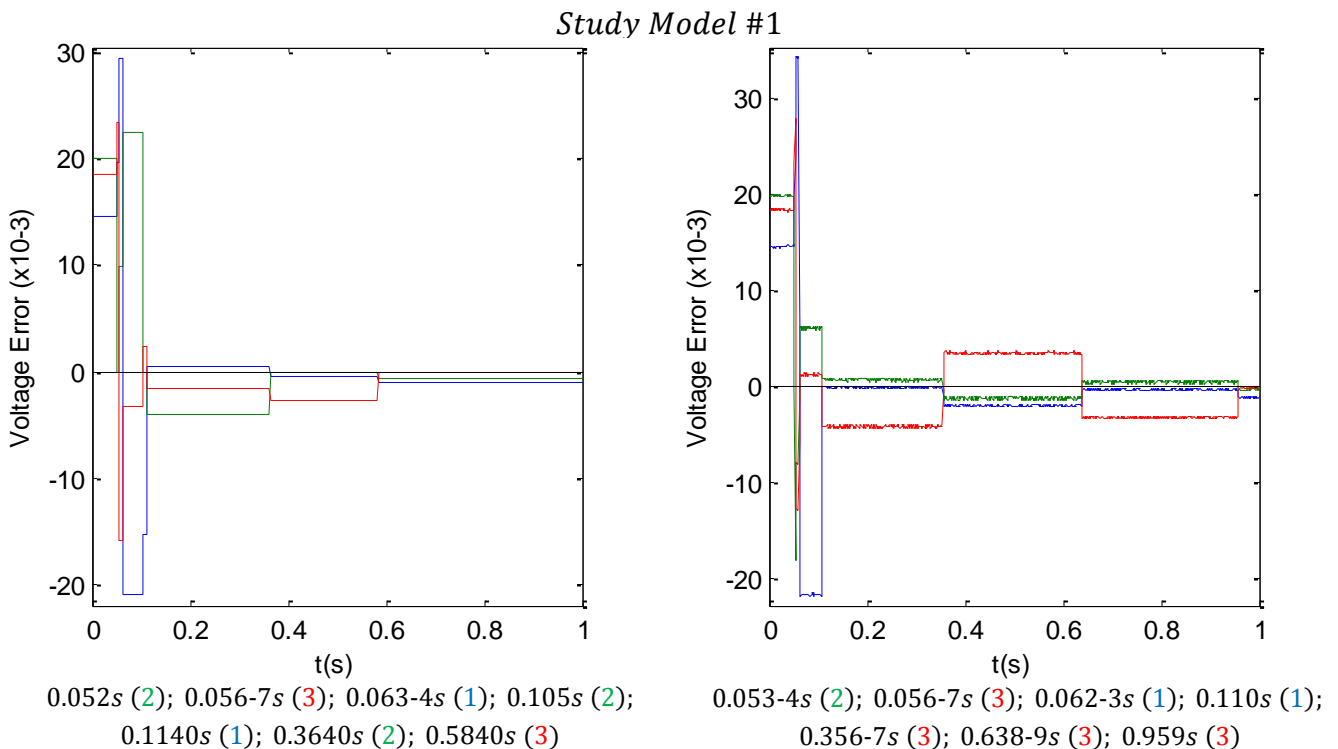


Fig. 6.3 Hypothetical voltage error curve, and its respective means taken from the entire area and sampled from the dashed demarcation. The latter, as we can see, is closer to the error at the endmost, and thus more adequate for the controller to use as a basis for the consequent power shift.

Limiting the controllers' intervention on a whole works for the system's benefit, as it avoids unnecessary shifts in active and reactive power that would come as a result of the natural oscillations in the nodal voltage. Yet, perhaps the most significant advantage this voltage control method brings to the table, aside from the drastically reduced number of corrective shifts, is that it practically guarantees that no two generating nodes will vary their injected power simultaneously. As mentioned in Chapter 3, when discussing the possibility of alternative control strategies, it's the concurrence between the operation of the various controllers that it's at the core of the instability issue for a decentralized power control scheme. For a discrete iterative process, it was the eigenvalues of the n -by- n matrix $[A]$ that determined whether or not the system was convergent (and oscillatory). The same remains valid for the continuous process, however here we can easily determine the eigenvalues beforehand, even without prior knowledge of the resistance matrix $[R]$. Assuring that a maximum of one controller i is acting at any given time, then we'll have a situation similar to (21), where the eigenvalues of $[A]$ will be equal to 1 and $1 - R_{ii}k_{ii} = 1 - \alpha$, considering $[k] = \alpha[R]$. The algorithm's convergence is thus guaranteed so long as $0 < \alpha < 2$, regardless of the number of DERs and their configuration throughout the feeder network.

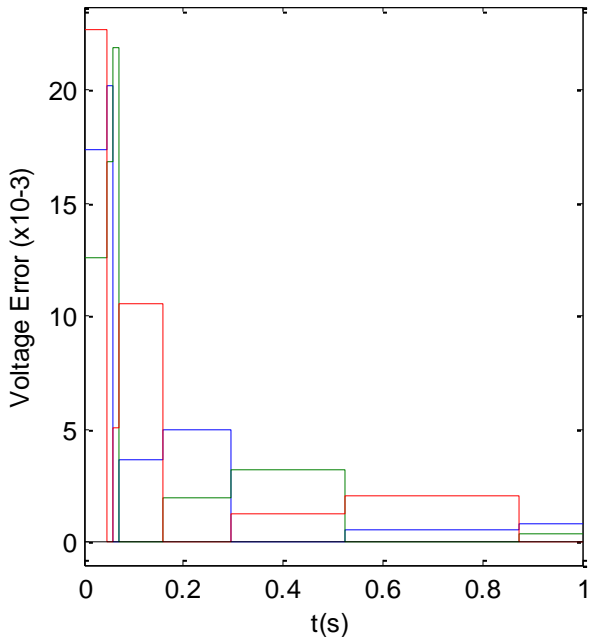
6.2 Voltage Error Behavior and System Performance

With this new paradigm in mind, we moved on to simulate the evolution of the voltage error for study models 1, 6, 9 and 14 (with the same initial conditions as in Chapter 4), using a variation of the previously utilized MATLAB code to reproduce the algorithm on a temporal scale. We've considered that each controller, upon activation, executes its power adjustment within a millisecond, sampling the last ten milliseconds of the voltage error for reference, with voltage error area set-point of $A_x = 10^{-3}$.

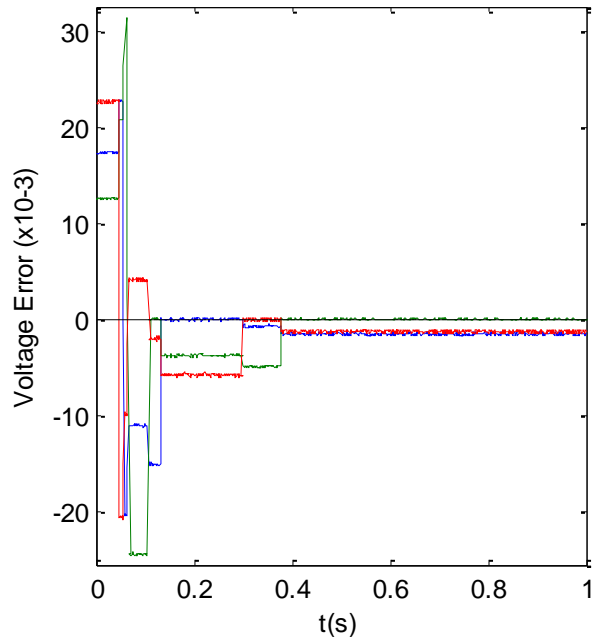


Figs. 6.4 and 6.5 Evolution of the state variable error for a continuous system, for study model 1, employing integration of the voltage error area, during a one second interval, with $\alpha = 1$.

Study Model #6



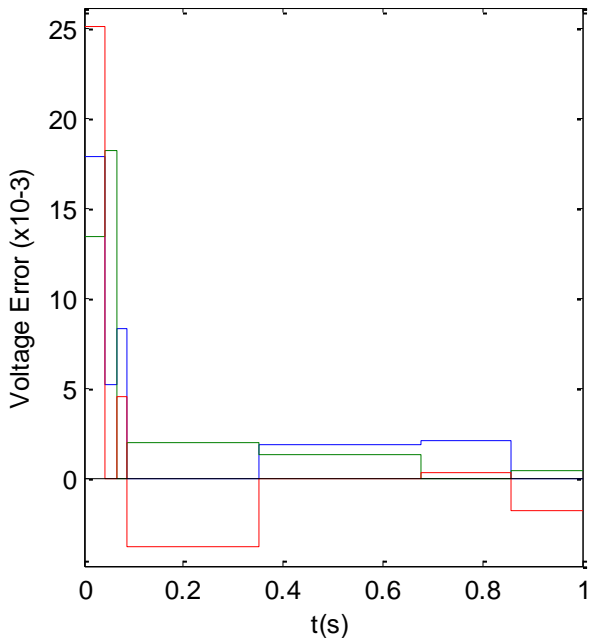
0.047s (3); 0.058s (1); 0.07s (2); 0.160s (3);
0.296s (1); 0.524s (2); 0.875s (3)



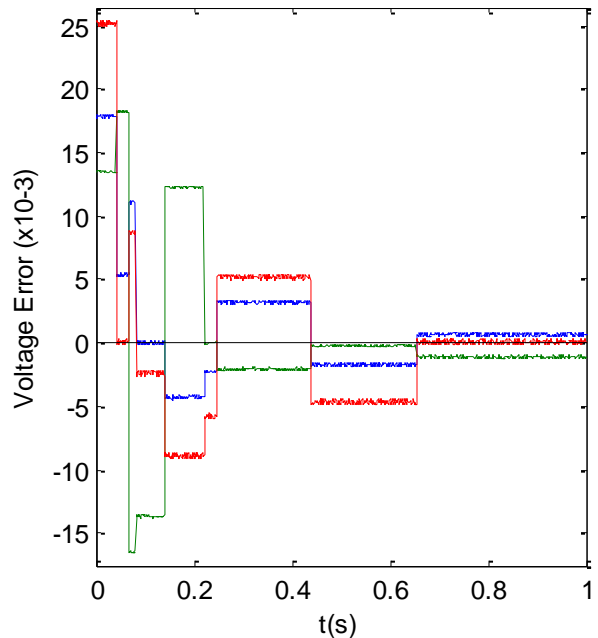
0.047-8s (3); 0.057-8s (1); 0.065-6s (2); 0.107s (2);
0.133s (1); 0.299s (2); 0.377s (2)

Figs. 6.6 and 6.7 Evolution of the state variable error for a continuous system, for study model 6, employing integration of the voltage error area, during a one second interval, with $\alpha = 1$.

Study Model #9



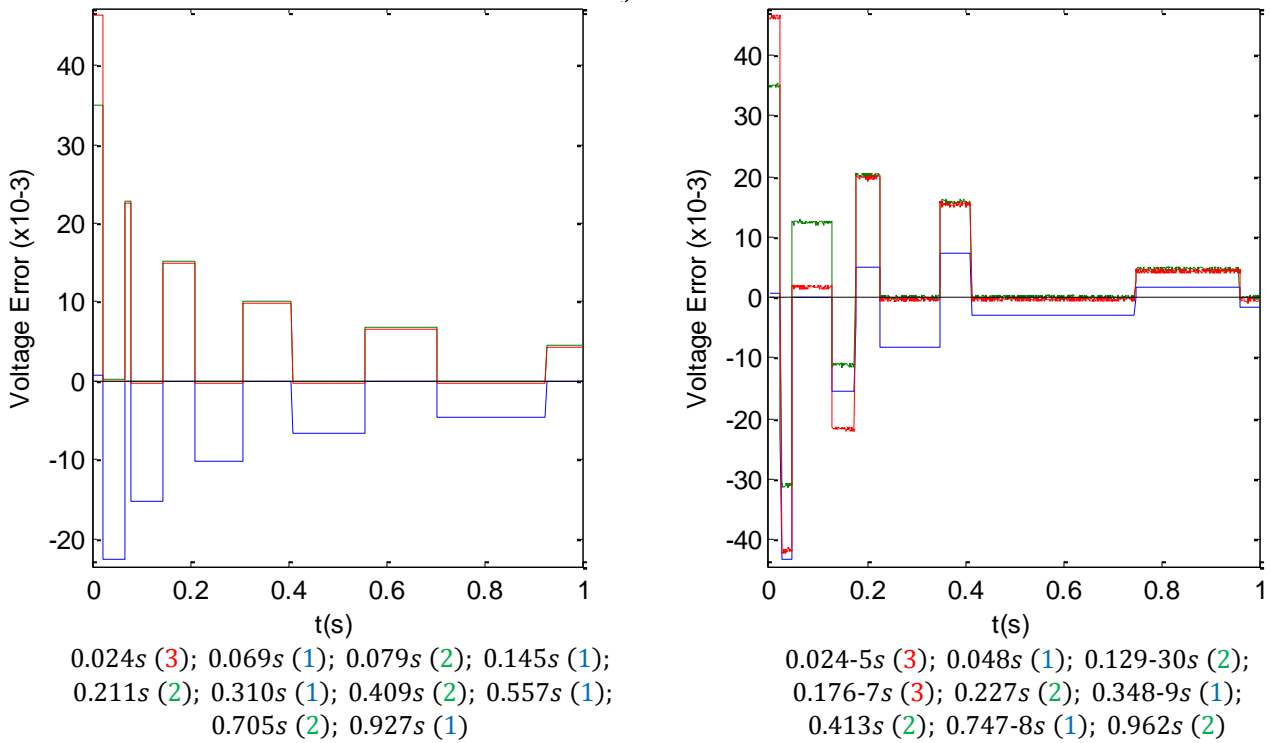
0.042s (3); 0.068s (2); 0.086s (1);
0.351s (3); 0.677s (2); 0.858 (1);



0.042s (3); 0.068-9s (2); 0.082s (1); 0.140-1s (2);
0.223s (2); 0.246-7s (3); 0.439-40s (3); 0.655s (3)

Figs. 6.8 and 6.9 Evolution of the state variable error for a continuous system, for study model 9, employing integration of the voltage error area, during a one second interval, with $\alpha = 1$.

Study Model #14



Figs. 6.10 and 6.11 Evolution of the state variable error for a continuous system, for study model 14, employing integration of the voltage error area, during a one second interval, with $\alpha = 1$.

Left graphs showcase the error progression without fluctuations in the nodal voltage, and opposite side with. Beneath each are the timestamps for each individual controller's activation. Note that any right graph represents only one possible outcome of the error's evolution, due to the randomized nature of the fluctuations. The DERs are again color coded, according to Table I and II.

As we can observe, although the voltage error does not converge in a manner similar as the examples in Chapter 4, there's at least a significant reduction in all cases during the presented time interval. Of particular note, study model 14 is able to curtail its error despite the common gain factor being equal to one, which would've resulted in instability before (where $\alpha = k_{stb_{ii}}/K_{ii} = 0.707$). This serves as evidence that this criteria for voltage control manages to avoid the drawbacks that crop up from concurrent alterations in the injected power throughout the grid, eliminating the concern of having to establish a specific α based on DG distribution. Not only that, given the nature of its controllers, this system will come to prioritize the correction of the current highest and most lasting discrepancies first, a fact which is corroborated by the timestamps in Figs. 6.4 through 6.11, another useful trait to have as to safeguard the network's health. Regarding the differences between the left and right sides, without and with voltage fluctuation respectively, the main standout appears to be that the latter is more prone to have larger amplitudes in its "oscillations". At any rate, these cases still manage to achieve a comparable reduction in error to their left counterparts, in both the presented graphs and in subsequent tests, for the same time interval.

6.3 Dynamic Error Sampling

Another standout aspect from the above graphs, those with fluctuations in particular, is that several of its timestamps have a double activation period (0.056-7s (3) in Model 1 for example), and are graphically paralleled by large oscillations in the voltage error (in that same instance, the error goes from approx. 0.03 to lower than -0.02). These are the result of an insufficient estimate on the controller's part, that is the sampled average error is inferior to the actual error at the onset of its activation, resulting in a shift of the injected power that does not lower (or increase) the nodal voltage past V^* with a single shift in power. As a consequence, the value of the error integral will still be above A_x , causing the controller to activate again immediately afterwards, using roughly the same sampled error as a basis. This effectively results in nodal voltage variation to double, often way past what is necessary to curtail its error. While this phenomenon might come as a consequence of the still iterative simulation model we're employing, it nonetheless highlights a concern that the sampling method displayed in Fig 6.3 might not be sufficient for the controller to gauge an accurate estimate of the voltage error. Not to mention, an increased activation period runs the risk of having two or more controllers operating simultaneously, losing the main advantage this type of controller has over its discrete equivalent. An alternative or expanded methodology for the controller to better estimate the voltage error comes then as advantageous.

The simplest solution would be to make it that $\alpha > 1$, so that the controller would naturally overcompensate for any possible discrepancies between the sampled and actual error, ensuring that it goes through zero (resetting A_x in the process) with a single adjustment in the injected power. However, while this may help to offset the random variations in the nodal voltage, it cannot be said to be entirely reliable. If α is too low, its effects might end up being negligible, while if it is too high, it may induce more of the same oscillations we're attempting to lessen. Simply reducing the sample period would likewise be a limited scope resolution.

A careful analysis of the graphs shows that, beyond these small fluctuations, it's again the generators' mutual influence on one another that lies at the heart of the issue. If within a controller's sampling period a change in the nodal voltage were to occur, due to a different controller's activation, then the average calculated by the former will be significantly different than its current error. (Notice again in Model #1 that all cases of double activation periods occur less than 10 milliseconds – the sample period – after the previous.) Going by the logic applied when first determining the sampling method, we can make it so that a controller is able to automatically readjust its sample period should it detect a significant rise or fall in its nodal voltage within a short interval of time. That is, it will shorten the sample period by placing its start point at the moment said variation takes place, as it's illustrated in Fig 6.12. Note that the fixed period will still remain in effect as to counteract any gradual changes in the nodal voltage that would not be detected otherwise (see the cosine wave in Fig 6.3). In essence, this means that the sample period is defined by whichever Δt_d or Δt_f is the smallest, while the common gain factor α should be chosen based on the expected amplitude of the voltage fluctuations.

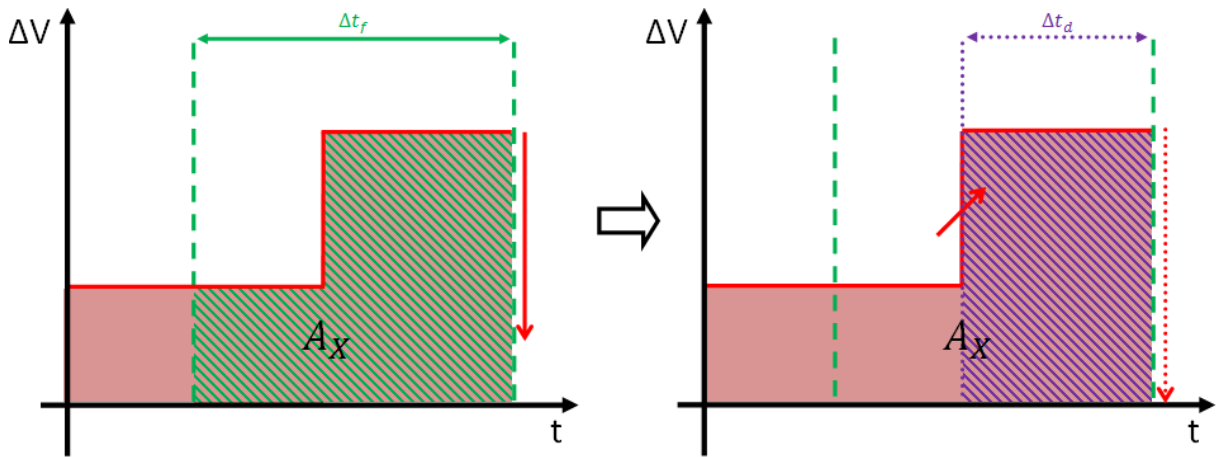
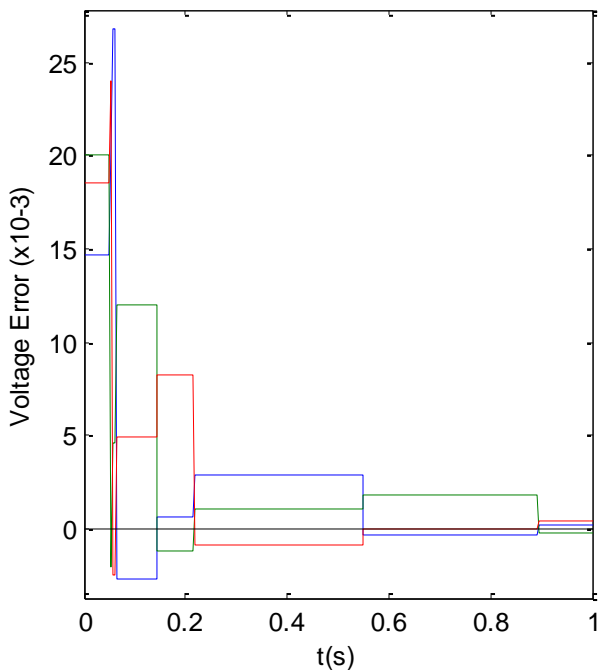


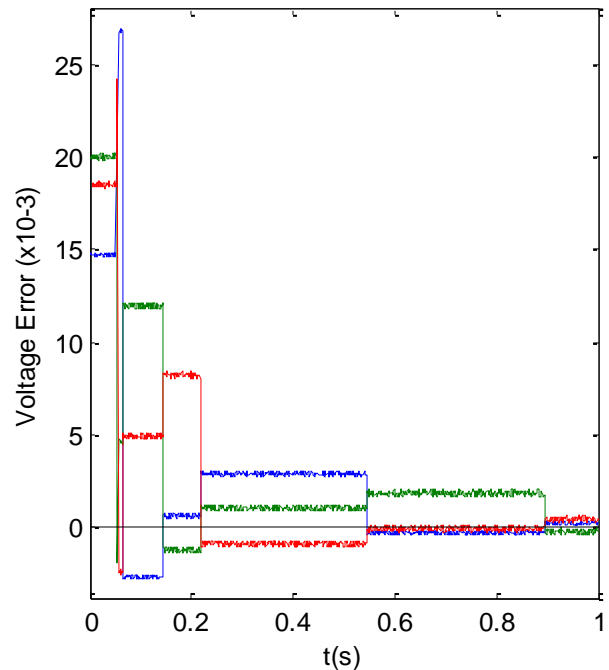
Fig. 6.12 Fixed interval sampling vs. dynamic interval sampling. As we can see, integrating the right dashed area will result in a more precise reduction of the voltage error than with the area on the left. The controller measures Δt_d by pinpointing the last instance where a substantial variation of the nodal voltage took place, as opposed to Δt_f which is fixed.

Adopting this new sampling methodology, and choosing a $\alpha = 1.1$, we repeated the previous set of simulations, with the same initial conditions. Each controller will readjust its sampling time if it detects a the nodal voltage variation larger than 10^{-3} within a millisecond. Again, left graphs showcase the error progression without fluctuations, and opposite side with.

Study Model #1



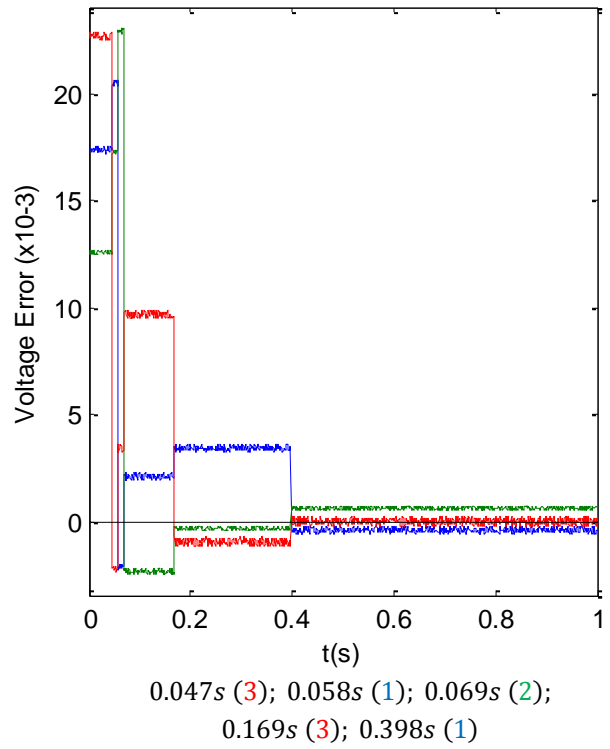
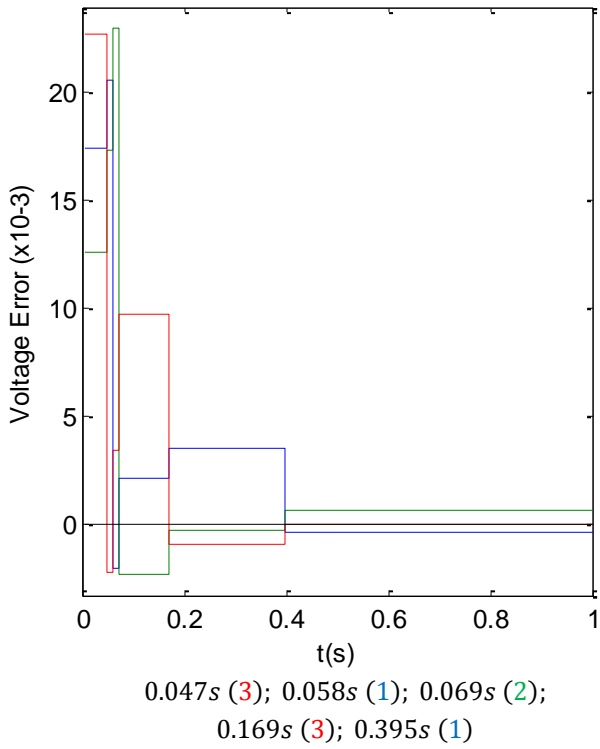
0.052s (2); 0.056s (3); 0.063s (1); 0.144s (1);
0.217s (3); 0.549s (1); 0.894s (2)



0.053s (2); 0.056s (3); 0.064s (1); 0.145s (1);
0.218s (3); 0.545s (1); 0.895s (2)

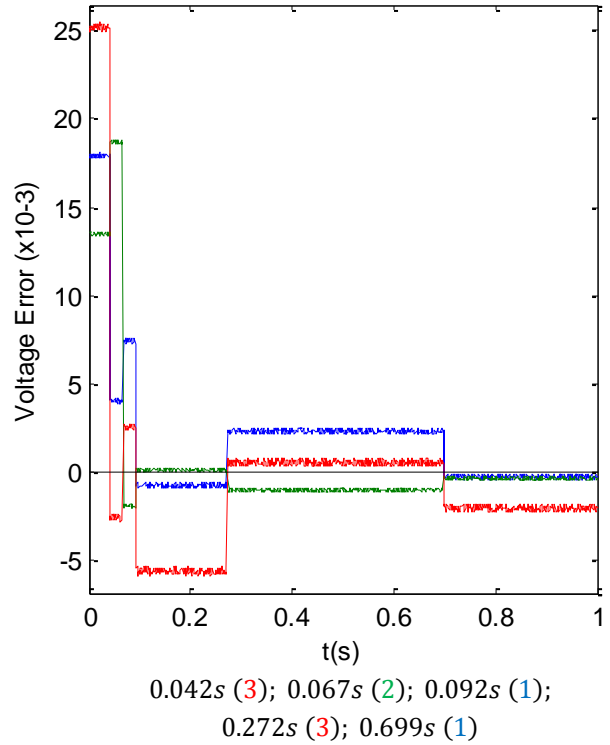
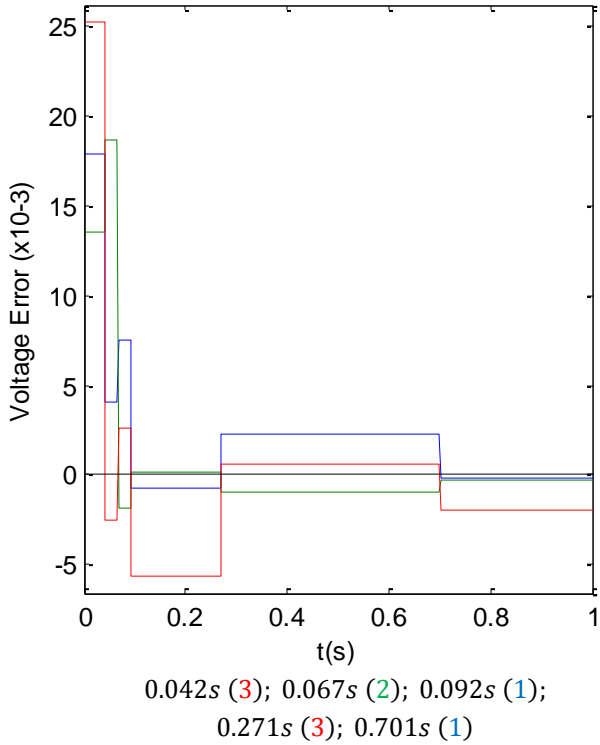
Figs. 6.13 and 6.14 Evolution of the state variable error for a continuous system, for study model 1, employing integration of the voltage error area and dynamic sampling, during a one second interval, with $\alpha = 1$.

Study Model #6



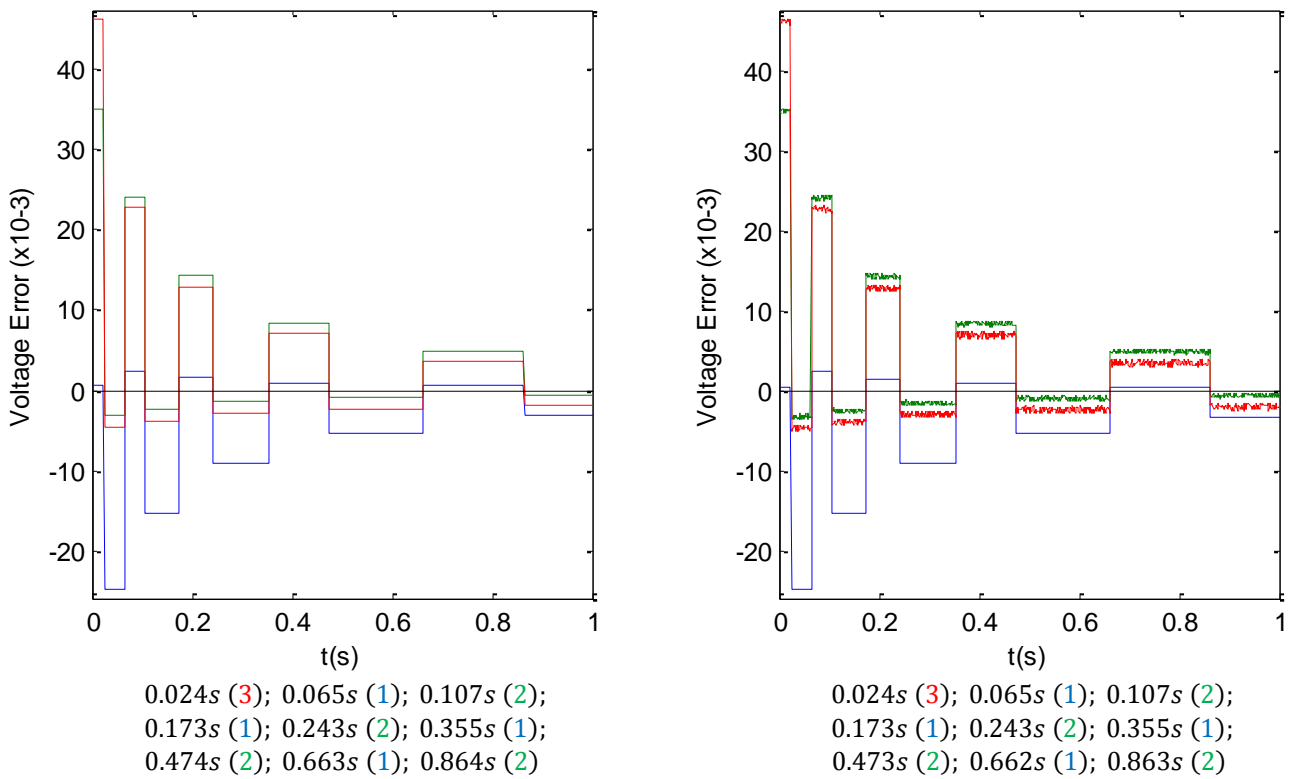
Figs. 6.15 and 6.16 Evolution of the state variable error for a continuous system, for study model 6, employing integration of the voltage error area and dynamic sampling, during a one second interval, with $\alpha = 1$.

Study Model #9



Figs. 6.17 and 6.18 Evolution of the state variable error for a continuous system, for study model 9, employing integration of the voltage error area and dynamic sampling, during a one second interval, with $\alpha = 1$.

Study Model #14

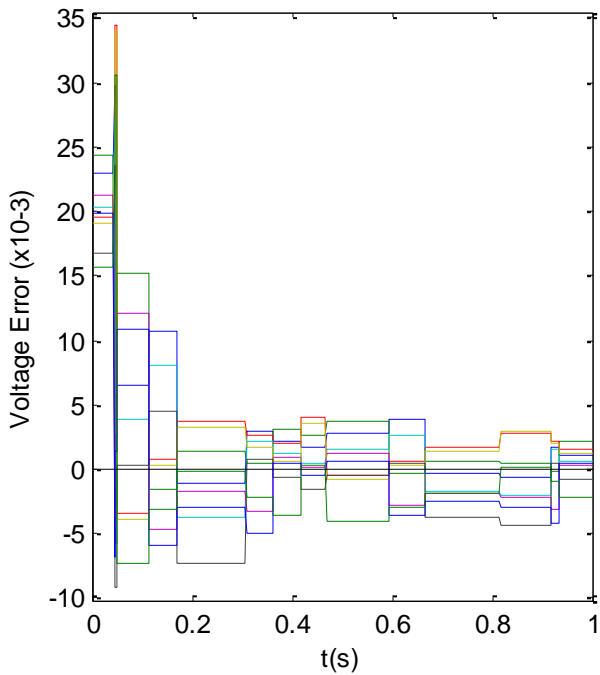


Figs. 6.19 and 6.20 Evolution of the state variable error for a continuous system, for study model 14, employing integration of the voltage error area and dynamic sampling, during a one second interval, with $\alpha = 1$.

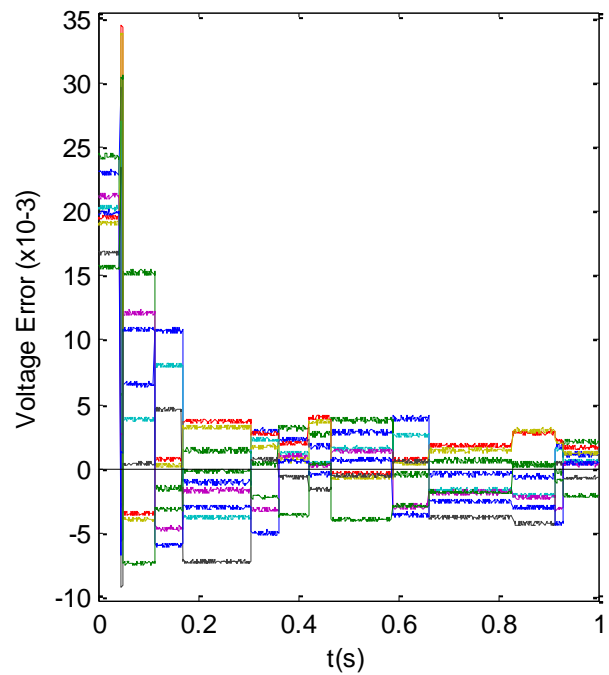
Side-by-side, it's readily obvious that the graphs on opposite sides are nearly identical, a fact that is further hammered in by their near equal timestamps. And unlike the examples on display in Figs 6.4 to 6.11, the error behavior with the added fluctuations remains more or less consistent, with only a few differences of a couple milliseconds in its timestamps from simulation to simulation. The large error oscillations that cropped up in the previous examples are also, for the most part, eliminated. Thus, it's presumable to say that the effect of these random fluctuations have on the system's error has been effectively curtailed, though only for relatively small amplitudes. Larger fluctuations will necessitate an increase in both α , again to make sure that A_x is reset during a single tick of the controller, and in the dynamic sampling voltage variation threshold, so that it can correctly detect the when its nodal voltage is being influenced by another generator's operation.

6.4 Applied to a Full Grid

Lastly, in the interest of obtaining a fuller picture, we can take another look at the example of a full grid scenario tested in Chapter 5. As Figs. 6.21 and 6.22 show, the two graphs also share the same degree of similarity seen in the previous cases, both visually and in their timestamps. Another noteworthy fact is that the controllers for generators 4, 5 and 6 never activate during the 1 second interval, relying solely on the surrounding DERs to correct their voltage deviation.



0.044s (2); 0.046s (1); 0.050s (3); 0.115s (2);
 0.170s (1); 0.308s (7); 0.361s (8); 0.418s (9);
 0.468s (3); 0.593s (2); 0.665s (1); 0.816s (9);
 0.917s (7); 0.934s (8)



0.044s (2); 0.046s (1); 0.050s (3); 0.115s (2);
 0.169s (1); 0.307s (7); 0.361s (8); 0.421s (9);
 0.467s (3); 0.590s (2); 0.661s (1); 0.828s (9);
 0.915s (7); 0.930s (8)

Figs. 6.21 and 6.22 Evolution of the state variable error in a full grid (9 DERs), following the same setup as the previous eight figures. Each color stands for one of the nine DERs connected to the feeder grid.

Compare it with the discrete method of voltage control, where all nine controllers would be operating concurrently, tripling the power shifts in relation to the 3 DER study models. Going back to Fig 6.1, without fluctuations it took 56 iterations for the discrete system to curtail the error below 10^{-4} , tallying about $56 \times 9 = 504$ shifts in the injected power total. Upon further testing, we found that for the voltage error integration it takes only 117, nearly 5 times less. (For study model 6, it was $16 \times 3 = 48$ against 7.) The discrepancy only increases if we were to factor in the fluctuations, were it took the former an average of 1500 iterations, meaning $1500 \times 9 = 13500$ shifts, to satisfy the requirements. This serves to highlight the other major advantageous that integrating the error area has over the discrete iterative process, that being reducing its reliance on the autonomous power controllers to safeguard the network's voltage profile.

Note also that all performance matters of the voltage integration system are tied to A_X : the lower its value, the faster the system will act upon the error. (For example, halving A_X in the above figures would result in the same graphs, only for a time interval of 0.5 seconds instead of 1.) However, there's an ostensible lower limit to this parameter dictated by the controllers' own response time, as it's paramount that their operation period do not overlap which, as stated before, could cause an imbalance in the system, similar to stability issues that plagued the discrete process.

Chapter 7

Conclusions

The significant expansion of microgeneration in recent years has resulted in a renewed focus on the issue of DG regulation within the pertaining academic community, given its noted impact on network quality of service, not to mention security and reliability. As placing the DNO in charge of the regulation process, the so-called centralized control strategy, carries significant associated costs and a crippling dependence on usually fickle communication links, decentralized approaches are being promoted as the more practical and economical alternatives. However, while appealing taken at a glance, several underlying concerns regarding the adoption of these control approaches, chiefly stemming from the single-phase nature of the DER elements, have gone unrecognized or inadequately defined so far. Their existence, and general ignorance of, poses a potential false step in the establishment of autonomous systems as the new paradigm in DG power control.

7.1 Summary

As underlined in the state-of-the-art, the avowed objective of this work was to propose such a theoretical operable control strategy, that could (in a future instance) be employed by micro-producers to regulate their own operation without the need of input or oversight from any external entity. Also anticipated in the opening chapter, a large portion of this study came to concern the identification and subsequent detailed examination of the most conspicuous stumbling blocks that arise with said independence, namely stability, performance and restrictions on the power output. In tandem, throughout the paper, we've strived to develop a voltage control scheme that could eliminate or minimize the impact of these inherent inadequacies, yielding two results in the form of the Alternating Q(V)/P(V) Controller (Table VIII - Chapter 3) and the Voltage Error Area Integration Controller (Chapter 6).

We started in Chapter 2 by demonstrating the principle behind the voltage rise phenomenon, that occurs in three-phase grids with single-phase DERs, and how it can be translated into a reduced resistance matrix $[R]$ for the a four-wire feeder circuit model. It's in the non-diagonal elements of this matrix, representing the generators' mutual influence on one another, that the heart of the studied issue of stability lies. Defining first both a set of fourteen basic study models, whose minute differences revealed the extensive effects DER distribution has on the system performance further ahead, and basic control algorithm, a criteria for convergence was established based on the eigenvalues of the derived matrix $[A]$. The existence of this benchmark, rooted in each controller specific power gain $[K]$ as opposed to the common gain α , allows us to calculate the maximum allowed gain $[k_{stb}]$ given a specific network's configuration, through $[R]$. It's this set of values, which define the algorithm's limitations for the convergent (and thus stable) behavior of the voltage error, that became our standard of comparison for the different network configurations and control options, as it gauges the former's robustness.

Chapter 3 dealt with the evolution of the base algorithm, transforming it into the one that was to be utilized in the succeeding simulations. We first arrived at the conclusion that the best option for the controllers was to base their specific power gain $[K]$ on the inverse impedance seen by their respective DER, as it counteracts the effects of the generators' distance to the source bus. Additionally, we've discovered that by eliminating the simultaneity of the control process, that is have no two controllers operating at the same time, any common gain factor α between 0 and 2 could guarantee the system's stability. Such methodology would later be studied in Chapter 6. Beyond gains and stability concerns, we also weighted in the physical characteristics of the equipment, which will invariably impose restrictions on the power injected into the grid by a generator, mathematically represented by a S_M radius semi-circle. While this limit curve does not compromise the algorithm convergence in itself, it may act as a roadblock, making it impossible for the nodal voltage to reach its set-point. Furthermore, in order for the system to successfully maneuver within its operational area, the controller will have to alternate between regulating its reactive, $Q(V)$, or its active power, $P(V)$, exclusively. In order to avoid any unnecessary drops in the injected active power, we opted for an algorithm that gives precedence to the former, meaning that will only fall back on the latter if it encounters the limit curve. Lastly, we identified the line segment (27) which contains all possible sets of solutions for the given initial conditions. This, and any line segment with the same slope, can be navigated by the system without it disturbing the voltage profile, which is helpful when a certain power factor is desired or when drops occur in the available active power.

With the fundamentals laid out, in Chapter 4 we proceeded to simulate the study models with the updated algorithm, using MATLAB. Being necessary to run the program, we began by computing a set of initial voltage values based on each study model, which naturally came to yield dissimilar results owing to the different positioning of the DERs in the 3bus-by-3phase grid and the occurrence of voltage rise. Also as expected, the effects of the latter are more pronounced in situations where there's more concentration of DG, both in busses and in phases. In general, what we can take from the simulations is that small differences in positioning of the generators produce non-negligible variations in both voltage error behavior and system performance, particularly for higher common gains. Alluded since the beginning, the collected results from the tests have indeed corroborated that an unbalanced distribution of generators throughout the grid's phases induces a higher lag, and a somewhat lower total power shift for both types due to same-phase reciprocal influences. The latter even resulted in some situations where the injected power counter-intuitively rose, despite the initial nodal voltage being greater than the set-point. Furthermore, the best performances are achieved within the oscillatory range of the common gain factor, typically found around $1.5[k_{osc}] = 0.75[k_{stb}]$. Last of all, an additional function was added to the algorithm, due to a situation encountered in one of the study models, to allow for more breathing space to the controller.

The follow-up Chapter 5 was dedicated to the expansion of the original network model, studying the system's response to a larger concentration of DG in the same 3-bus network and the effects of increasing the impedance (i.e. electrical distance) between those same busses. Unsurprisingly, the inclusion of more DERs further lowers the maximum common gain factor α , weakening the robustness of the system, though not to the extent that was initially feared, with its value leveling when two of the phases are filled. Nevertheless, each extra element contributes with yet another degree of unwanted complexity, as can be noted in the obtained sets for each set of initial nodal voltage based on the number of connected generators. Performance with high concentration of DG is mostly tied with the initial conditions of the system, its biggest hinder being instances of anchoring, where one (or more) voltage error is corrected well ahead of its peers. This in turn will cause its respective controller to act as an anchor to the remainder, as it tries to hold its own nodal voltage in place. Thus, the system will correct more swiftly its overall voltage profile if the detected errors progress towards zero at a similar pace. Spacing wise, the conclusion we reached was that in order to isolate the generating busses more effectively, the relative distance between concurrent ones has to be maximized, rather than applying simple increments in line impedance. The resulting grid would have its busses not equidistant from one another, but rather spaced in logarithmic fashion, which allows us to obtain a higher maximum common gain factor with the same distance between the most downstream and upstream bus.

Finally, in Chapter 6, we saw to the proposal of continuous basis algorithm, as opposed to the discrete one used till that point, as part of a voltage error integration based controller. The impetus for elaborating on this methodology stemmed mainly from the erratic patterns in system performance when applying a small random fluctuation factor to the nodal voltage, whose lag is on average substantially higher, especially with a large number of DERs. In essence, by adopting this method, a controller's operation would only be triggered when the voltage error integration area surpasses a certain set limit, then readjusting the injected power based on a sample of said area. Not only would this curtail the impact natural voltage fluctuations have on the system's operation but, more importantly, it removes the simultaneous aspect of the control process, assuming that no two controller's operations can overlap. As mentioned above, a large share of the stability issue in decentralized voltage control is thus eliminated, removing any pressing concerns over the distribution of the DERs over the feeder, though power limits and performance remain a matter of consequence. Another benefit came with the shorter number of power shifts necessary to reach a solution set, that is to correct the same initial voltage error, compared to the discrete algorithm.

7.2 Outlook

In conclusion, the results of this thesis demonstrate that implementing a decentralized voltage control strategy for DG in a LV network can indeed be feasible, in theory. Despite the numerous issues that plague it, such as the pervasive threat of instable behavior and lacking performance, it is possible to circumvent them through adequate planning of the controllers' gains and adjustments to their algorithm. However, as noted by German military theorist Helmuth von Moltke, "*No battle plan survives contact with the enemy*". That's to say, when theory is pitted against the real world, the latter will invariably come out on top.

In spite of our efforts to factor in several limiting factors into our calculations and solutions, such as restrictions on injected power and voltage fluctuations, the results obtained throughout this work were still drawn from a simplified scenario rather than a realistic one. And even presented with such model conditions – a constant- parameter network model, a constant reactance-to-resistance ratio ($x \gg r$), no external perturbations in injected power, ideal initial conditions, a balanced load for non-generating nodes, instant reaction times, etc. – we've still encountered a significant number of complications, that can prove nonetheless critical to the control system's operation, and possibly a death knell to the near-future widespread adoption of decentralized control strategies. Future, more in-depth and in practice, studies are thus believed to be required to properly gauge the realistic viability of the autonomous option in real-life LV distribution networks. It's nonetheless hoped that the provided strategies, even if not viable as practical solutions, can at least serve as a stepping stone towards the formulation of a workable decentralized control scheme, much like the original base algorithm was expanded throughout the work in response to the encountered issues.

More importantly, throughout the course of this thesis, it was our intention to draw attention to the inherent limitations of decentralized voltage control, shining a light on a previously poorly defined field of research, and hopefully stimulate a broader discussion within the pertaining academia on the topic.

Bibliography

- [1] I. I. E. Agency, Trends in Photovoltaic Applications—Survey Report of Selected IEA Countries Between 1992 and 2007, 2008.
- [2] I. I. E. Agency, Trends in Photovoltaic Applications—Survey Report of Selected IEA Countries Between 1992 and 2009, 2010.
- [3] E. E. P. I. Association, Global Market Outlook for Photovoltaics Until 2014, 2010.
- [4] J. Deutch, and E. Steinfeld, “A Duel in the Sun: The Solar Photovoltaics Technology Conflict between China and the United States,” in *Report for the MIT Future of Solar Energy Study*. Cambridge, MA, USA: Mass. Inst. Technol., May 2013.
- [5] M. Bolen, and F. Hassan, Integration of Distributed Generation in the Power System. Piscataway, NJ, USA: Wiley/IEEE Press, pp. 88, 2011.
- [6] P. M. Carvalho, L. A. Ferreira, and J. J. Santana, “Single-Phase Generation Headroom in Low-Voltage Distribution Networks Under Reduced Circuit Characterization,” *IEEE Trans. Power Syst.*, Vol. 30, no. 2, pp. 1006-1011, March 2015.
- [7] C. L. Masters, “Voltage rise: The big issue when connecting embedded generation to long 11 kV overhead lines,” *Inst. Elect. Eng. Power Eng. J.*, vol. 16, pp. 5-12, Feb. 2002.
- [8] P. F. Ferreira, P. M. S. Carvalho, L. A. F. M. Ferreira, and M. D. Ilic, “Distributed Energy Resources Integration Challenges in Low-Voltage Networks: Voltage Control Limitations and Risk of Cascading,” *IEEE Trans. Sustain. Energy*, vol. 4, no. 1, pp. 82–88, Jan. 2013.
- [9] P. H. Nguyen, J. M. A. Myrzik, and W. L. Kling, “Coordination of voltage regulation in active networks,” in *Proc. T&D. IEEE/PES Transm. Distrib. Conf.*, pp. 1-6, 2008.
- [10] R. Tontoski, and L. A. C. Lopes, “Voltage regulation in radial distribution feeders with high penetration of photovoltaic,” in *Proc. IEEE Energy 2030 Conf.*, pp. 1-7, 2008.
- [11] R. Tontoski, L. A. C. Lopes, and H. M. T. El-Fouly, “Coordinated active power curtailment of grid connected PV inverters for overvoltage prevention,” *IEEE Trans. Sustain. Energy*, vol. 2, no. 2, pp. 139-147, Apr. 2011.
- [12] M. H. J. Bollen, and A. Sannino, “Voltage control with inverter-based distributed generation,” *IEEE Trans. Power Del.*, vol. 20, no. 1, pp. 519–520, Jan. 2005.
- [13] C. M. Hird, H. Leite, N. Jenkins, and H. Li, “Network voltage controller for distributed generation,” *Proc. Inst. Elect. Eng., Gen., Transm., Distrib.*, vol. 151, no. 2, pp. 150–156, Mar. 2004.
- [14] A. E. Kiprakis, and A. R. Wallace, “Maximizing energy capture from distributed generators in weak networks,” *Proc. Inst. Elect. Eng., Gen., Transm., Distrib.*, vol. 152, no. 5, pp. 611–618, Sep. 2004.
- [15] P. M. S. Carvalho, Pedro F. Correia, and Luís A. F. M. Ferreira, “Distributed Reactive Power Generation Control for Voltage Rise Mitigation in Distribution Networks,” *IEEE Trans. On Power Systems*, vol. 23, no. 2, pp. 766–772, May 2008.
- [16] J. Ragazzini, and L. Zadeh, “The analysis of sampled-data systems,” *Trans. AIEE*, vol. 71, pt. II, pp. 225.234, 1952.
- [17] Vytautas Bielinckas, “Efficiency of Solar Harvesting,” *Materials, Energy and Sustainable Growth: Netherlands*, Leewarden, 2012.
- [18] Prabha Kundur, “Power System Stability and Control,” *The EPRI Power System Engineering Series*, McGraw-Hill, Inc., pp. 191-196, 1994.

Annex A – MATLAB Code for Discrete Controller

```

%%%%%%%%%%%%%%%%%%%%%%%%%%%%%%%%%%%%%%%%%%%%%%%%%%%%%%%%%%%%%%%%%%%%%%%%
%%Discrete alternating Q(V)/P(V) controller%%
%%%%%%%%%%%%%%%%%%%%%%%%%%%%%%%%%%%%%%%%%%%%%%%%%%%%%%%%%%%%%%%%%%%%%%%%

clc; clear all; clf;

%reactance-to-resistance ratio
XoR=.1;

%grid position matrix: 0-empty node, 1-generating node
% 0 1 2 3 4 ...
%R 0 - 0 - |0 - 0 - 0 -...|
%S 0 - 0 - |0 - 0 - 0 -...|
%T 0 - 0 - |0 - 0 - 0 -...|
%
% |<-start point
pDER=[ 1 0 0 ;
       0 1 0 ;
       0 0 1 ];
%number of elements (DERs)
nDER=nnz(pDER);

%voltage set-point
vx=1.1;

%build reduced circuit resistance matrix and calculate initial voltage
[R,v0]=matrixbuild(pDER);

%reactance, conductance and susceptance matrices
X=XoR*R;G=R^-1;B=X^-1;

%common gain factor
alpha=1.0;
%controller power gains, active (kp) and reactive (kq)
k=diag(R).^-1*alpha;kp=k;kq=k/XoR;

%eigenvalues
lamb=eig(eye(nnz(pDER))-R*diag(k));

%setting initial values
%%voltage
v=v0;
%%active power
p0(1:nDER,1)=0.95;
%%reactive power
q0(1:nDER,1)=-0.3;
%%maximum apparent power == semi-circle radius
sM=1.035;
%%maximum available active power
pA(1:nDER,1)=sM;

%initial condition variable: equation (24)
c0=(G*(vx-v0)+p0)*XoR^-1+q0;

%system checks
%%checks if system is stable
if any(abs(lamb)>1)
    disp('--System is instable')
    return
%%checks if set-point is reachable under current conditions
elseif ini cond error(c0,sM,XoR,pA)==0
    return
end

%record initialization
vout(:,1)=v0; p=p0; pout(:,1)=p0; q=q0; qout(:,1)=q0; lag=0;

%number of iterations
N=100;

```

```

%main loop
for i=2:N

    %maximum active and reactive power
    pM=min(sqrt(sM^2-q.^2),pA);
    qM=sqrt(sM^2-p.^2);

    %runs through all DERs
    for j=abs(1:nDER)
        %activates P(V) if next activation of Q(V) puts apparent power over
        %the limit
        if abs(q(j)+kq(j)*(vx-v(j)))>abs(qM(j))
            %activates meanshiftpoint function when necessary (see Section 4.5)
            if p(j)+kp(j)*(vx-v(j))>pM(j) || p(j)+kp(j)*(vx-v(j))<=0
                [p(j) q(j)]=meanshiftpoint(p(j),q(j),XoR,sM,pA(j));
            end
            %executes active power shift
            p(j)=p(j)+kp(j)*(vx-v(j));
            %keeps power within limits
            p(j)=min(pM(j),max(0,p(j)));
            %otherwise activates Q(V) per standard
        else
            %executes reactive power shift
            q(j)=q(j)+kq(j)*(vx-v(j));
            %keeps power within limits
            q(j)=min(qM(j),max(-qM(j),q(j)));
        end
    end

    %updates voltage based on previous shifts
    v=v0+R*(p-p0)+X*(q-q0);

    %adds random fluctuation factor (if wanted)
    %v=v-0.01*(v0-vx)+0.02*(v0-vx).*rand(nDER,1);

    %updates record
    vout(:,i)=v; pout(:,i)=p; qout(:,i)=q;

    %checks if error threshold has been reached to estimate the lag
    if lag==0 && (mean(abs(v-vx))<10^-4)
        lag=i-1;
    end
end

%final active power drop curtailment
[p q]=setlineadj(p,q,p0,q0,sM,XoR,1);
v=v0+R*(p-p0)+X*(q-q0); vout(:,i)=v; pout(:,i)=p; qout(:,i)=q;

%chose plot: 1-[P,Q] cartesian plot, 2-voltage error
plottype=0;

if plottype==1
    youtp(1)=sM;
    youtn(1)=-sM;
    xout(1)=0;
    for j=2:3*N+1
        youtp(j)=youtp(j-1)-(sM)/(3*N);
        youtn(j)=-youtp(j);
        xout(j)=sqrt((sM)^2-youtp(j)^2);
    end
    for i=1:nDER
        hold on
        plot(pout(i,1:N),qout(i,1:N), xout,youtp,'k', xout,youtn,'k')
        hold on
    end
    axis([min(min(pout))-0.01 max(max(pout))+0.01 min(min(qout))-0.005 max(max(qout))+0.005])
    line([0 sM],[0 0], 'Color','k','LineStyle',':');
    xlabel('P (pu)')
    ylabel('Q (pu)')
elseif plottype==2
    plot(0:N-1,(vout(:,i)-vx)*10^3)
    axis([-0.1 N (min(min(vout-vx))-0.001)*10^3 (max(max(vout-vx))+0.001)*10^3])
    xlabel('Iterations')
    ylabel('Voltage Error (x10^-3)')
    line([0 N],[0 0], 'Color','k','LineStyle',':');
end

```

Annex B – MATLAB Code for Continuous Controller

```

%%%%%%%%%%%%%%%%%%%%%%%%%%%%%%%%%%%%%%%%%%%%%%%%%%%%%%%%%%%%%%%%%%%%%%%%
%%Voltage error area integration alternating Q(V)/P(V) controller%%
%%%%%%%%%%%%%%%%%%%%%%%%%%%%%%%%%%%%%%%%%%%%%%%%%%%%%%%%%%%%%%%%%%%%%%%%
clc; clf; clear all

%reactance-to-resistance ratio
XoR=.1;

%grid position matrix: 0-empty node, 1-generating node
% 0 1 2 3 4 ...
%R 0 - 0 - |0 - 0 - 0 -...|
%S 0 - 0 - |0 - 0 - 0 -...|
%T 0 - 0 - |0 - 0 - 0 -...|
% |<-start point
pDER=[ 1 0 0 ;
       0 1 0 ;
       0 0 1 ];
%number of elements (DERs)
nDER=nnz(pDER);

%voltage set-point
vx=1.1;

%build reduced circuit resistance matrix and calculate initial voltage
[R,v0]=matrixbuild(pDER);

%reactance, conductance and susceptance matrices
X=XoR*R;G=R^-1;B=X^-1;

%common gain factor
alpha=1.1;
%controller power gains, active (kp) and reactive (kq)
k=diag(R).^-1*alpha;kp=k;kq=k/XoR;

%eigenvalues
lamb=eig(eye(nnz(pDER))-R*diag(k));

%setting initial values
%%voltage
v=v0;
%%initial error
verr(:,1)=vx-v0;
%%voltage variation
dvout(1:nDER,1)=0;
%%active power
p0(1:nDER,1)=0.95;
%%reactive power
q0(1:nDER,1)=-0.3;
%%maximum apparent power == semi-circle radius
sM=1.035;
%%maximum available active power
pA(1:nDER,1)=sM;

%initial condition variable: equation (24)
c0=(G*(vx-v0)+p0)*XoR^-1+q0;

%system checks
%%checks if system is stable
if any(abs(lamb)>1)
    disp('--System is instable')
    return
%%checks if set-point is reachable under current conditions
elseif ini_cond_error(c0,sM,XoR,pA)==0
    return
end

%record initialization
vout(:,1)=v0; p=p0; pout(:,1)=p0; q=q0; qout(:,1)=q0; lag=0;

%operation timespan (in milliseconds)
N=1000*1.0;

```

```

%voltage error area set-point
Ax=1;

%sampling timespan (in milliseconds)
n=10;

%time parameters initialization
A(1:nDER)=0; trig(1:N)=0; temp(1:nDER)=0; lerr(1:nDER)=0; ss(1:nDER)=1;

for i=2:N %alterar k para i

    %maximum active and reactive power
    pM=min(sqrt(sM^2-q.^2),pA);
    qM=sqrt(sM^2-p.^2);

    %stops two controllers from acting in the same iteration of the loop
    %this better simulates an actual continuous base controller
    flag=0;

    %runs through all DERs
    for j=1:nDER

        %resets time parameters if voltage error switches signal
        if i~=2 && ((verr(j,i-1)/verr(j,i-2))<=0 || abs(verr(j,i-1))<10^-9)
            A(j)=0; temp(j)=0; ss(j)=i-1;
        end

        %accrues error area and timer
        A(j)=A(j)+verr(j,i-1)/1;
        temp(j)=temp(j)+1;

        %detects large shift in voltage, sets new sample border
        if abs(dvout(j,i-1))>1*10^-3
            ss(j)=i-1;
        end

        %detects when error area surpasses set-point
        if ( abs(A(j))>=Ax ) && flag==0
            %records trigger time
            trig(i)=j;

            %adjusts sample border
            if k-1-ss(j)>n
                ss(j)=i-1-n;
            end
            span=numel(verr(j,ss(j):i-1));

            %activates P(V) if next activation of Q(V) puts apparent power
            %over the limit
            if abs(q(j)+kq(j)*sum(verr(j,ss(j):i-1))/span)>abs(qM(j))
                %activates meanshiftpoint function when necessary
                if p(j)+kp(j)*sum(verr(j,ss(j):i-1))/span>pM(j) ||
                p(j)+kp(j)*sum(verr(j,ss(j):i-1))/span<=0
                    [p(j) q(j)]=meanshiftpoint(p(j),q(j),XoR,sM,pA(j));
                end
                %executes active power shift based on average error
                p(j)=p(j)+kp(j)*sum(verr(j,ss(j):i-1))/span;
                %keeps power within limits
                p(j)=min(pM(j),max(-pM(j),p(j)));
                %otherwise activates Q(V) per standard
            else
                %executes reactive power shift based on average error
                q(j)=q(j)+kq(j)*sum(verr(j,ss(j):i-1))/span;
                %keeps power within limits
                q(j)=min(qM(j),max(-qM(j),q(j)));
            end
            flag=1;
        end
    end

    %updates voltage based on previous shifts
    v=v0+R*(p-p0)+X*(q-q0);

    %adds random fluctuation factor (if wanted)
    %v=v-0.01*(v0-vx)+0.02*(v0-vx).*rand(nDER,1);

```

```

%updates record
vout(:,i)=v; verr(:,i)=vx-v; dvout(:,i)=v-vout(:,i-1);
pout(:,i)=p; qout(:,i)=q; Aout(:,i)=A;

%checks if error threshold has been reached to estimate the lag (in s)
if lag==0 && (mean(abs(v-vx))<10^-4)
    lag=(i-1)*10^-3;
end

end

%triggers record
[row col val]=find(trig);
trig=[col/1000 ; val];
ct=trig(1, size(trig,2))*1000;

%chose plot: 1-[P,Q] cartesian plot, 2-voltage error
plottype=0;

t=(1:N)/1000;
if plottype==1
    youtp(1)=sM;
    youtn(1)=-sM;
    xout(1)=0;
    for j=2:3*N+1
        youtp(j)=youtp(j-1)-(sM)/(3*N);
        youtn(j)=-youtp(j);
        xout(j)=sqrt((sM)^2-youtp(j)^2);
    end
    for i=1:nDER
        hold on
        plot( pout(i,1:N),qout(i,1:N), xout,youtp,'k', xout,youtn,'k')
        hold on
    end
    axis([min(min(pout))-0.01 max(max(pout))+0.01 min(min(qout))-0.005 max(max(qout))+0.005])
    line([0 sM],[0 0], 'Color','k', 'LineStyle',':');
    xlabel('P (pu)')
    ylabel('Q (pu)')
elseif plottype==2
    plot(t, (vout(:,:)-vx)*10^3)
    line([0 N/1000],[0 0], 'Color','k')
    axis([0 N/1000 (min(min(vout-vx))-0.001)*10^3 (max(max(vout-vx))+0.001)*10^3])
    xlabel('t(s)')
    ylabel('Voltage Error (x10^-3)')
end
end

```

Annex C – MATLAB Code for *ini_cond_error* Func.

```
%%%%%%%%%%%%%%%%%%%%%%%%%%%%%%%%%%%%%%%%%%%%%%%%%%%%%%%%%%%%%%%%%%%%%%%%
%%Function checks if given initial conditions%
%%allow the system to reach the set-point %%
%%%%%%%%%%%%%%%%%%%%%%%%%%%%%%%%%%%%%%%%%%%%%%%%%%%%%%%%%%%%%%%%%%%%%%%%
function [check] = ini_cond_error(c0,sM,XoR,pA)

err(1:4)=0;

%coefficients of function (23), solved for pf
a=1+XoR^-2; b=-2*c0*XoR^-1; c=c0.^2-sM^2;

%checks (26)
if any( sqrt(1+XoR^2)*sM - abs(c0*XoR) < 0 )
    err(1)=1;
end
%checks (28), lower limit
if any(c0<-sM)
    err(2)=1;
end
%checks (28), higher limit
if any(c0>sM*XoR^-1*sqrt(1+XoR^2))
    err(3)=1;
end
%checks for available active power
if pA(1)<min(roots([a b(1) c(1)])) || pA(2)<min(roots([a b(2) c(2)])) || pA(3)<min(roots([a
b(3) c(3)]))
    err(4)=1;
end

%error message
if any(err~=0)
    check=0;
    disp('Initial conditions do not allow for successful correction')
    if err(1)==1
        disp('--Inequality 25 violated')
    end
    if err(2)==1
        disp('--Inequality 27 (lower) violated')
    end
    if err(3)==1
        disp('--Inequality 27 (higher) violated')
    end
    if err(4)==1
        disp('--Not enough active power available')
    end
end
else
    check=1;
end
```


Annex D – MATLAB Code for *matrixbuild* Func.

```

%%%%%%%%%%%%%%%%%%%%%%%%%%%%%%%%%%%%%%%%%%%%%%%%%%%%%%%%%%%%%%%%%%%%%%%%
%%Function builds resistance matrix under reduced circuit conditions and%%
%%then calculates the powerflow to determine the initial voltage values %%
%%%%%%%%%%%%%%%%%%%%%%%%%%%%%%%%%%%%%%%%%%%%%%%%%%%%%%%%%%%%%%%%%%%%%%%%

function [R,v0] = matrixbuild(pDER)

%bus-to-bus line impedance
zz=0.2;

N=numel(pDER); NZ=nnz(pDER);
R(1:NZ,1:NZ)=0; pos(1:NZ,3)=0;
count=0; nDER=1; z=zz*4;

for i=1:N/3

    %runs through the three phases
    for j=abs(1:3)
        count=count+1;
        %if it detects a DER...
        if pDER(j,i)~=0

            %...it calculates the distance of its associated non-diagonal
            R(nDER,nDER:NZ)=-z/4;
            R(nDER:NZ,nDER)=-z/4;
            %...and its own...
            R(nDER,nDER)=z;

            %saves DER position on the grid
            pos(nDER,:)=[count,j,i];

            %checks for same-phase DERs
            for k=1:i-1
                if pDER(j,k)~=0
                    %changes matrix term accordingly
                    R(nDER,pDER(j,k))=R(pDER(j,k),pDER(j,k));
                    R(pDER(j,k),nDER)=R(pDER(j,k),pDER(j,k));
                end
            end
            pDER(j,i)=nDER;
            nDER=nDER+1;
        end
    end
    %moves to next downstream bus
    z=z+zz*2;
end

%generated voltage, up until 9 DERs (+9 are randomized between 0.96-0.97)
vg=[0.9615 0.9601 0.9651 0.9642 0.9632 0.9656 0.9677 0.9645 0.9690 0.96+0.0099*rand(1,NZ-9)];

%factors samme-phase co-generation into the generated voltage
for j=1:3
    for i=nonzeros(pDER(j,:))
        vg(i)=vg(i)+(nnz(pDER(j,:))-1)*0.1;
    end
end

A = R;
b = ones(NZ,1)*1.1 - vg(1:NZ);
f = ones(NZ,1);
[x,fval,exitflag,output,lambda] = linprog(f,[],[],A,b);

g(1:N)=0;
for i=1:NZ
    g(pos(i,1))=-x(i);
end

a(2+N/3:2)=0; a(1,1)=1; a(1,2)=2;
for i=2:1+N/3
    a(i,1)=a(i-1,1)+1;
    a(i,2)=a(i-1,2)+1;
end
nn=length(a)+1;

```

```

sb = 100; %kVA
vb = .4; %kV
ib = sb/sqrt(3)/vb; %A
zb = vb^2/sb*1e3 ; %Ohm
z(1:nn) = zz;

%load map
sr (1:nn) = [ 0+1i*0 0+1i*0 g(1:3:N)+1i*0];
ss (1:nn) = [ 0+1i*0 0+1i*0 g(2:3:N)+1i*0];
st (1:nn) = [ 0+1i*0 0+1i*0 g(3:3:N)+1i*0];
s = [sr; ss; st];

%set loads for unconnected nodes
for i=3:length(s)
    cog=nnz(s(:,i));
    for j=1:3
        if s(j,i)==0 && cog>=1
            s(j,i)=s(j,i)+0.1;
        end
    end
end

%calculate power flow
[vphase, vneutral, eps] = pf3ph(a, z, s, 1.06, 1., 50);

%retrieves value for the DER nodes
for k=1:NZ
    v0(k)=vphase(pos(k,2),pos(k,3)+2);
end
v0=v0';

%set mean v0 as 1.12 (if wanted)
% v0=v0+(1.12-mean(v0));

```

Annex E – MATLAB Code for *pf3ph* Func.

```
%%%%%%%%%%%%%%%%%%%%%%%%%%%%%%%%%%%%%%%%%%%%%%%%%%%%%%%%%%%%%%%%%%%%%%%%%%%%%%
%%Function that calculates powerflow%%
%%Created by Prof. Pedro Carvalho %%
%%%%%%%%%%%%%%%%%%%%%%%%%%%%%%%%%%%%%%%%%%%%%%%%%%%%%%%%%%%%%%%%%%%%%%%%%%%%%%
function [mvp, mvn, eps, in] = pf3ph (t, z, s, vr, el, ni)
p=t(:,1); f=t(:,2); w=length(p)+1;
vp(1,1:w) = vr; al=exp(-j*pi*2/3);vn(1:3,1:w)=0.0;
for h=2:3 vp(h,1:w)=vp(h-1,1:w)*al; end
va = vp-vn; ia=conj(s.*abs(va).^el./va);
for it=1:ni va=vp-vn; ip=conj(s.*abs(va).^el./va); in=-sum(ip);
for k=w-1:-1:1 n=f(k); m=p(k); in=-sum(ip); ip(:,m)=ip(:,m)+ip(:,n); end
eps = norm(max(abs([ia-ip])));

% if (eps>1e-4) ia=ip; mvp=0;mvn=0;eps=inf; else mvp=abs(vp-vn);
% mvn=abs(vn(1,:)); return; end

mvp=abs(vp-vn);
mvn=abs(vn(1,:));

for k=1:w-1 n=f(k); m=p(k); vn(:,n)=vn(:,m)-z(k)*in(n);
vp(:,n)=vp(:,m)-z(k)*ip(:,n); end; ia=ip; end % pms carvalho 2010
```

Annex F – MATLAB Code for *setlineadj* Func.

```
%%%%%%%%%%%%%%%%%%%%%%%%%%%%%%%%%%%%%%%%%%%%%%%%%%%%%%%%%%%%%%%%%%%%%%%%%%%%%%
%%Function that minimizes active power variation based on (27)%
%%%%%%%%%%%%%%%%%%%%%%%%%%%%%%%%%%%%%%%%%%%%%%%%%%%%%%%%%%%%%%%%%%%%%%%%%%%%%%
function [padj qadj] = setlineadj(p,q,p0,q0,sM,XoR,mode)

padj=p; qadj=q;

if mode==1
    c0=q+XoR^-1*p;
    for j=1:3
        if sqrt(p0(j)^2+(-XoR^-1*p0(j)+c0(j))^2)<=sM
            padj(j)=p0(j);
            qadj(j)=-XoR^-1*p0(j)+c0(j);
        else
            if p(j)<p0(j)
                padj(j)=max(roots([-XoR^-1]^2+1 2*c0(j)*(-XoR^-1) c0(j)^2-sM^2]));
            else
                padj(j)=min(roots([-XoR^-1]^2+1 2*c0(j)*(-XoR^-1) c0(j)^2-sM^2]));
            end
            qadj(j)=-XoR^-1*padj(j)+c0(j);
        end
    end
end
end
```